

POLITECNICO DI TORINO
MASTER OF SCIENCE IN CIVIL ENGINEERING



**Politecnico
di Torino**



UNIVERSITY OF
ILLINOIS CHICAGO

College of Engineering

Master's degree thesis

Scaled Model of the Messina Bridge:
Numerical Analysis and Experimental Setup
considering Soil-Structure Interaction under
Seismic Excitation

Supervisors:

Prof. Gian Paolo Cimellaro
Prof. Farhad Ansari

Candidate:

Kevin Visaggi

ACADEMIC YEAR 2024/2025

Abstract

This study investigates the seismic behavior of the Messina suspension bridge, focusing on the influence of soil conditions during seismic events. Three soil profiles were selected, representing soft, medium, and stiff soil conditions, combined with two distinct seismic ground motions, resulting in six scenarios.

A finite element model (FEM) was developed to assess the dynamic response of the bridge, including deck displacements and cable tension variations under different conditions. To validate the numerical results, a 1:265 scaled model of the bridge was constructed in the laboratory.

Experimental measurements included deck displacements recorded via Linear Variable Differential Transformers (LVDT) at mid-span, dynamic characteristics captured through accelerometers, and cable tension variations monitored using Fiber Bragg Grating (FBG) sensors. The results provide insights into the bridge's seismic response across different soil conditions, highlighting key structural behaviors under dynamic loading.

The analysis of displacement reveals that softer soil conditions lead to higher midspan displacements during seismic excitation, with the near-fault case generally exhibiting larger displacements compared to the far-fault case. However, the fixed foundation configuration in the MTR scenario deviates from this trend, likely due to local dynamic effects between the cables, tower, and foundation.

In terms of cable tension, a similar trend was observed: softer soil conditions resulted in lower cable tension under seismic excitation. Interestingly, in the case of MTR, the high-stiffness foundation configuration exhibited lower tension than the medium stiffness scenarios, indicating potential dynamic interactions or damping effects not seen in the other cases. These findings underscore the importance of soil-structure interaction in the seismic performance of suspension bridges.

The results highlight that the compression scale factor in the model may have diminished the effect of near-fault seismic excitation, leading to more similar outcomes in cable tension despite the differences in seismic ground motions. These insights pave the way for further experimental and numerical investigations into the seismic behavior of suspension bridges, with potential applications in improving seismic design strategies.

Acknowledgments

Prima di ogni altra persona che ha contribuito a questo percorso, devo ringraziare la mia famiglia: i miei genitori, Denis e Selene, per tutto ciò che hanno fatto per me in questi anni. Nonostante le distanze e i periodi difficili, sono sempre stati al mio fianco, pronti a supportarmi e a darmi la forza necessaria per superare ogni sfida che questo cammino mi ha posto davanti. Senza di loro, probabilmente nulla di tutto questo sarebbe stato possibile.

Voglio inoltre ringraziare il Professor Cimellaro e il Professor Ansari per l'opportunità che mi hanno dato. Questo progetto è stato fin da subito una sfida stimolante, che mi ha permesso di lavorare su uno dei miei ambiti preferiti dell'ingegneria civile, i ponti, e che mi ha concesso di esplorare per la prima volta il mondo americano. La mia gratitudine nei loro confronti sarà sempre immensa. Un ringraziamento speciale anche a Chengwei, che è stato un punto di riferimento nei momenti di difficoltà e mi ha sempre offerto il suo aiuto nei momenti più complessi di questi sei mesi di tesi.

Un'altra persona che è stata un pilastro per me in questo percorso è Mattia, che di tutte le battaglie fatte insieme è sempre stato una spalla su cui contare, su ogni lezione, corso, esame fatto insieme. E ovviamente non posso anche che ringraziare Marco, Antonio e Luca quali sono stati, sono e saranno amici di sempre.

Infine, un piccolo ringraziamento al me che ha intrapreso questo percorso. Nonostante tutte le difficoltà di questi anni, non hai mollato, non ti sei arreso, e quando lo hai fatto, sei stato comunque in grado di resistere. Con la speranza che questo sia solo l'inizio della rincorsa verso il lavoro dei miei sogni.

Before acknowledging anyone else who contributed to this journey, I must first thank my family—my parents, Denis and Selene—for everything they have done for me over the years. Despite the distance and difficult times, they have always been by my side, ready to support me and give me the strength needed to overcome every challenge this path has placed before me. Without them, none of this would have been possible.

I also want to express my gratitude to Professor Cimellaro and Professor Ansari for the opportunity they have given me. From the very beginning, this project has been an exciting challenge that allowed me to work on one of my favorite topics in civil engineering—bridges—while also giving me the chance to explore the American academic world for the first time. My appreciation for them will always be immense. A special thanks also goes to Chengwei, who has been a great support in difficult moments and has always offered his help during the most challenging times of these six months.

Another person who has been a pillar for me throughout this journey is Mattia, who, through all the battles we've faced together, has always been a shoulder to lean on during every lesson, course, and exam we've taken together. And of course, I cannot forget to thank Marco, Antonio, and Luca, who have been, are, and will always be lifelong friends.

Finally, a small acknowledgment to myself for embarking on this journey. Despite all the difficulties of these years, you never gave up, you never surrendered, and even when you did so, you still managed to push through. I hope this is just the beginning of the race toward achieving the job of my dreams.

Contents

Abstract	3
Acknowledgments	5
List of Figures	12
1 Introduction	13
2 Suspension Bridges	14
2.1 Structural Systems	14
2.2 Historical Review	18
2.2.1 1° Generation Type	23
2.2.2 2° Generation Type	28
2.2.3 3° Generation Type	29
3 Messina Suspension Bridge	31
3.1 Location	31
3.2 Evolution of the Project	32
3.3 Final Design Project (Progetto Definitivo)	39
3.3.1 Main Characteristics of the Bridge	39
3.3.2 Deck	40
3.3.3 Suspension System	41
3.3.4 Towers	43
3.3.5 Anchorage Blocks	44
4 Scaling Procedures and Design Model	45
4.1 Similarity Conditions	45
4.1.1 Geometric scaling	45
4.1.2 Physical Scaling Properties	46
4.2 Bridge Model	48
4.2.1 Geometry	48
4.2.2 Materials	48
4.2.3 Boundary Conditions	50
4.2.4 Static Analysis	51
4.2.5 Dynamic Analysis	51
5 Finite Element Model Analysis (FEM)	53
5.1 Model Assumptions	53
5.2 Suspension Bridge Wizard	53
5.2.1 Node Coordinates & Heights	54
5.2.2 Hangers Distance	55

CONTENTS

- 5.2.3 Properties 55
- 5.2.4 Deck System 55
- 5.3 Final Model 57
 - 5.3.1 Boundary Conditions 58
 - 5.3.2 Loads 59
- 5.4 Suspension Bridge Analysis 60
- 5.5 Construction Stage Analysis 60
- 5.6 Eigenvalue Analysis 62
- 5.7 Time History Analysis 64

- 6 Construction Stage 66**
 - 6.1 Laboratory Capacity 66
 - 6.2 Materials Preparation 66
 - 6.2.1 Hanger Anchorages 66
 - 6.2.2 Bridge Deck 68
 - 6.2.3 Plate Masses 69
 - 6.2.4 Towers 71
 - 6.2.5 Wall Anchorage 73
 - 6.3 Bridge Assembling 73

- 7 Experimental Set-up Test 77**
 - 7.1 Ground Motion 77
 - 7.1.1 Near-Fault and Far-Fault 77
 - 7.1.2 Selection of Seismic Records for Testing 78
 - 7.2 Soil-Foundation System 85
 - 7.2.1 Box-Spring System 85
 - 7.3 Sensors and Instrumentation 87
 - 7.3.1 Shakers 87
 - 7.3.2 Accelerometers and LVDT 88
 - 7.3.3 Fiber Bragg Gratings (FBG) 89

- 8 Results 91**

- 9 Conclusions 94**

List of Figures

2.1	Structural components of a suspension bridge	14
2.2	Reaction forces at supports for a cable and a beam simply-supported	15
2.3	Sag and horizontal force relationship in a cable structure	15
2.4	Comparison of deflection in a cable/beam- based systems subjected to point load	16
2.5	Comparison of deflection in a cable/beam- based systems under non-uniform load	16
2.6	Single-span suspension bridge	17
2.7	Three-span suspension bridges	17
2.8	Suspension system with inclined hangers	18
2.9	Self-anchored suspension bridge	18
2.10	Jacob’s Creek Bridge, the first suspension bridge in Pennsylvania 1801	18
2.11	Wynch Bridge in 1741	19
2.12	Chain Bridge over the Merrimac River, between Amesbury and Newburyport.	20
2.13	Eyebar connection invented by Brown [8]	21
2.14	Menai Bridge in UK, in 1826	21
2.15	Grand Pont Suspendu, Fribourg, 1834.	22
2.16	Wheeling suspension bridge rebuilt by John Roebling	23
2.17	Niagara Railways Suspension Bridge, in 1855	24
2.18	Brooklyn bridge across the East River between Manhattan and Long Island,1883	25
2.19	Manhattan Bridge, in 1909	25
2.20	Golden Gate across the San Francisco Bay, completed in 1937. Source: Wikipedia	26
2.21	Tacoma Narrow Bridge, in 1940 Source: wikipedia	27
2.22	Additional trusses in the Golden Gate Bridge, after the Tacoma collapse	27
2.23	Severn Bridge, in 1966	28
2.24	Lillebælt Suspension Bridge in Denmark, 1970	29
2.25	Canakkale Bridge, in Turkey	30
2.26	3° generation cross-section type	30
3.1	Location of the Messina suspension bridge project.	31
3.2	The tunnel solution proposed by Carlo Alberto Navone in 1870	32
3.3	Representation of the Messina bridge proposed by Steinman	34
3.4	Grant Alan and Partners, Covell and Partners, Inbucon international project	35
3.5	Gruppo Lambertini project	36
3.6	Gruppo Musmeci project	36
3.7	Gruppo Ponte Messina SpA project	36

LIST OF FIGURES

3.8	Arch. Eugenio Montuori with the collaboration of Calini e Lionel Pavlo	37
3.9	Technital SpA project	37
3.10	Lateral view of the Messina Bridge	40
3.11	Multi-box deck-section of the Messina Bridge	40
3.12	Lengths of single boxes of the deck	41
3.13	Single box girder for road	41
3.14	Single box girder for rail	41
3.15	Main suspension system of the bridge	42
3.16	Hangers pattern according to design documents	42
3.17	Towers design of the Messina Bridge	43
3.18	Towers legs cross-section	44
3.19	Anchoring system for main cables	44
4.1	Laboratory in Chicago	46
4.2	Drawing of the model realized in the laboratory	50
4.3	Cad drawing for the towers	50
4.4	Cad drawing for the deck configuration	50
5.1	Suspension bridge wizard with dimensions of the scaled model in the laboratory	53
5.2	Representation of all geometric points to be implemented in the model	54
5.3	Deck-system window	55
5.4	Hangers cross-sections in the FEM model (diameter 0.6 mm)	56
5.5	Main cables cross-sections in the FEM model	56
5.6	Deck cross-section in the FEM model	56
5.7	Towers cross-section in the FEM model	56
5.8	FEM model developed on Midas Civil	57
5.9	Tower- sidespan detail	57
5.10	Rigid boundary conditions	58
5.11	Elastic boundary conditions	58
5.12	Spring-stiffness detail	59
5.13	Nodal loads applied to the model to simulate additional masses	59
5.14	Nodes of the suspension system to be updated	60
5.15	Construction stage analysis	61
5.16	Null vertical deformation of the suspension system after applying the load pattern	61
5.17	Tension forces in main cables after load applied	61
5.18	Eigenvalue analysis control window	62
5.19	First vibration mode: horizontal mode shape	63
5.20	Second vibration mode: horizontal mode shape	63
5.21	Third vibration mode: vertical mode shape	63
5.22	Fourth vibration mode: horizontal mode shape	63
5.23	Fifth vibration mode: vertical mode shape	63

5.24	Time history load case	65
6.1	Raw material for hangers anchorages	66
6.2	Couple of nuts inserted in the bar every 3.81 cm (1.5 inches)	66
6.3	Band saw used for cutting the bars in single pieces	67
6.4	Final anchorages for hangers	67
6.5	Details of the drilling process and the no-slippery connection system for the hanger.	68
6.6	Raw bars for the bridge's deck.	68
6.7	Cross-section of the bridge's deck bars HSS $1\frac{1}{4} \times 1\frac{1}{4} \times \frac{1}{8}$	68
6.8	Plates weight for matching dynamic properties of the bridge	69
6.9	Steps in preparing plates for hanger connections: incision, drilling, and refinement of holes.	70
6.10	Final plates after the whole process	70
6.11	Rectangular shape bars for the tower's legs	71
6.12	Combined Caption for Both Images	71
6.13	Completed tower	72
6.14	Details of the anchoring system.	73
6.15	Tower-cable system.	74
6.16	Hanger positioned at the correct distance.	75
6.17	Welding process of the mass plates onto the deck.	76
6.18	Completed bridge and tensioned hanging system.	76
7.1	Ground motions recorded at (a) 1994 Northridge earthquake, and (b) 1952 Kern County earthquake.	77
7.2	Velocity time history with pulse behaviour and without	78
7.3	6th April 2009 Aquila earthquake	79
7.4	Site of the Aquila earthquake with accelerometers stations [23]	79
7.5	Legend based of the PGA intensity (cm/s^2) [23]	80
7.6	AQV station (Near-Fault)[23]	81
7.7	Illustration of a vertical cross section through a rupture plane and main important distances measurements	81
7.8	AQK station accelerograms records for East-West and North-South direction	82
7.9	MTR station (Far-Fault) [23]	82
7.10	AQK EW and MTR NS time-history Acceleration, Velocity, Displacement	83
7.11	Spectral acceleration of AQK and MTR.	84
7.12	Time scaled acceleration time-history records	84
7.13	Time and PGA scaled acceleration time-history records	85
7.14	Spring-box system	86
7.15	Different components of the Spring-box system	86
7.16	Base plate with roll bearings	86
7.17	Whole system set-up	86
7.18	Shaker used for the experimental analysis	87

LIST OF FIGURES

7.19 Accelerometer used for calculating the dynamic properties of the bridge 88

7.20 LVDT used to calculate displacement in midspan 88

7.21 Example of calibration for FBG sensors 89

8.1 Displacement midspan results 91

8.2 Most loaded main-cable results 91

8.3 Most loaded hangers tension results 92

8.4 Base shear z direction East tower results 93

8.5 Base shear y direction East tower results 93

1 Introduction

Suspension bridges are a type of structure that exhibit good seismic resilience due to their flexibility and very high fundamental vibration period [1]. Their ability to withstand earthquakes stems from their capacity to deform and dissipate energy, reducing the forces transmitted to the main structural components. However, due to their long spans and low natural frequencies, these structures are particularly sensitive to ground motion with dominant low-frequency content, typical of near-fault earthquakes [2], which can amplify dynamic effects, leading to large displacements, increased cable forces, and potential resonance phenomena.

The influence of Soil-Structure Interaction (SSI) is a critical factor in accurately predicting the real structural response of a system. Therefore, traditional numerical models often assume fixed-base conditions, which can lead to discrepancies between theoretical and actual structural behavior. Incorporating SSI effects allows for a more realistic representation of the interaction between the bridge foundation and the underlying soil, providing valuable insights into the dynamic performance of the structure.

Two main methods for modeling SSI effects are commonly found in the literature: the Direct approach and the Substructure approach. The Direct approach integrates all components—structure, foundation, and soil—into a single numerical model, allowing the system to be analyzed as a whole under external excitation. While this method provides a detailed and comprehensive representation, it is computationally demanding and resource-intensive, making it less commonly used in practical applications [3]. In contrast, the Substructure approach simplifies the system by representing the interaction between the structure, foundation, and soil using a combination of springs and dampers, significantly reducing computational complexity while maintaining reasonable accuracy. [4]

This study investigates the seismic response of a suspension bridge considering different soil conditions to assess the impact of SSI. Three soil profiles—soft, medium, and stiff—are examined in combination with two distinct seismic ground motions, resulting in six total scenarios. A numerical analysis is performed to evaluate key dynamic parameters such as deck displacements and cable forces. To validate these findings, experimental testing is conducted on a 1:265 scaled model of the Messina Bridge. The results aim to provide a better understanding of the role of soil flexibility in suspension bridge seismic behavior, offering insights that could enhance future bridge design and seismic mitigation strategies.

2 Suspension Bridges

2.1 Structural Systems

Suspension bridges are a type of bridge primarily used to span very long distances. The reasons why this structural system is particularly suited for such applications will be further explored in the following chapters.

The main components of a suspension bridge, as shown in Figure 2.1, are listed below:

- **Main cables**
- **Hangers (or suspenders)**
- **Deck**
- **Towers**
- **Anchor blocks**

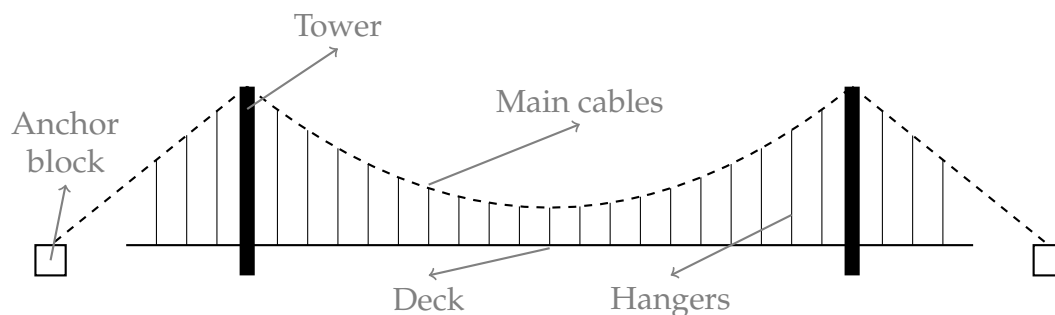


Figure 2.1: *Structural components of a suspension bridge*

For suspension bridges, the deck is carried completely and connected to the main cables throughout the vertical cable system (suspenders/hangers). Main cables are pulled and anchored to massive concrete blocks, that allow to bridge to obtain the wished shape of themselves. The towers provide essential support for the main cables, transferring the forces directly to the foundation level.

Before going in detail in the structural system, it is worth to introduce basic principles behind the suspension system.

Firstly, it is important to distinguish the cable system from the beam one. It is known, that a simply-supported beam scheme uniformly vertically loaded, has two equal vertical reaction forces, while for a cable, 2 horizontal opposite forces arise for equilibrium of the system, as shown in Figure 2.2.

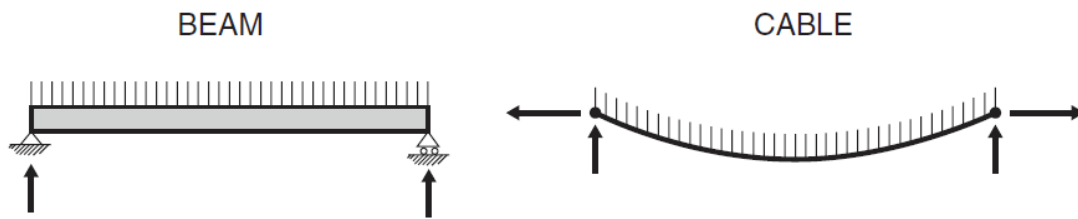


Figure 2.2: Reaction forces at supports for a cable and a beam simply-supported

In fact, if for simply-supported beam vertically loaded, the horizontal forces of supports are null, for a cable configuration, they play a very critical role. Therefore, the horizontal force is inversely proportional to the sag (k in the Figure 2.3). This principle holds true not only for a basic cable but also for suspension bridges. A greater sag can be associated with a reduction in the material required for the towers. However, as the tension in the cable increases, the towers must be sufficiently strong to resist the forces exerted by the cables.

It is clear at this point, that the shape of the cable in the design phase of a suspension bridge, or from another point of view the sag-to-span ratio, is the most important factor to assess to guarantee the correct performance of the whole bridge. According to [5], the optimal range of sag-to-span ratio that can ensure the right amount of stiffness with a modest towers height, is between $1/9$ and $1/11$.

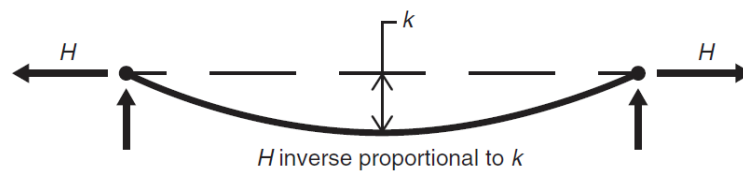


Figure 2.3: Sag and horizontal force relationship in a cable structure

It can be demonstrated that, in systems with small cable diameters and purely tensile forces, a cable-based structure is often the most efficient structural solution when compared to a massive girder. However, examining the complete structural system reveals that suspension bridges require more than just cables. Massive concrete anchor blocks are essential to secure the cables, while tall towers are necessary to transfer forces into the ground. Additionally, several other structural components play an important role in ensuring the stability and functionality of the system. Despite these complexities, suspension systems remain highly efficient for spanning long distances. For shorter spans, however, alternative structural systems should be carefully considered. Another drawback of cable systems is their response to non-uniform loading. While for beam-based structures a point load does not significantly affect the deflection shape of the beam, in a suspension system, a point load can dramatically alter the shape of the cable, as it is shown in the following picture.

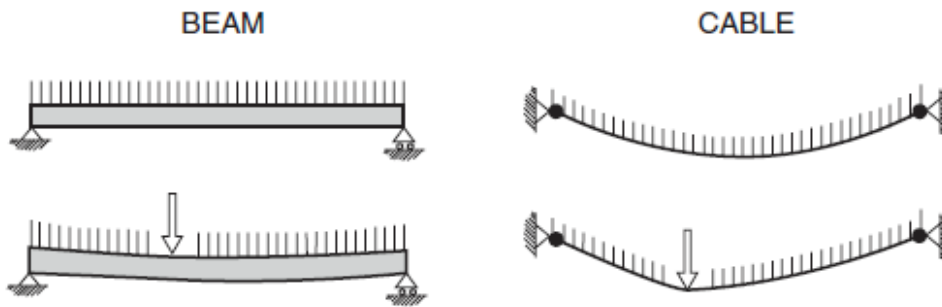


Figure 2.4: Comparison of deflection in a cable/beam- based systems subjected to point load

The reason of that, is because the cable has to reach the funicular shape under the applied loads to reach the global equilibrium of the system, and it can be demonstrated that a cable under its own self-weight (almost uniform), will deflect following the funicular shape. If an additional live load is applied, the more the live load will be non-uniform, the more the cable will change its geometry, instead of deflecting under its own elongation (elastic strain component) [6].

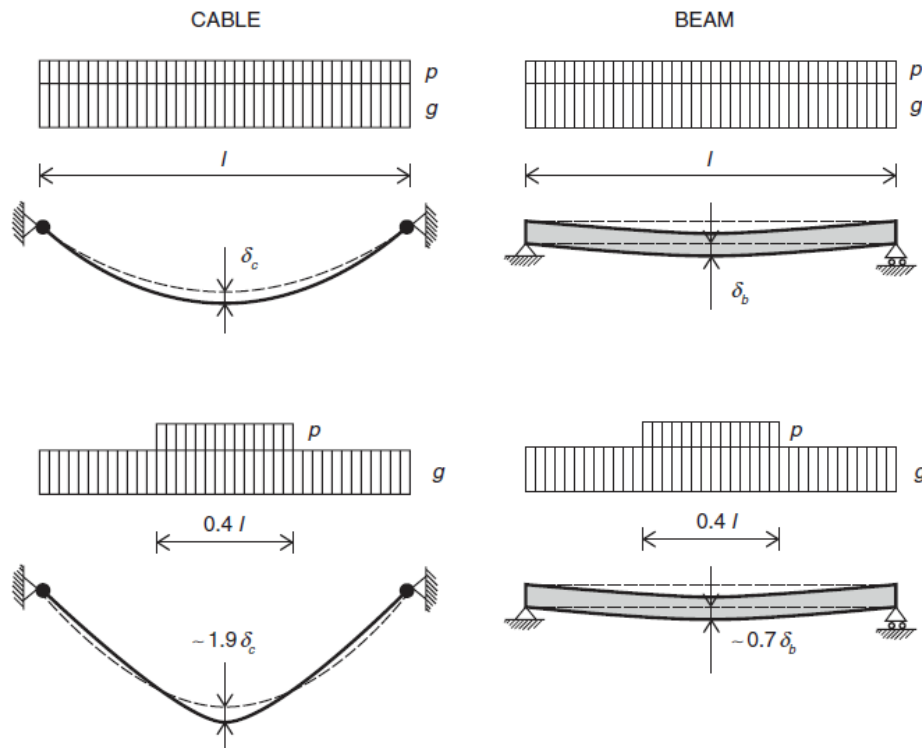


Figure 2.5: Comparison of deflection in a cable/beam- based systems under non-uniform load

After reviewing the most important factors that influence the design of a cable structure, several suspension bridge schemes used along the last decades will be presented.

Firstly, the single span case will be introduced, where suspenders are placed only in the main span. This configuration works efficiently if the length of sidespan main cables is not too large (because of sag effect), where top of the pylon are well restrained by the anchor cables block.

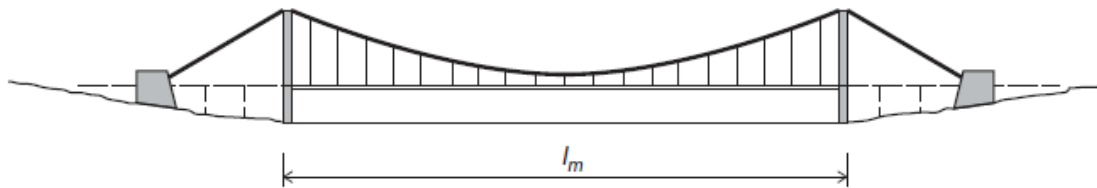


Figure 2.6: Single-span suspension bridge

However, the most common suspension bridge structural scheme is the three span type. In this configuration, the length of sidespans plays a significantly role in the performance of the bridge, as it is going to be explained in the following.

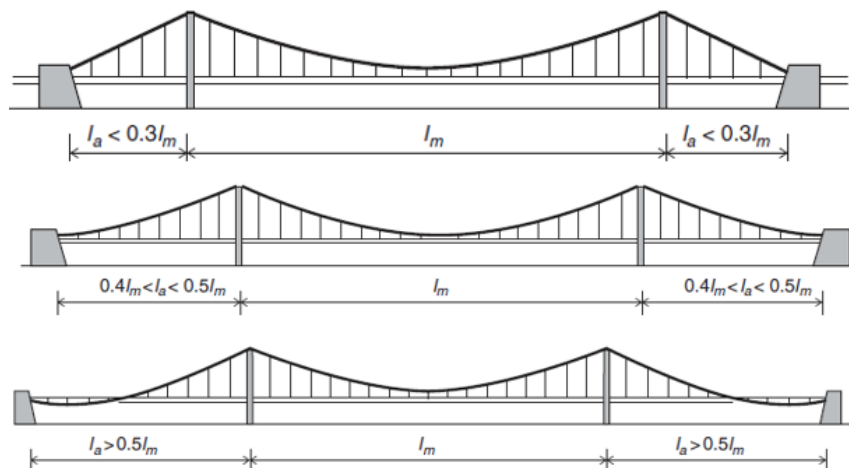


Figure 2.7: Three-span suspension bridges

For short sidespans (less than 30% of the main span), the deformational characteristics of the side cables are significantly reduced, resulting in better structural performance. However, when the sidespan length approaches 50% of the main span, the bridge achieves greater aesthetic appeal due to its symmetry around the towers. Despite this visual advantage, such a configuration markedly reduces the structural efficiency of the bridge, as it induces a large sag in the side-span cables. Further increasing the sidespan length beyond 50% leads to an even more

unfavorable condition, where the cables may dip below the deck level, resulting in poor deformational behavior and compromised structural performance.

Less common solutions are the one with inclined hangers and the self-anchored configuration. The former is used to create a truss system on the way that the shear force can be absorbed by tension and compression elements. By knowing that cables cannot carry compression force, the condition for which this system works, is based on the initial tensile force coming from the dead load, that must be greater than the compressive force coming from the live load.



Figure 2.8: *Suspension system with inclined hangers*

The last solution mentioned before, the self-anchored one, required a very large deck cross-section, not having anymore concrete anchor blocks in order to transfer the forces from main cables. Despite this solution seems very efficient, as no more concrete blocks are required, the dead load resulted from this increment of deck section, makes this solution less attractive.



Figure 2.9: *Self-anchored suspension bridge*

2.2 Historical Review

The suspension structural system using ropes, chains or cables has been used since ancient times [6]. The first suspension bridge in the modern era is attributed to the Jacob's Creek Bridge, built by James Finley (1762-1828) in Pennsylvania in 1801.

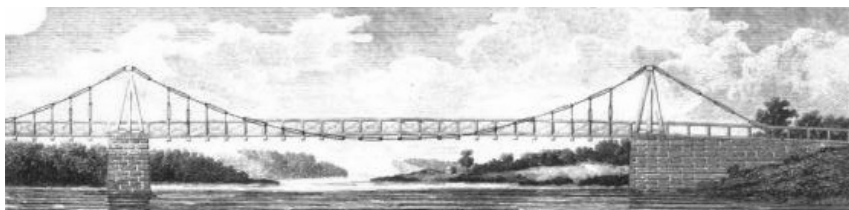


Figure 2.10: *Jacob's Creek Bridge, the first suspension bridge in Pennsylvania 1801*

At the beginning of 1800, several suspension bridge projects were started to be built, following the idea of James Finley. In detail, catenaries composed by eyebar with pinned connection links, were employed as main load-carrying element, creating very massive and stiff chains elements. By comparing this new structural solution with previous primitive suspension bridges, as the Winch Bridge Figure (2.11), it is possible to comprehend how James Finley solved issues of this ancient structural schemes.

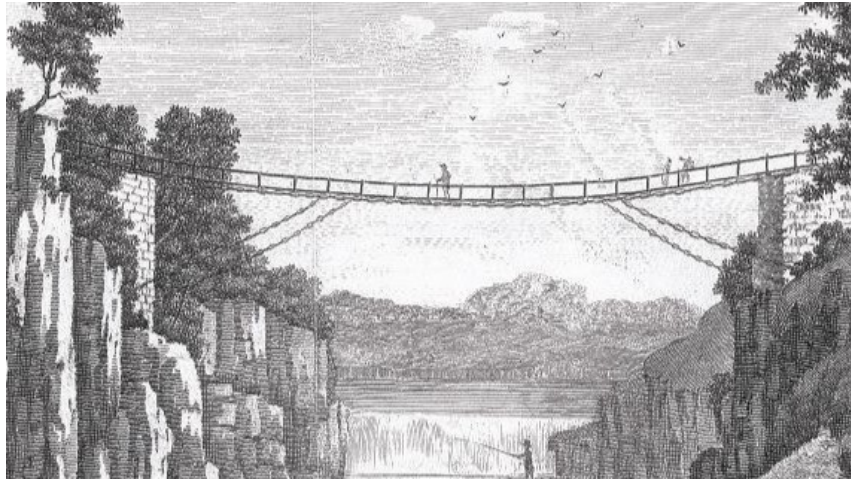


Figure 2.11: *Wynch Bridge in 1741 [Photograph]. (2017). Northeast History Tour.*
<https://northeasthistorytour.blogspot.com/2017/12/wynch-bridge-teesdale-ny904279.html>

In fact, despite the Winch Bridge could be considered a suspension bridge with a cable system, there are different issues that distinguish this bridge from modern types. First of all, analyzing the stabilizing iron chains, that are useful against later actions, like wind, they are also part of the deck itself, making it become a different structural scheme. Secondly, at that time, the main traffic typology was horse-drawn carriages, while in the modern era cars, and vehicles are the main ones. It is intuitive to think that the stiffness of the deck was not enough to sustain high loads, and the flexibility should have been reduced avoiding excessive deformations.

James Finley was able to overcome those issues with the Jacob's Creek Bridge, as already mentioned. In detail he stated that using many hangers, could have brought to a better distribution of loads, reducing extreme stresses on main cables. Moreover, he was the first one who identify the importance of stiffening the deck in suspension bridges. In the early 1800s, after the first was built, suspension bridges became well-known within Western civilization for some time, but they were viewed as dangerous and primitive structures. They were largely associated with less advanced societies and were primarily used as temporary or emergency bridges by the military. Despite this reputation, the suspension system became really famous and new bridges with this technology spread out across

2 SUSPENSION BRIDGES

frontier America because of its "lightness, robustness, ease of construction, and easy maintenance" [7]. Therefore, multiple suspension bridges were built in next years pushing more the span's length, coming up with the Essex-Merrimac Bridge with a single span of 72 m, built by Finley, in the state of Massachusetts across the Merrimac River in 1810.



Figure 2.12: *Chain Bridge over the Merrimac River, between Amesbury and Newburyport. Photograph from 1840. Digital Commonwealth.*

<https://ark.digitalcommonwealth.org/ark:/50959/tq57q707r>

In the same way, in Europe, during the late 18th and early 19th centuries, Brown (1779–1852) advanced Finley's concept of the modern suspension bridge, marking the beginning of a new era for bridge design in Britain. Around 1808, he developed a bar chain system consisting of round or flat bars with holes at each end, designed to address the limitations in strength found in traditional link chains made of iron rings (Figure 2.13).

The British engineer Thomas Telford, in 1826, worked and realized the Menai Bridge between the British mainland and the Isle of Anglesey, with a main span measured of 176 m.

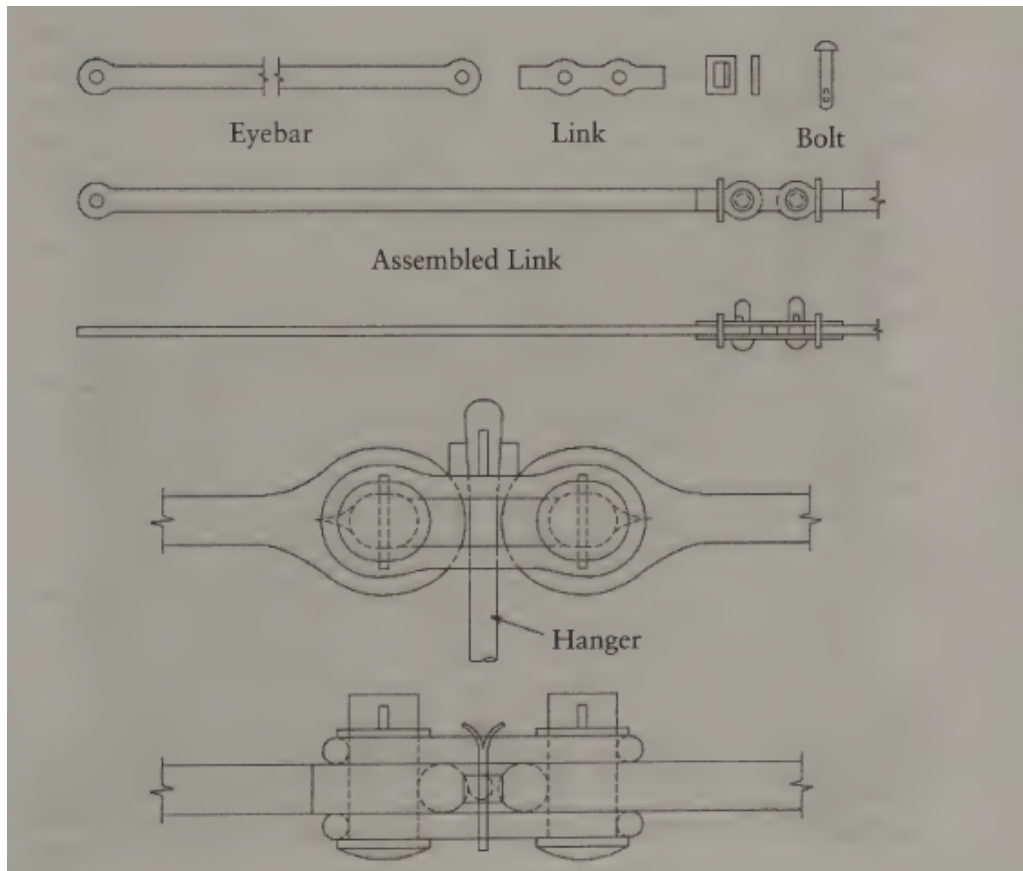


Figure 2.13: *Eyebar connection invented by Brown [8]*



Figure 2.14: *Menai Bridge in UK, in 1826*

2 SUSPENSION BRIDGES

Moving in 1834, for several decades, the longest main span suspension bridge composed by wires instead of a chain system, was attributed to the Grand Pont Suspendu in Fribourg (Switzerland). With a main span of 273 m, this bridge was composed of over 1000 wires, grouped in 20 strands (Figure 2.15).

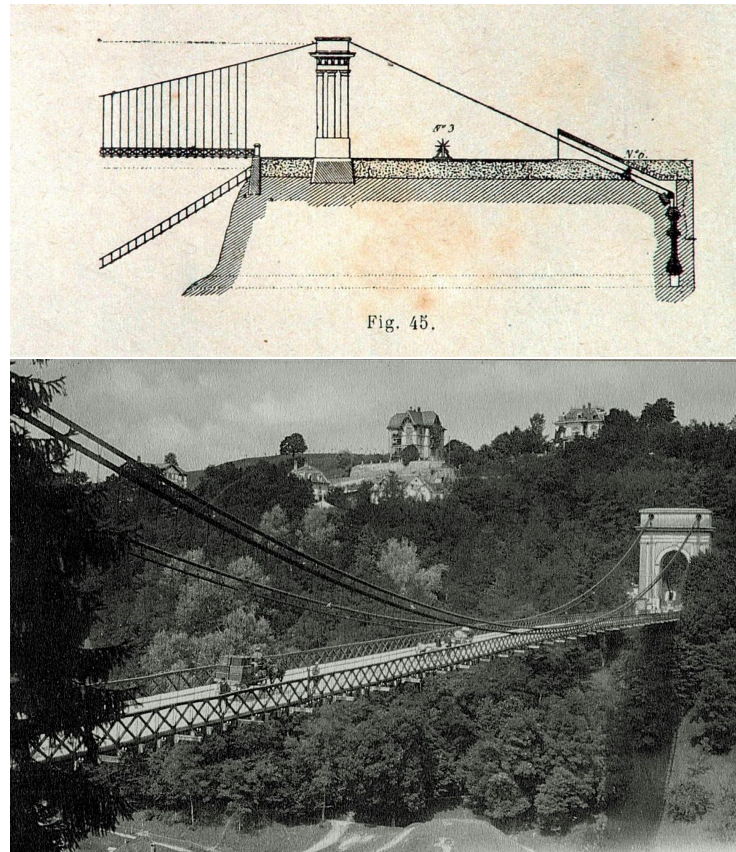


Figure 2.15: *Grand Pont Suspendu, Fribourg, 1834.*

<https://notrehistoire.ch/entries/pz89wrqEY0o>,

<https://structurae.net/en/structures/grand-pont-suspendu>

In the same century, despite the widespread adoption of suspension bridges worldwide, this structural system faced several accidents. Analyzing the failures of that era, many bridge collapses were attributed to wind-related problems, though not all failures were caused by this issue. For instance, one of the most notable failures of Brown's suspension bridges was the collapse of the Tees Railway Suspension Bridge in North Yorkshire, England. With a modest span of 86 meters, the bridge was originally designed for horse-drawn carriages. However, as the demand for railways increased, the bridge was adapted for railway use. This adaptation ultimately led to its failure, highlighting the fact that the importance of deck stiffness was not yet fully understood at the time.

A significant figure in the history of suspension bridges was Charles Ellet Jr. (1810–1862). Born in America, in early 20, he moved to Paris, France, to study civil engineering at the École Polytechnique. During his time in Europe, he visited several countries to study and analyze various structural suspension systems. After completing his studies in France, he came back to his country and imported wire-style suspension bridges to America, a design that was already widely adopted across Europe, especially in France. Charles Ellet Jr.'s first suspension bridge was the Schuylkill River Bridge, completed in 1841 with a span of 109 meters. The success of this project not only boosted the adoption of modern wire-style suspension bridges in America but also significantly increased Ellet's reputation.

Years later, he obtained several construction contracts, culminating in the Wheeling Bridge in West Virginia, which opened to traffic in 1849. This project was particularly remarkable for its main span of 308 meters, the longest in the world at the time, surpassing the previous record held by the Grand Pont Suspendu.

In 1854, just after 5 years from the realization, the Wheeling Bridge collapsed due to a storm, marking the ending point of his professional career. It is interesting to mention that the bridge collapsed due to low stiffness in the structural scheme, typical of all bridges realized before at that time and especially in France.

2.2.1 1° Generation Type

Some years later the collapse of the Wheeling Bridge, John Roebling (1806-1869), was the first one to understand the 1854 failure. The reconstruction of the bridge, shown in Figure 2.16, was entrusted to Roebling. He addressed the issue by increasing the deck's stiffness through the implementation of a stiffening truss system and the addition of stay cables from the towers.



Figure 2.16: *Wheeling suspension bridge rebuilt by John Roebling*
<https://sah-archipedia.org/buildings/WV-01-WH22>

2 SUSPENSION BRIDGES

John Roebling understood the meaning of "stiffening" in suspension bridges, a concept clearly demonstrated in Figure 2.17, which depicts the Niagara Railway Suspension Bridge designed by him, from 1851 to 1855. Roebling, in fact, separated the upper girder for railroad and the lower one, addressed for roadway. In between these two, wood members and steel rods are connected to each other, to create a rigid truss system enhancing the bridge's overall stiffness and stability.



Figure 2.17: *Niagara Railways Suspension Bridge, in 1855*

<https://www.structuremag.org/article/john-a-roeblings-niagara-river-railroad-suspension-bridge-1855/>

In the following years, Roebling gained a lot of success, and the suspension bridge system became one of the most suitable and reliable for long span bridges. In 1883, the Brooklyn Bridge (Figure 2.18), one of the most iconic in modern suspension bridges era, was opened to the traffic, but Roebling died in 1869, just after the beginning of the construction. The bridge finalized by his son's wife Emily, has a main span of 486 m, with 2 side span of 286 m.

The Brooklyn Bridge represented a turning point in the evolution of suspension bridge design. From that moment on, future generations of engineers were encouraged to place greater emphasis on mathematical modeling in structural design. Prior to this, the Linear Elastic Theory, developed by Rankine in 1858, had been employed to calculate and analyze the behavior of suspension bridges. The construction of the Brooklyn Bridge signaled the beginning of a more advanced and precise approach, the so-called "Deflection Theory". While a more



Figure 2.18: *Brooklyn bridge across the East River between Manhattan and Long Island, 1883*
<https://asliceofbrooklyn.com/6-odd-and-interesting-facts-about-the-brooklyn-bridge-part-1/>

detailed explanation of both theories will follow in subsequent chapters, it is important to highlight that the Deflection Theory enabled a significant reduction in the stiffness of the deck without compromising the bridge's safety. As a result, the construction of suspension bridges with progressively longer spans became possible, continuously pushing the boundaries of bridge length.

The first bridge realized with this theory was the Manhattan Bridge, in 1909, with a main span of 451 m.



Figure 2.19: *Manhattan Bridge, in 1909*
<https://asliceofbrooklyn.com/7-things-you-didnt-know-about-the-manhattan-bridge/>

2 SUSPENSION BRIDGES

The "Deflection Theory", following its success with the Manhattan Bridge, became the standard method for designing suspension bridges. From that point onward, numerous suspension systems were constructed using this innovative approach. The stiffening trusses evolved to become increasingly slender, enabling the construction of bridges with greater spans, culminating in the completion of the Golden Gate Bridge in 1937. This iconic structure features a main span of 1,280 meters, notable for its remarkably low stiffening truss depth-to-span ratio of just 1:168, an unprecedented achievement for its time.



Figure 2.20: *Golden Gate across the San Francisco Bay, completed in 1937. Source: Wikipedia*

Another peculiar aspect of this bridge, was that at the first design, so how it was realized at the beginning, the structural stiffening comprehended just 3 plane trusses, two vertical below the main cables and on transversal below the deck plane. This arrangement of trusses resulted a system with a very low torsional stiffness, an issue of suspension bridges that at that time was not completely understood. Therefore, the aerodynamic stability of suspension bridges, had started to be studied after the Tacoma Narrow bridge. This bridge realized in 1940, surpassed the Golden Gate Bridge in terms of truss depth-to-span ratio, being 1:340. The main span with 853 m, was extremely low comparing the width-to-span ratio of 1:72, going beyond ever previous practice (the Golden Gate was 1:47).

This bridge exhibited nearly zero torsional stiffness, beginning to oscillate almost immediately after its opening. Within a few months of service, it collapsed under a relatively modest wind. This event marked the beginning of in-depth

studies into the aerodynamic behavior of suspension bridges, leading to significant improvements in torsional stiffness in subsequent designs. In response to these findings, the engineers of the Golden Gate Bridge reinforced its structural system with additional bracings to improve its torsional rigidity.



Figure 2.21: *Tacoma Narrow Bridge, in 1940* Source: wikipedia

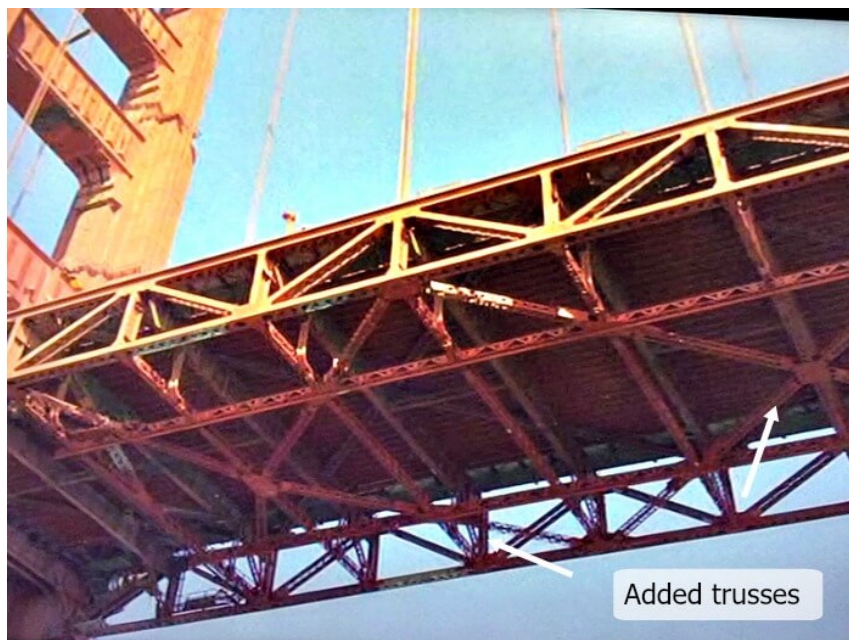


Figure 2.22: *Additional trusses in the Golden Gate Bridge, after the Tacoma collapse*

2.2.2 2° Generation Type

Following the Tacoma Narrow Bridge collapse, as already said, aerodynamic studies of suspension bridges gained a significant consideration increasing the stiffening truss torsional stiffness up to the 1966, where Sir Gilbert Roberts substituted the standard truss system with a streamlined deck shape.

The Severn Bridge concept, designed by Robert, in fact in terms of truss depth-to-span ratio was very close to the Tacoma case study, being 1:324 (main span of 988 m). This new type of cross-section, represented a sort of turning point in the design of suspension bridges, the so-called 2° generation bridges.



Figure 2.23: *Severn Bridge, in 1966*

<https://www.southwalesargus.co.uk/news/18923409.crossing-river-severn-bridges-built/>

Differently from what was realized in the Tacoma bridge, in fact, in the Severn Bridge the sharp edges of the plate girders in the first generation-type, was substituted by streamlined shape. This innovation significantly reduced the wind resistance and mitigated aerodynamic instability. Furthermore, the new section type featured a high torsional stiffness, addressing the near-zero torsional rigidity that contributed to the Tacoma Narrows collapse.

During the 1970s, the application of the streamlined box section became widespread and in 1970, the Lillebælt Suspension Bridge in Denmark, designed by C. Ostensfeld, was built.



Figure 2.24: *Lillebælt Suspension Bridge in Denmark, 1970*

From this point, several bridges have been built all around the world, following the Severn Bridge concept, pushing the main span every time. In the following some of the most iconic bridges of the second generation are listed.

Table 2.1: *Most Iconic Suspension Bridges 2° generation-type*

Bridge Name	Country	Year	Main Span (m)
First Bosphorus Bridge	Turkey	1973	1,074
Humber Bridge	United Kingdom	1981	1,410
Ōshima Bridge	Japan	1987	1,540
Second Bosphorus Bridge	Turkey	1988	1,090
Great Belt Bridge	Denmark	1998	1,624
Jiangyin Yangtze River Bridge	China	1997	1,385

2.2.3 3° Generation Type

The third and last generation of suspension bridges, nowadays employed for very long spans), following the so-called Messina type, have a type of deck similar in shape to the second generation ones, with an aerodynamic scaffolding, but with addition of holes inside. These holes have been idealized to let the wind passing through them, increasing the aerodynamic stability also for very long span.

Nowadays, the longest suspension bridge in the world, with a main span of 2023 m, inaugurated and open to the traffic in 2022, is the Canakkale Bridge, in Turkey.

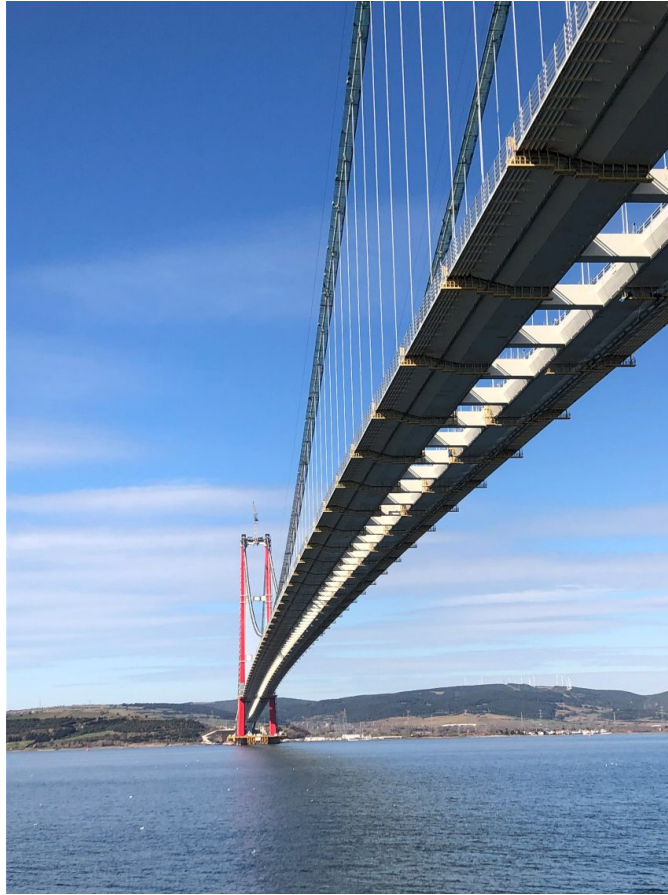


Figure 2.25: *Canakkale Bridge, in Turkey*

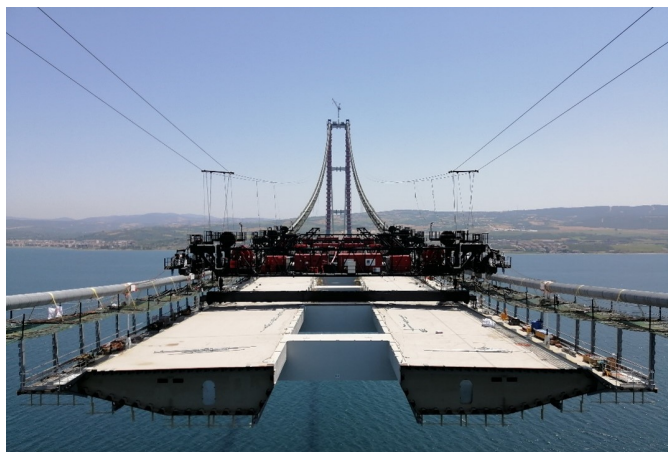


Figure 2.26: *3° generation cross-section type*

In Italy instead, the Messina Bridge, focus of this study, is classified as a third-generation bridge and is currently in the design phase, close to the construction stage. Its key characteristics will be discussed in Chapter 3.

3 Messina Suspension Bridge

3.1 Location

The location of the Messina suspension bridge will be located across the Messina Strait in Italy, between the Sicily and Calabria regions (also rest of the Italian Peninsula) . In detail, the structure will connect Torre Faro (Sicily side) with Villa San Giovanni (Calabria one) as it is represented in following picture:



Figure 3.1: Location of the Messina suspension bridge project. (2023).
<https://www.independent.co.uk/news/world/europe/sicily-bridge-plan-revived-by-italian-government-despite-concerns-over-earthquakes-and-the-mafia-a6674181.html>

The Strait of Messina is a portion of the sea that connects the Ionian Sea in the south with the Tyrrhenian Sea in the north. The distance between the two lands is variable along the two coasts, having points in which the distance is 16 km, to a minimum of around 3 km. This area is notable for its significant underwater depth, reaching up to 200 meters in some places. Additionally, this region of Italy is classified as a high-seismicity zone.

The bridge project has been characterizing over the years by multiple challenges including engineering, environmental, and logistical issues. In the next chapter, it will be explained briefly the history of the project and all the main stages of it.

3.2 Evolution of the Project

The history of this bridge dates back to ancient Roman times, when rudimentary methods were attempted to cross the Strait of Messina [9]. The initial proposal to connect the Italian Peninsula with the Sicily island in the modern era, goes back to the Italian Unification, driven by the desire to create a continuous kingdom. One very prominent character of the history of this bridge has been Alfredo Cottrau, expert in construction of bridges and structures at that time. In 1866, in fact, was in charge to study the project and find a solution that was able to connect the strait. At the end of his studies, Cottrau concluded that building a bridge between the two lands was impossible. This assertion was based on the depth of the Strait's waters and the intense currents, which would make constructing the bridge piers nearly unfeasible, except in case of very significant financial resources.

In the years that followed, up until the end of the Second World War, no one was able to overcome the challenges that Cottrau had identified in previous years.

In the same years, Carlo Navone in 1870, presented another solution for overcoming the strait. The proposed idea was to built a tunnel underwater with a depth of 33 m under the seabed (Figure 3.2).

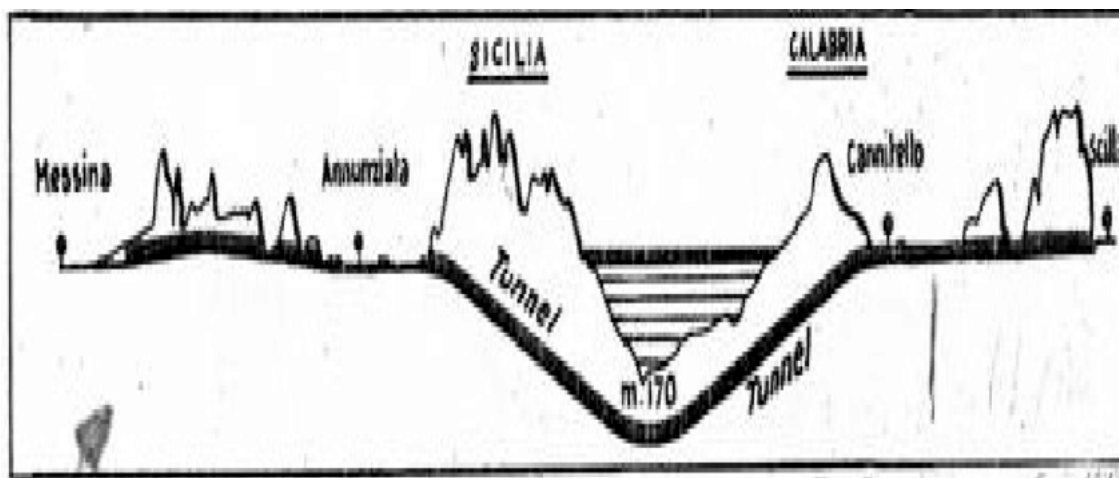


Figure 3.2: The tunnel solution proposed by Carlo Alberto Navone in 1870

https://www.researchgate.net/figure/Progetto-di-tunnel-sottomarino-di-Carlo-Albero-Navone-1870_fig5_327118372

One of the worst critic that this project obtained, was the fact that the time to cross the strait, was almost similar to the one of the actual period, as ships.

Some years later, early 1880, two big projects were presented to the Italian Government, one bridge and one tunnel. The first one, proposed by Giambastiani Biadego e Pennacchio was the idea of a suspension bridge with five multiple spans, while the second project was a tunnel propose by the engineer Federico Gabelli. However, after several economical evaluations, The idea for a connection between the strait was gradually abandoned.

It is after the First World War, that the engineer Vismara, restarted again the idea of the connection. His idea, proposed in 1921, was an underwater gallery [10].

In 1934, engineer Antonino Calabretta presented another bridge project, which featured three spans with a parabolic side structure. However, with the onset of the African War, the idea of building the bridge became completely irrelevant. After the Second World War, Italy's economic growth had a direct impact on the transportation system, leading to improvements in various transport lines. However, it became evident that the system was inefficient when it came to crossing the Strait of Messina. The idea of a permanent connection was partially abandoned until the late 1960s, when the focus shifted to improving the ferry system instead.

In 1953, the "Messina Bridge" group, which had been formed within the Italian Steel Constructors Association (ACAI) and included the most prominent Italian metallurgical and industrial companies, presented a preliminary project. This project had been commissioned from engineer David Steinman, with the group committing to further develop the design at its own expense, an investment estimated at around 600 million lire (italian currency). Another very important project was proposed by the engineer Nino Del Bosco who introduced an ambitious plan for an artificial land bridge between the Sicilian and Calabrian coasts (3,336 meters). Given that the seabed depth in the area does not exceed 120 meters, the land embankment would have been constructed from the sea floor, rising 10 meters above water level. At its deepest point (120 meters), the embankment would have reached a width of 350 meters. On top of it, there would have been infrastructure for cables, pipes, and other utilities. The railway, would reach the highest point of the structure, 55 meters above sea level, where a reinforced concrete arch bridge would be placed. Below, a 75-meter-wide navigable channel would allow large ships to pass through.

The proposal also included a second bridge and an additional wide channel to allow for the passage of medium and small ships. However, this project faced significant criticism and was quickly forgotten.

Several project's ideas were presented along post bellic period, and remarkable importance was attributed to the Steinman's project, already mentioned above. This project, in collaboration with another italian-american engineer Mario Palmieri, included a three span bridge with a stiffening girder (central span around 1500 m [11]), with towers located in the sea (foundations in the seabed).



Figure 3.3: Representation of the Messina bridge proposed by Steinman
https://www.researchgate.net/figure/Rappresentazione-del-ponte-progettato-da-DB-Steinman_fig3_369538113

Multiple thoughts and doubts have moved this project, being that the longest bridge built at that time was the Golden Gate in San Francisco, with a span length of 1260 m. Steinman conducted extensive researches and studies for guarantee to the structure enough stiffness against seismic and wind actions under the aerodynamic point of view.

The ACAI was particularly favorable to the construction of the bridge, after being illustrated all the benefits and advantages that this bridge would have brought to the country in term of economy growth, but also in transportation system. However, various entities required further investigation about the feasibility of the bridge regarding geological assessments. The professor of the Polytechnic of Milan Luigi Solaini, in fact declared the ambiguity of the foundation layout inside the sea, and that was unknown the realization of the bridge [12].

Furthermore, several issues arose in parallel with the project. Many engineers expressed concerns about the technical aspects of the bridge, while others raised objections regarding its environmental and social impacts, and still others questioned its economic feasibility.

Despite all the uncertainties and contrasted social opinions, with the law '27 Gennaio 1955 n. 2', the Sicilian Region allocated 100 million lire (italian currency), for initiating the geological studies [13]. In parallel, in 1955, the society 'Ponte di

Messina' was established by Ilva, Ansaldo, Italcementi, Falk, and others, companies that were among the pillars of the Italian economy at the time, to promote engineering and environmental studies aimed for creating a permanent road and rail connection between Sicily and the Italian mainland.

Despite the excitement surrounding the project, the following years saw numerous debates and opinions from both the general public and technical experts, including engineers. These discussions led to the emergence of new concerns and doubts, leaving the project in limbo.

An apparently turning point, was in 1969, where ANAS (Azienda Nazionale Autonoma delle Strade Statali) in collaboration with FS (Ferrovie dello Stato), created a contest for which it should have been found the right project for the Messina bridge. There were 143 projects in total, of which 125 were mostly Italian, 8 American, 3 from England, 3 from France, and 1 each from Germany, Sweden, Argentina, and Somalia. It took almost two years to rank all the projects, where among the top positions, only a tunnel was presented, while others were all bridges or structures above the sea level. In the following the first 6 winner of the contest ([14]) will be presented:

1. Tunnel anchored to bedsea throughout steel cables

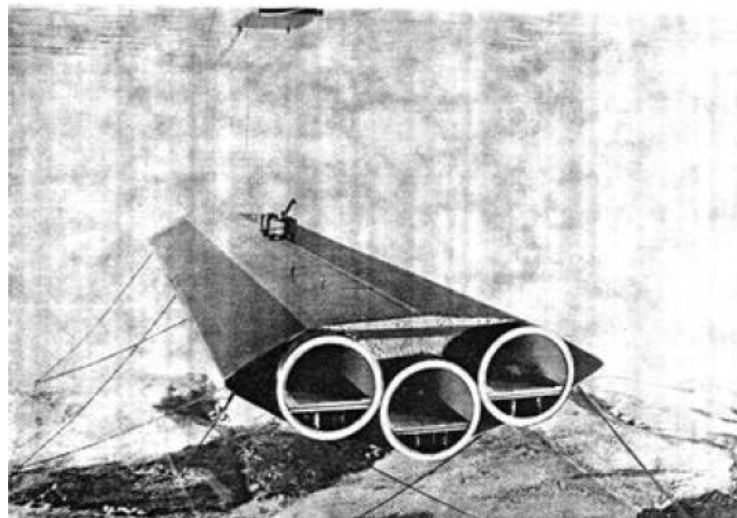


Figure 3.4: *Grant Alan and Partners, Covell and Partners, Inbucon international project*

3 MESSINA SUSPENSION BRIDGE

2. Cable-stayed bridge, three spans (540m + 1300m + 540m)

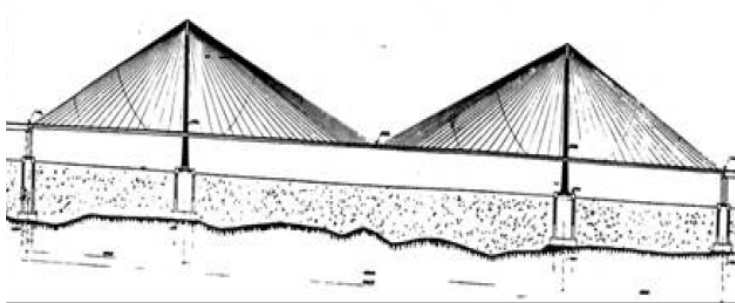


Figure 3.5: *Gruppo Lambertini project*

3. Suspension bridge with just a span of 3000 m

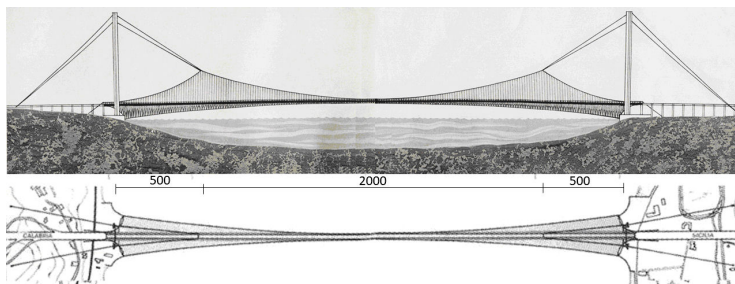


Figure 3.6: *Gruppo Musmeci project*

4. Suspension bridge with three spans (central one 1600m)



Figure 3.7: *Gruppo Ponte Messina SpA project*

5. Suspension bridge with four spans

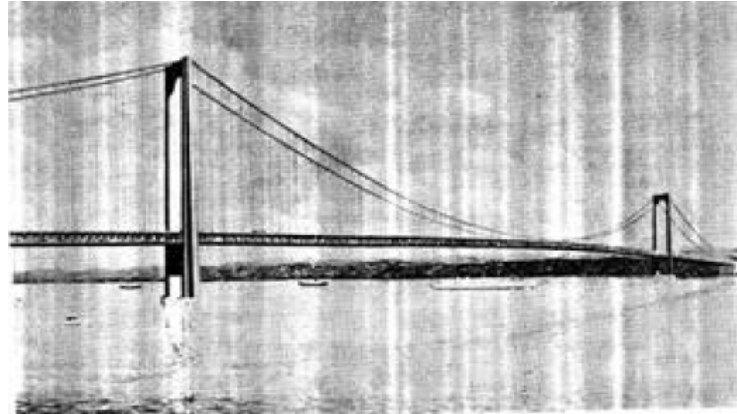


Figure 3.8: Arch. Eugenio Montuori with the collaboration of Calini e Lionel Pavlo

6. Suspension bridge with five spans

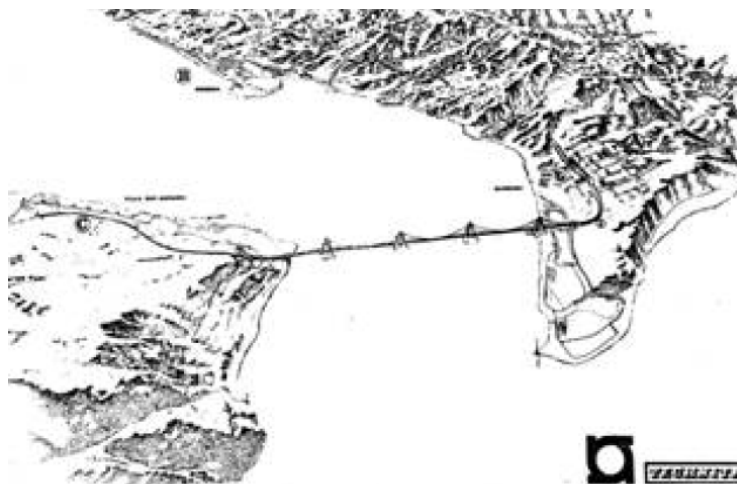


Figure 3.9: Technital SpA project

Despite the successful outcome of the competition, there was still controversy, mainly due to the delays in decision-making regarding the Messina Bridge. In 1971, the Italian government passed 'La Legge n. 1158' which authorized the creation of a private company, responsible for the design, construction, and management of the bridge. The company was to have shares held by IRI, Fiat, ANAS, Region of Sicily, and Region of Calabria.

In the summer of 1977, the feasibility studies conducted by the "Messina Bridge Group," which included several Italian industries, were completed. After about ten years of studying the preparatory phase of the project, the group proposed a solution that had all the necessary safety and reliability features. According

to these studies, the construction of a suspension bridge with a single span of 3,400 meters, with supporting cables anchored to the extremities of the bridge, was considered feasible and economically viable. The bridge would have been in steel with a deck's height of 70 meters above sea level, with towers reaching 380 meters. The proposed width of 66 meters, it was designed to accommodate a double railway track in the center, and two three-lane roadways on both side, along with sidewalks and emergency lanes. The stability and wind resistance of the bridge were also tested through experiments carried out by the Fiat-Impresit group, using a full-scale model in the wind tunnel at Fiat's Orbassano center near Turin.

The initial enthusiasm for the project was quickly stopped by engineer Riccardo Morandi, a leading expert in bridges and earthquakes. He sustained that serious seismic studies should have been carried out before the construction (seismic studies have never been developed).

Due also to the steady pressure from the European Union, that wanted the infrastructure in the Messina Bridge for opening also the market towards African States, in 1981 raised the society Stretto di Messina S.p.A which succeeded the Messina Bridge Group and was established with a majority share of 51% held by IRI-Italstat. The remaining shares were equally divided among the State Railways Authority, ANAS, the Region of Sicily, and the Region of Calabria, each holding 12.25%. The company's capital was entirely public.

On June 16, 1986, Stretto di Messina SpA presented a new feasibility study, which included designs phase, costs of the structure, and reliability of three solutions, underground, through the sea, and aerial. Among these, the suspension bridge was deemed the most technically feasible and economically viable option compared to the alternatives.

In 1992, under Calarco guide, head of the Stretto di Messina SpA group, it was presented the design project 'Progetto di massima definitivo', in which different aspect of the bridge were evaluated, as the timeline of the constructions, costs, environmental technical studies.

After seven years of design phase, in the 'Progetto di massima definitivo', several aspect of the bridge were changed and revised. In details: the bridge was suspended with a unique span (multi-box girder with aerodynamic shape), letting the towers on the two lands, avoiding the marine currents problem. Two towers of 376 m height each one has been designed to sustain the huge suspend main cables.

At the beginning of 2000, despite the project was labeled as a "strategic infrastructure" and promoted by the European Union, there were many questions raised by the people who opposed to the construction of the bridge. Several doubts raised regarding benefits of the local populations, the toll that would cost the road and who would collect it and other economical and political aspects.

In October 2005, during the third Berlusconi government, the association of companies Eurolink, led by Impregilo S.p.A., won the bidding to become the general contractor for the construction of the bridge offering 3.88 billion euros.

Since 2005, the general contractor Eurolink, transfer the responsibility for the final and detailed design of the project was assigned (by contract) to the following companies, qualified in the field of suspension bridges and part of the Eurolink consortium:

- **COWI A/S** (Denmark), structural design.
- **Dissing+Weitling** (Denmark), design and drafting.
- **Buckland & Taylor Ltd.** (Canada), structural design.
- **Sund & Bælt A/S** (Denmark).

On September 2009, the agreement between the Società Stretto di Messina and Eurolink was stipulated with the aim to restart the construction activities of the bridge.

The final design ('Progetto Definitivo') was approved by the CDA (Consiglio di amministrazione) on 29th July 2011. On 1st March 2013, all contractual agreements signed by the Stretto di Messina Company were terminated, and the company was put into liquidation, effectively shelving the project once again.

On 31st March 2023, the Italian government under the guide of Giorgia Meloni, signed the 'decreto Legge 35/2023' that reactivated the Stretto di Messina S.p.A. company with the intent of resuming the process for the construction of the bridge. As stated by Minister Matteo Salvini, the objective is to open the bridge to traffic by 2032.

The updated 2011 final design ('Progetto Definitivo'), was approved again by the new CDA of the concessionary company on 15th February 2024.

The whole study and project have been developed considering the updated version of the bridge design documentation available in [15].

3.3 Final Design Project (Progetto Definitivo)

The final solution expressed in the "Progetto definitivo", with some updates and changes of the 2011 version, as explained in the previous chapter, will be explained in detail in this paragraph, where all documents and details are listed from the official site of the Stretto di Messina website before mentioned.

3.3.1 Main Characteristics of the Bridge

The Messina Strait Bridge is a suspension bridge with three spans, two sidespan very short compared to the extremely long central span (183+3300+183 m) with a total length of 3666 m, as it depicted in the following picture:

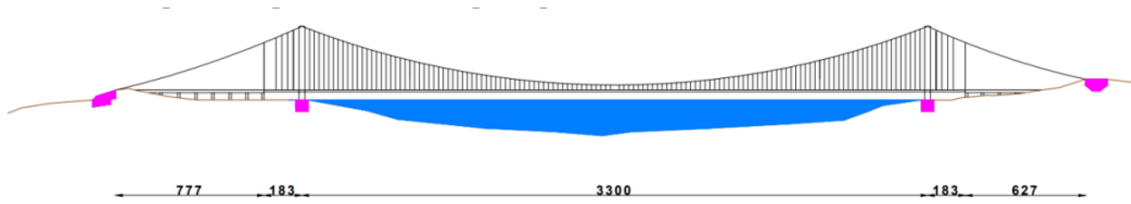


Figure 3.10: *Lateral view of the Messina Bridge*

The two concrete anchor blocks will be placed with a distance of 777 m from the last hanger of the bridge on the left, and 627 m from the right side. It is worth mentioning again that the actual longest suspension bridge is the Çanakkale Bridge with a central span of over 2023 m. In the following chapters, main characteristics of the Messina Bridge will be reported.

3.3.2 Deck

The deck of the Messina bridge is a wing multi-box section (known also as Third generation deck, as explained in the Chapter 2.2), completely in steel. The idea behind this choice, is to have a very light deck, but aerodynamically stable, able to sustain wind gust velocity up to 275 km/h [15]. The main characteristics of the deck are: total width of the deck 60 m, with distance between the two main cables of around 52 m; the bridge is design for 3 road lanes for cars with a central railway. The deck cross-section is presented like in Figure 3.11:

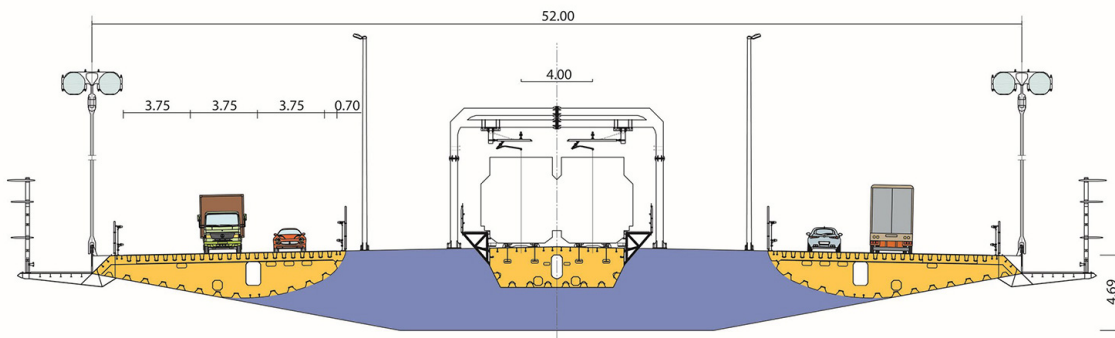


Figure 3.11: *Multi-box deck-section of the Messina Bridge*

In detail, singles box girders width are 14 m for the road type and 7.5 m for the railway's one each one connected in between with cross girders, as depicted in the following pictures:

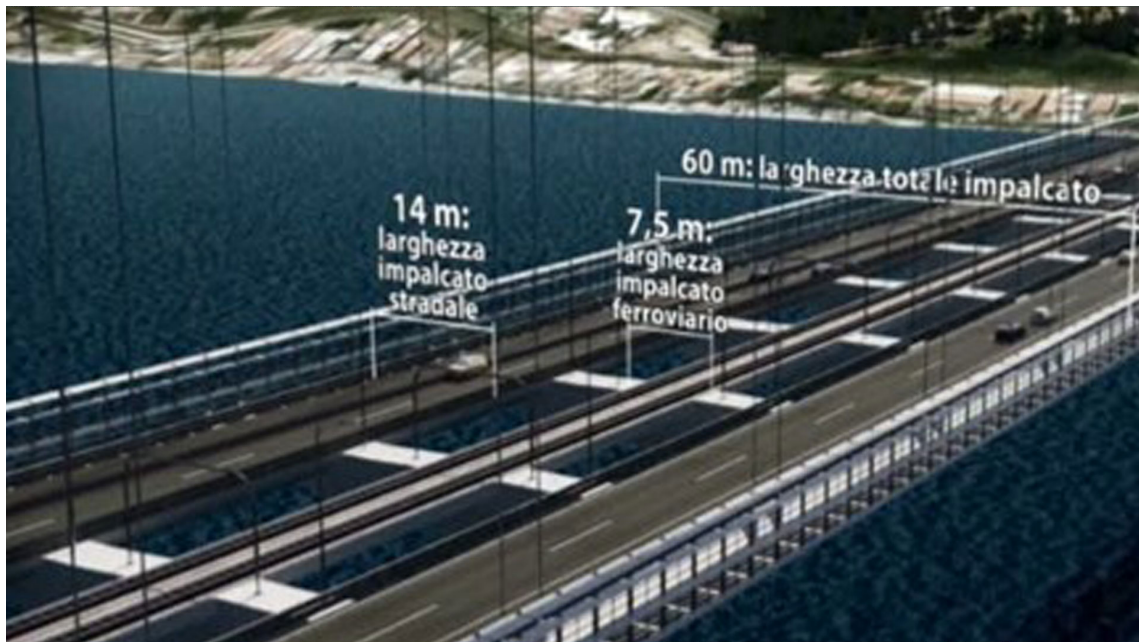


Figure 3.12: Lengths of single boxes of the deck

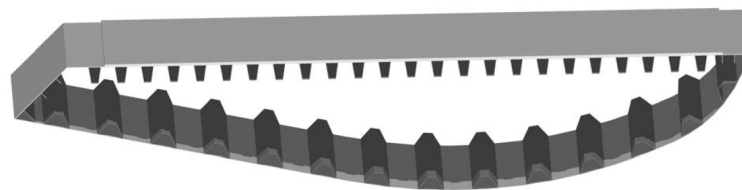


Figure 3.13: Single box girder for road

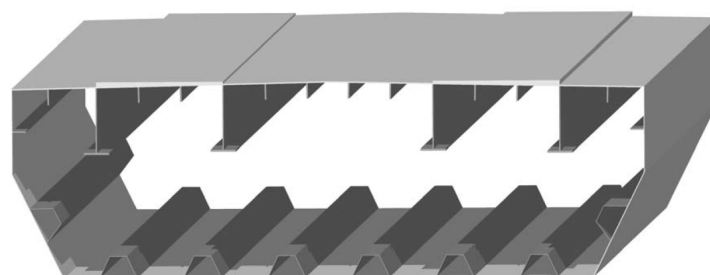


Figure 3.14: Single box girder for rail

3.3.3 Suspension System

The main suspension system which has the job to sustain the whole deck (main cables), is composed by a couple of cables for each side. The material used

3 MESSINA SUSPENSION BRIDGE

for the main suspension system is a high-strength steel with the technique of Prefabricated Parallel Wire Strand (PPWS). As already mentioned the distance between the two couple of cables is around 52 m. Entering in more detail in the single couple of cables, center-to-center distance between the two cables is around 2 m, with a diameter (of the single cable) of around 1.26 m after the whole process of compaction, as illustrated in next Figure 3.15.

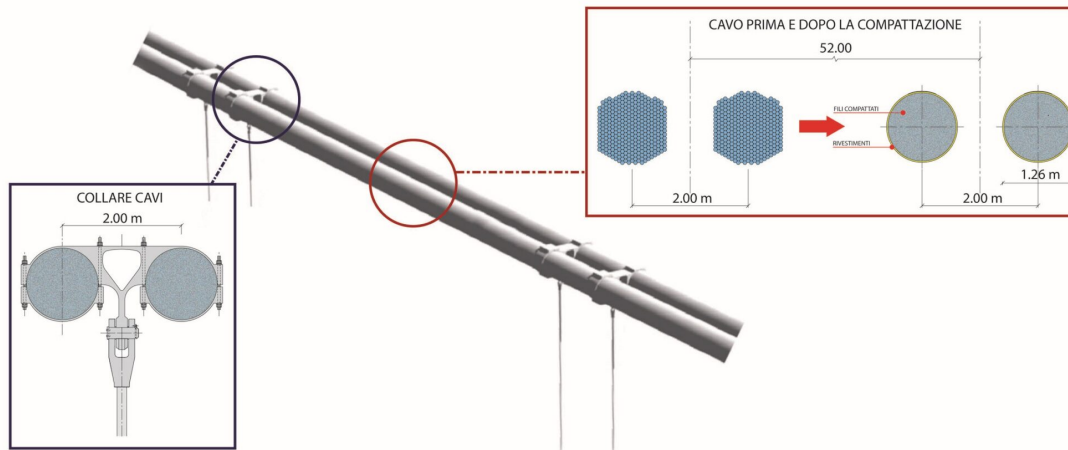


Figure 3.15: Main suspension system of the bridge

Every cable, is composed by 349 strands, each one made of 127 wires; in total the number of wires for each cable is 44'323. The total length of the main suspension system is of around 5300 m, concrete block-to-block distance. An estimation of the dead load of the 4 cables combined together is approximately 170'000 ton.

For the suspenders (hangers) instead, they are placed every 30 m along the bridge, always made of high strength steel. Also hangers as well, are placed in couples as it is shown in Figure 3.17, on the right. From the design document calculations, it has been revealed that different diameters have been used for hangers with a specific pattern, as it is going to be illustrated in the next figure.

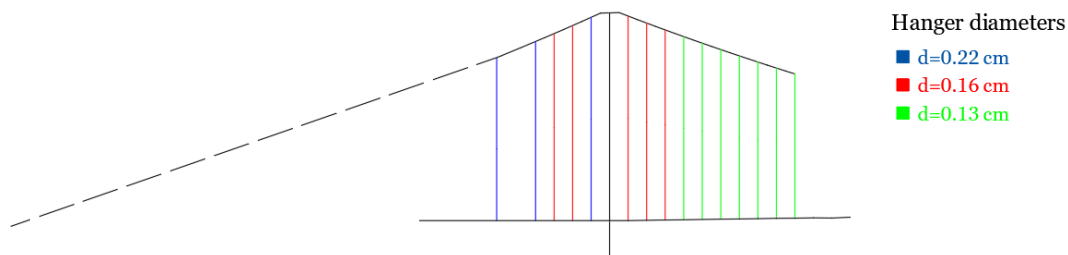


Figure 3.16: Hangers pattern according to design documents

3.3.4 Towers

The towers of the bridge are built with 2 inclined legs connected by three cross-beams. Center-to-center distance of the top towers is 52 m, while the base is around 78 m; the height of the towers reaches 399 m composed by 22 precast segments, as shown in Figure 3.17.

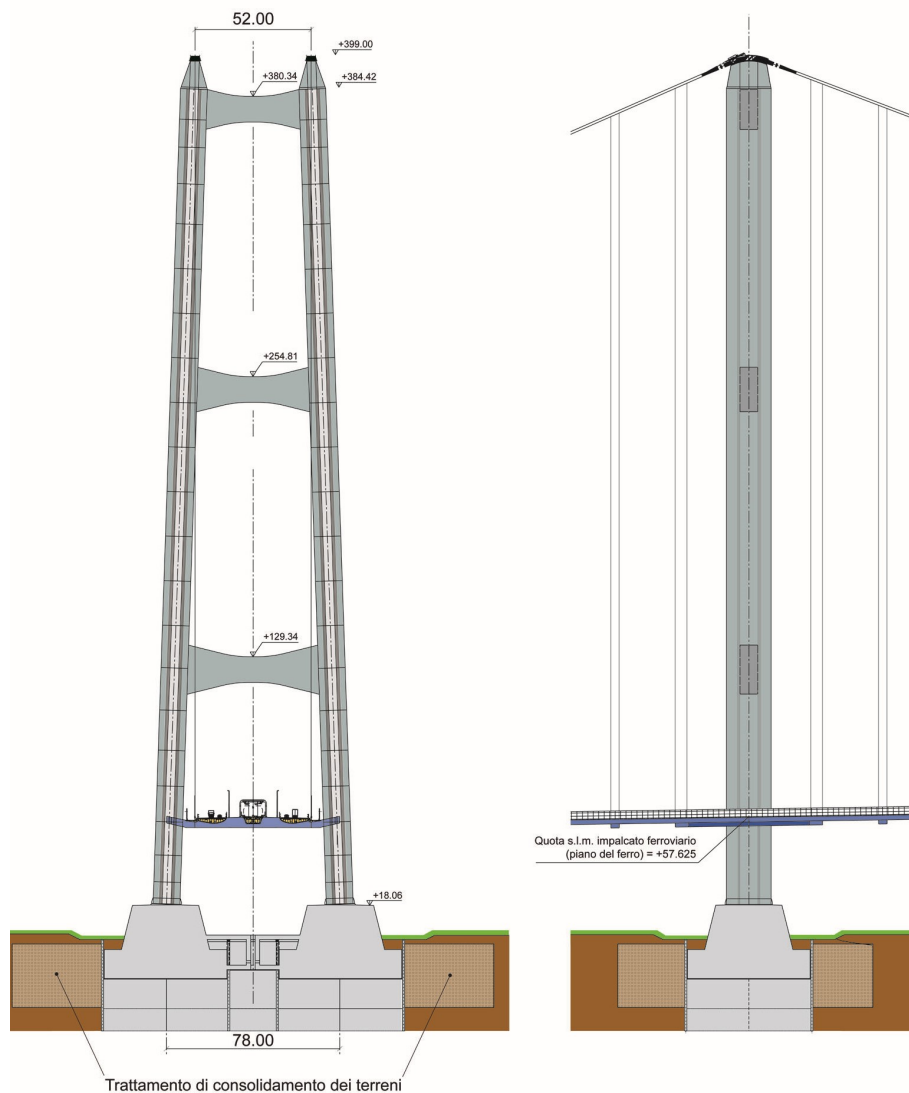


Figure 3.17: Towers design of the Messina Bridge

The cross-section of legs is an octagonal shape 20x12 m, with a maximum height of 20 m (the single segment). The FEM model realized in the official documents, before mentioned, show the following cross-section:

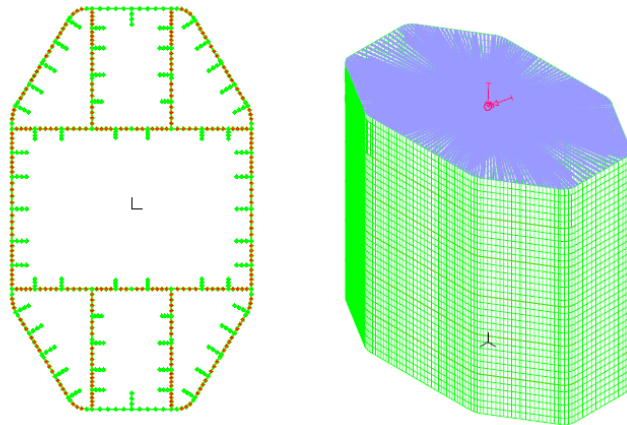


Figure 3.18: *Towers legs cross-section*

The foundation system is composed by 2 shallow foundations, with a circular cross-section connected by a massive cross-beam (the footings diameter of Sicilia side is different from Calabria one, 55 and 48 m).

3.3.5 Anchorage Blocks

Massive concrete anchorage blocks are constructed, with most of their volume backfilled to minimize visual impact. The total volume of concrete used is approximately 533,000 m³. The Figure 3.19 illustrates the main characteristics of the anchoring system.

It is worth noting that the heights of the two anchorage blocks differ, reflecting the varying landscape conditions at the sites. On the Sicily side, the anchoring block is positioned at 53.50 m above sea level, whereas on the Calabria side, it is located at 118 m.

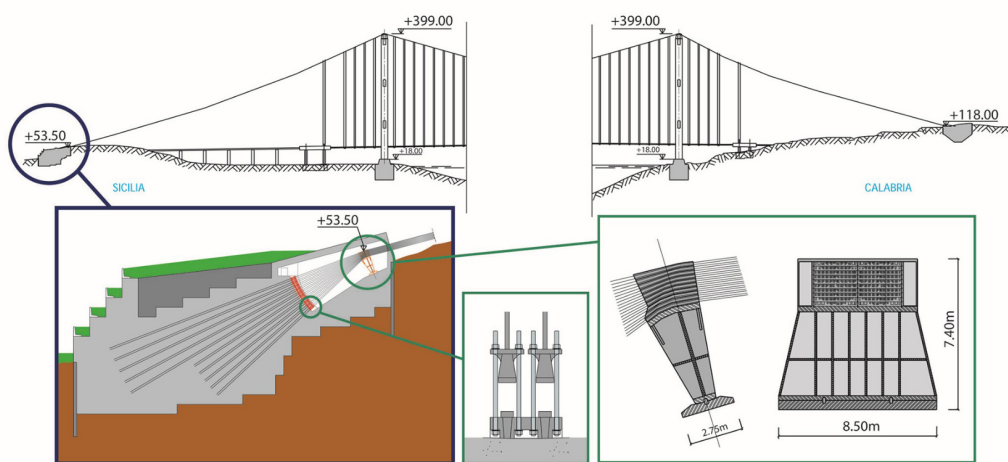


Figure 3.19: *Anchoring system for main cables*

4 Scaling Procedures and Design Model

4.1 Similarity Conditions

Structural scaled models have always played a very important role in structural engineering for research or design processes. In detail, they are usefully employed for large-scale projects where there might be new and innovative structural solutions never tested. As it is defined by [16]:

"A structural model is any structural element or assembly of structural elements built to a reduced scale (in comparison with full size structures) which is to be tested, and for which laws of similitude must be employed to interpret test results."

There are several types of structural models, and in this chapter only the characteristics of the one employed in this study will be explained in detail.

First of all, it is necessary to define that the model used in this experiment is an elastic model. Therefore, this model cannot predict the inelastic behavior of the structure, such as the post-yielding response, despite the same material as the prototype structure (steel) being adopted.

In the following, all considerations that were taken into account for the modeling-strategy are explained.

4.1.1 Geometric scaling

Firstly, the geometric scale has been necessary to be decided for the model. In detail, the limited size of the laboratory had to be the major constraint for the geometric scaling procedure. After multiple considerations, the entire laboratory length was used to build the structural model (Figure 4.1).

It has been selected according to laboratory size a scaling factor for the bridge of $\frac{1}{265}$. This choice is the result of practical and logistical evaluations. A smaller scale could have been used, but given that the prototype structure (full-scale) is a very long suspension bridge, a smaller scale would have posed several challenges during the construction phase. Working with extremely small components would have made the process more complex and tedious.



Figure 4.1: *Laboratory in Chicago*

4.1.2 Physical Scaling Properties

By having decided on the total scale of the bridge, to ensure that dynamic properties of the scaled model reflect the behavior of the real bridge, similarity laws were employed. According to the Buckingham's theorem [17], any physical phenomenon can be reduced to an equation expressed in a set of dimensionless products:

$$\pi_1 = \phi(\pi_2, \pi_3, \pi_4, \dots, \pi_n)$$

By rewriting this equation in terms of scaled and prototype model the results is going to be:

$$\frac{\pi_{1p}}{\pi_{1m}} = \frac{\phi(\pi_{2p}, \pi_{3p}, \pi_{4p}, \dots, \pi_{np})}{\phi(\pi_{2m}, \pi_{3m}, \pi_{4m}, \dots, \pi_{nm})}$$

Now, by looking in detail single dimensionless properties, the perfect similarity between the model and the prototype is reached if every condition is the same for both, where:

$$\pi_{2p} = \pi_{2m}$$

$$\pi_{3p} = \pi_{3m}$$

...

$$\pi_{np} = \pi_{nm}$$

so that the previous equation becomes:

$$\frac{\pi_{1p}}{\pi_{1m}} = \frac{\phi(\pi_{2p}, \pi_{3p}, \pi_{4p}, \dots, \pi_{np})}{\phi(\pi_{2m}, \pi_{3m}, \pi_{4m}, \dots, \pi_{nm})} = 1$$

It is worth to mention that the complete similarity most of the times is difficult to reach, because of the several variables that should be considered in a model. Therefore, in this case, a "distorted model" is adopted.

In the case study of this research, multiple considerations have been adopted for the scaling model. In detail, scaling factors of physical quantities are expressed in the following:

Table 4.1: *Scaling factors for physical quantities.*

Physical Quantity	Similarity Relation	Dimension	Scaling Factor
Length (L)	S_L	L	$\frac{1}{265} = 0.0038$
Elastic Modulus (E)	S_E	FL^{-2}	1
Acceleration (a)	S_a	LT^{-2}	1
Stress (σ)	S_σ	FL^{-2}	1
Force (F)	S_F	F	$(\frac{1}{265})^2 = 0.000014$
Strain (ε)	S_ε	-	1
Time (t)	S_t	$T = L^{1/2}$	$(\frac{1}{265})^{1/2} = 0.0614$

First of all, same material has been employed, being both bridges built in steel, therefore the elastic modulus scaling factor is the unity. Consequently to this, also stresses are the same as well. Considering that the model is immerse in the gravity field, as the prototype, for this research the acceleration scale factor has been employed as 1[18].

4.2 Bridge Model

4.2.1 Geometry

The configuration of scaled model details is presented in Figure 4.2, where the total height of towers is 1.51 m and the length of the bridge is 13.83 m (12.45 m the central span and 0.69 m sidespans). By moving to the deck configuration, a square cross-section 31.75 x 31.75 x 3.175 mm (HSS square 1 1/4 x 1 1/4 x 1/8 inch) was selected to match natural frequency requirements from similarity law. From the latter, the target natural period of the model estimated was $T_{mod} = 2.045$ s, being the prototype's one $T_{prot} = 33.17$ s.

$$T_{mod} = T_{prot} \cdot S_t = 33.17 \cdot \left(\frac{1}{265}\right)^{\left(\frac{1}{2}\right)} = 2.045 \text{ sec}$$

It is well known that for a suspension bridge, also lower modes shapes are significant somehow, but being the first one transversal, the most significant for this research, the selection of the cross-section has been based on that. For achieving the final configuration, FE model has been employed [4] for the eigenvalues problem, that will be described better in next chapters. In order to meet the natural period requirement, additional mass was added to the deck at each hanger locations to get as close as possible to the target period. However, due to material and logistical limitations, the target period could not be fully reached, because of the significant number of additional masses that should have been placed on the deck. A reasonable compromise between the amount of mass and the final error, simulating several cases, was found adding a flat steel plate mass of 1.5 kg with attached below 2 steel cubes of weight of 1 kg for each hanger. The suspension system, instead, was perfectly scaled from the prototype bridge, using for main cables a diameter of 6.35 mm; regarding hangers, as well, same pattern of the prototype's configuration has been adopted with diameters of 0.5-0.6-0.8 mm. In Table 4.2, are reported half of the hangers sizes, being symmetric the bridge that have been employed for this scaled model.

4.2.2 Materials

Main cables are made of 304 stainless-steel composed by 7 strands each one with 19 wires ($f_y = 241$ MPa, $f_u = 520$ MPa, $E=200$ GPa). For the suspenders, high-strength steel was adopted ($f_y = 1500$ MPa, $f_u = 1800$ MPa, $E=200$ GPa).

Regarding the whole structure, as it was already mentioned, structural steel was employed, for the deck and towers .

Table 4.2: *Hangers length of half of the bridge*

	REAL MODEL			SCALED MODEL		
	N°	Coordinates [m]	Length [m] (ft)	Diameter [m] (in)	Length [m] (ft)	Diameter [mm] (in)
SIDESPAN	1	-1833	264 (866.18)	0.22 (8.66)	0.996 (3.27)	0.8 (0.0315)
	2	-1770	290 (951.49)	0.22 (8.66)	1.095 (3.59)	0.8 (0.0315)
	3	-1740	303 (994.14)	0.16 (6.30)	1.137 (3.75)	0.6 (0.0236)
	4	-1710	316 (1036.80)	0.16 (6.30)	1.19 (3.90)	0.6 (0.0236)
	5	-1680	329 (1079.45)	0.22 (8.66)	1.24 (4.07)	0.8 (0.0315)
	6	-1620	331 (1086.01)	0.16 (6.30)	1.25 (4.10)	0.6 (0.0236)
	7	-1590	320 (1049.92)	0.16 (6.30)	1.2 (3.96)	0.6 (0.0236)
	8	-1560	308 (1010.55)	0.16 (6.30)	1.164 (3.81)	0.6 (0.0236)
	9	-1530	296 (971.18)	0.13 (5.12)	1.119 (3.67)	0.5 (0.0197)
	10	-1500	285 (935.09)	0.13 (5.12)	1.076 (3.53)	0.5 (0.0197)
11	-1470	274 (898.99)	0.13 (5.12)	1.033 (3.39)	0.5 (0.0197)	
12	-1440	264 (866.18)	0.13 (5.12)	0.996 (3.27)	0.5 (0.0197)	
13	-1410	253 (830.09)	0.13 (5.12)	0.958 (3.13)	0.5 (0.0197)	
14	-1380	243 (797.28)	0.13 (5.12)	0.921 (3.01)	0.5 (0.0197)	
15	-1350	233 (764.47)	0.13 (5.12)	0.885 (2.89)	0.5 (0.0197)	
16	-1320	224 (734.94)	0.13 (5.12)	0.848 (2.77)	0.5 (0.0197)	
17	-1290	215 (705.42)	0.13 (5.12)	0.811 (2.66)	0.5 (0.0197)	
18	-1260	205 (672.61)	0.13 (5.12)	0.773 (2.54)	0.5 (0.0197)	
19	-1230	196 (643.08)	0.13 (5.12)	0.736 (2.43)	0.5 (0.0197)	
20	-1200	187 (613.55)	0.13 (5.12)	0.699 (2.32)	0.5 (0.0197)	
21	-1170	178 (584.02)	0.13 (5.12)	0.662 (2.20)	0.5 (0.0197)	
22	-1140	170 (557.77)	0.13 (5.12)	0.637 (2.11)	0.5 (0.0197)	
23	-1110	162 (531.52)	0.13 (5.12)	0.610 (2.01)	0.5 (0.0197)	
24	-1080	153 (501.99)	0.13 (5.12)	0.577 (1.89)	0.5 (0.0197)	
25	-1050	146 (479.03)	0.13 (5.12)	0.550 (1.81)	0.5 (0.0197)	
26	-1020	138 (452.78)	0.13 (5.12)	0.518 (1.71)	0.5 (0.0197)	
27	-990	131 (429.81)	0.13 (5.12)	0.496 (1.62)	0.5 (0.0197)	
28	-960	124 (406.84)	0.13 (5.12)	0.471 (1.54)	0.5 (0.0197)	
29	-930	117 (383.88)	0.13 (5.12)	0.446 (1.45)	0.5 (0.0197)	
30	-900	110 (360.91)	0.13 (5.12)	0.415 (1.36)	0.5 (0.0197)	
MAIN SPAN	31	-870	103 (337.94)	0.13 (5.12)	0.389 (1.28)	0.5 (0.0197)
	32	-840	97 (318.26)	0.13 (5.12)	0.366 (1.20)	0.5 (0.0197)
	33	-810	91 (298.57)	0.13 (5.12)	0.343 (1.13)	0.5 (0.0197)
	34	-780	85 (278.89)	0.13 (5.12)	0.320 (1.05)	0.5 (0.0197)
	35	-750	79 (259.20)	0.13 (5.12)	0.298 (0.98)	0.5 (0.0197)
	36	-720	74 (242.79)	0.13 (5.12)	0.281 (0.92)	0.5 (0.0197)
	37	-690	68 (223.11)	0.13 (5.12)	0.258 (0.85)	0.5 (0.0197)
	38	-660	64 (209.98)	0.13 (5.12)	0.244 (0.80)	0.5 (0.0197)
	39	-630	60 (196.86)	0.13 (5.12)	0.226 (0.74)	0.5 (0.0197)
	40	-600	56 (183.74)	0.13 (5.12)	0.212 (0.70)	0.5 (0.0197)
	41	-570	52 (170.61)	0.13 (5.12)	0.196 (0.64)	0.5 (0.0197)
	42	-540	49 (160.77)	0.13 (5.12)	0.185 (0.61)	0.5 (0.0197)
	43	-510	45 (147.65)	0.13 (5.12)	0.170 (0.56)	0.5 (0.0197)
	44	-480	41 (134.52)	0.13 (5.12)	0.155 (0.51)	0.5 (0.0197)
	45	-450	37 (121.40)	0.13 (5.12)	0.140 (0.46)	0.5 (0.0197)
	46	-420	34 (111.55)	0.13 (5.12)	0.128 (0.42)	0.5 (0.0197)
	47	-390	30 (98.43)	0.13 (5.12)	0.113 (0.37)	0.5 (0.0197)
	48	-360	27 (88.59)	0.13 (5.12)	0.102 (0.34)	0.5 (0.0197)
	49	-330	24 (78.74)	0.13 (5.12)	0.091 (0.30)	0.5 (0.0197)
	50	-300	21 (68.90)	0.13 (5.12)	0.079 (0.26)	0.5 (0.0197)
	51	-270	19 (62.34)	0.13 (5.12)	0.072 (0.24)	0.5 (0.0197)
	52	-240	17 (55.78)	0.13 (5.12)	0.064 (0.21)	0.5 (0.0197)
	53	-210	15 (49.22)	0.13 (5.12)	0.057 (0.18)	0.5 (0.0197)
	54	-180	13 (42.65)	0.13 (5.12)	0.049 (0.16)	0.5 (0.0197)
	55	-150	11 (36.09)	0.13 (5.12)	0.042 (0.13)	0.5 (0.0197)
	56	-120	10 (32.81)	0.13 (5.12)	0.038 (0.12)	0.5 (0.0197)
	57	-90	9 (29.53)	0.13 (5.12)	0.034 (0.11)	0.5 (0.0197)
	58	-60	8 (26.25)	0.13 (5.12)	0.030 (0.10)	0.5 (0.0197)
	59	-30	7 (22.97)	0.13 (5.12)	0.026 (0.09)	0.5 (0.0197)
	60	0	7 (22.97)	0.13 (5.12)	0.026 (0.09)	0.5 (0.0197)

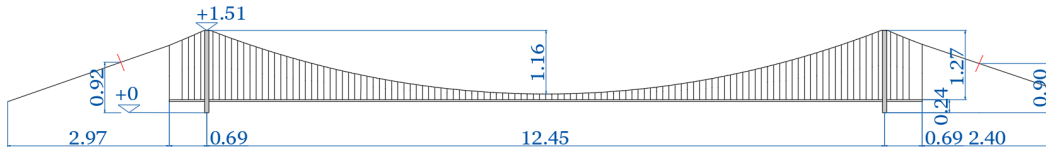


Figure 4.2: Drawing of the model realized in the laboratory

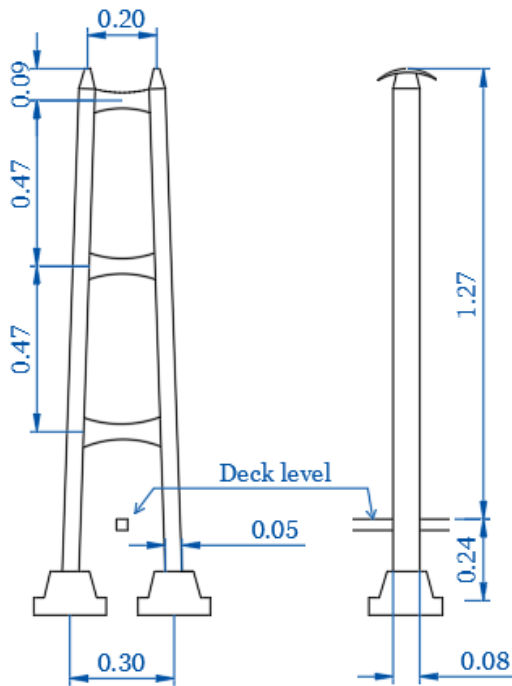


Figure 4.3: Cad drawing for the towers

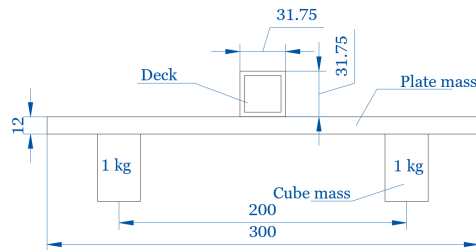


Figure 4.4: Cad drawing for the deck configuration

4.2.3 Boundary Conditions

The boundary conditions of the bridge, are the same of the prototype bridge, having at the two main cable ends fixed configuration, longitudinal roller in correspondence of the two tower-deck joints and a final roller and one hinge for the two extremities of the deck. For the towers base, Soil-Structure interaction springs with different stiffness have been used, simulating the different scenarios implemented in this research. Boundary conditions will be explained better also in the next chapter where it will be illustrated how the FEM model has been realized.

4.2.4 Static Analysis

For the static analysis, it was important to obtain the same cables/hanger stresses according to similarity laws previously mentioned. In detail, considering hangers case, the relation between the stresses of prototype-scaled model can be expressed:

$$\frac{P_{prot}}{A_{prot}} = \frac{P_{model}}{A_{model}}$$

Developing the equation, using the scaling factor for the force S_F , the force of each hanger :

$$P_{model} = P_{prot} * \frac{1}{265^2}$$

The P_{prot} comes from the deck weight of 23 t/m (230 kN/m). Multiplying the deck weight per unit length times the distance between each hanger, 30 m, it is possible to find that the each hanger in the real scale bridge should resist a weight of around:

$$P_{prot} = 230kN/m * 30m = 6900kN$$

Coming back at the equation of similarity for stresses, the equivalent weight to be attached at each hanger is:

$$P_{model} = \frac{6900}{265^2} = 0.098kN \approx 10kg$$

As already mentioned, this weight would have been unpracticable in size, where there would not have been enough space for the connection, and also for stresses in main cables, that would have overcome the yielding point of the material (in the prototype, high-strength steel has been employed also for main cables, while in the scaled model normal steel has been considered).

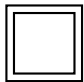
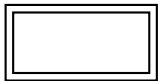
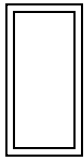
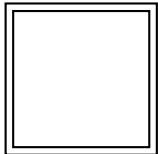

4.2.5 Dynamic Analysis

The dynamic analysis, in detail the eigenvalue one, has been developed to obtain the best configuration to get as close as possible to the target value of natural frequency of the bridge model (2.045 s), firstly without considering any additional mass.

Several FEM models have been developed and the whole procedure will be described in the next chapter. In the Table 4.3, results in terms of natural frequencies are represented for different cross-sections scenarios.

The section selected to maximize the natural period without any additional masses was the HSS square $1 \frac{1}{4} \times 1 \frac{1}{4} \times \frac{1}{8}$, depicted also the Figure 4.4.

Table 4.3: *Dynamic results of different cross-sections*

Section Name	Drawing Section	Natural Period [s]
HSS 1 $\frac{1}{4}$ x 1 $\frac{1}{4}$		0.77
HSS 2 x 1		0.53
HSS 1 x 2		0.69
HSS 2 x 2		0.48
HSS 3 x 2		0.45

It has been demonstrated that the thickness of the tube has not a huge difference in dynamic analysis because of the ratio stiffness and mass strictly correlated in the eigenvalue analysis.

5 Finite Element Model Analysis (FEM)

In order to have a better understanding of the dynamic properties of the scale bridge model, a FEM (Finite Element Model) has been developed by using MIDAS Civil Software [19].

5.1 Model Assumptions

For practical reasons, several assumptions were made in the model. The first assumption was to represent the deck as a straight line, disregarding the inclination of the central span, which was fixed at 24 cm. A secondary assumption concerned the anchoring point coordinates, was assuming the latter at the same height (z-coordinate) as the deck, spanning the entire length of the bridge, from anchorage to anchorage (in the real model in the laboratory main cable ends have been cut in a certain point of the length).

Regarding the suspension system, each pair of cables (main cables and hangers) was replaced with a single cable due to the very small distance between each pair after scaling.

5.2 Suspension Bridge Wizard

The model has been built using the wizard function for suspension bridges available in MIDAS Civil, for creating and generating the 2D-3D model of the suspension system which is able to calculate the initial undeformed lengths of main cables and hangers. The initial screen display is presented like the following picture:

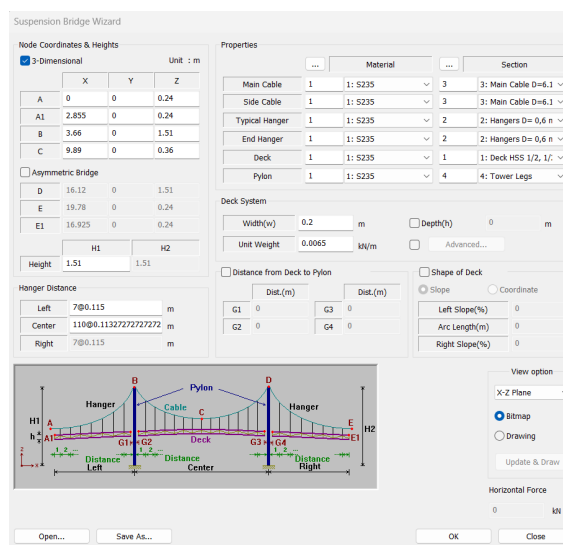


Figure 5.1: Suspension bridge wizard with dimensions of the scaled model in the laboratory

Every step is going to be explained in next sub-chapters.

5.2.1 Node Coordinates & Heights

In this section all the geometric characteristics of the bridge were implemented. In detail, all coordinates are well-illustrated here in the following:

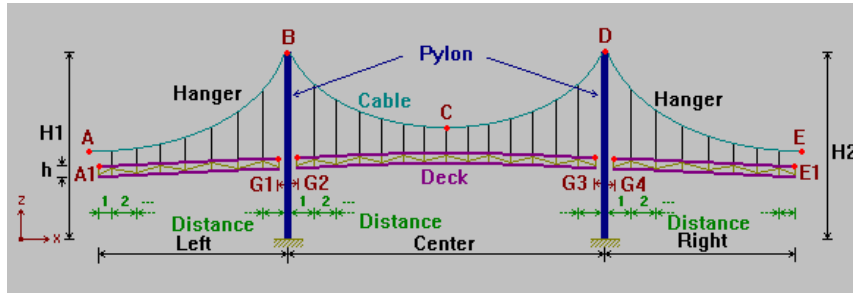


Figure 5.2: Representation of all geometric points to be implemented in the model

All the dimensions are based on the lab model created and explained in the Chapter 4. It is worth to mention that the nonlinear analysis generated by the wizard tool, under specific conditions, does not reach the numerical convergence of the problem. This due to the fact that at the beginning of the numerical problem, if suspension system is not loaded enough, cable elements can result in compression, giving the final error in convergence. For the study case following values has been implemented:

Table 5.1: Geometric Characteristics - Suspension Bridge Points

Point	x [m]	y [m]	z [m]
A	0.00	0.00	0.24
A1	2.86	0.00	0.24
B	3.66	0.00	1.51
C	9.89	0.00	0.36

It is worth to mention that the point C (sag point), according to the real scaled bridge that has been realized in the laboratory, it is going to have a coordinate of 0.27 m, considering a straight deck. Following the nonlinear analysis generated by the wizard model, 0.36 m is the first value for which the analysis reach convergence in the problem. This discrepancy has been mitigated by acknowledging that the actual laboratory configuration does not have a perfectly straight deck but instead has a slight upward bend. This upward curvature reduces the error by bringing the physical configuration closer to the modeled value.

By moving to the height of the tower, it has been fixed to a value of 1.51 m, as it has been designed and scaled. The bridge has been modeled as a symmetric one, so the right side of the bridge is going to be mirrored.

5.2.2 Hangers Distance

For the hangers distance, it was important to implement the right and perfect subdivision of the different bridge's lengths. In detail the distance are the following, as illustrated in Figure 5.1:

Table 5.2: *Hanger distance*

Length	Distance
Left side	7@0.115
Central span	110@0.11327
Right side	7@0.115

In order to model the right number of hangers, 7 space every 0.115 m have been implemented (6 hangers), going to modify the configuration of the bridge in the following steps. However the central span has been divided in order to obtain the right number of hangers.

5.2.3 Properties

By exploring the properties of the model, for the material, different types of steel have been employed for this project, that as already mentioned, for the deck structural steel, while for the cables high-strength steel have been adopted.

Regarding the cross-sections of the different components, the ones explained in previous chapters have been assumed for the model. More specific, main cables and hangers, have been modeled as a circular cross-section with respectively a diameter of 6.12 mm and 0.5-0.6-0.8 mm.

The deck instead, has been modeled with an HSS square $1 \frac{1}{4} \times 1 \frac{1}{4} \times \frac{1}{8}$. For the towers, always a box section have been used, following the HSS $3 \times 2 \times \frac{1}{12}$.

5.2.4 Deck System

The deck system section is presented as the following:

The image shows a software window titled "Deck System". It contains four input fields and one button. The first row has "Width(w)" with a value of "0.2" and unit "m", and "Depth(h)" with a value of "0" and unit "m". The second row has "Unit Weight" with a value of "0.0279" and unit "kN/m", and an "Advanced..." button.

Figure 5.3: *Deck-system window*

where the width of the deck corresponds to the distance between the two main cables, and the unit weight is the linear mass of the deck HSS square $1 \frac{1}{4} \times 1 \frac{1}{4} \times \frac{1}{8}$.

5 FINITE ELEMENT MODEL ANALYSIS (FEM)

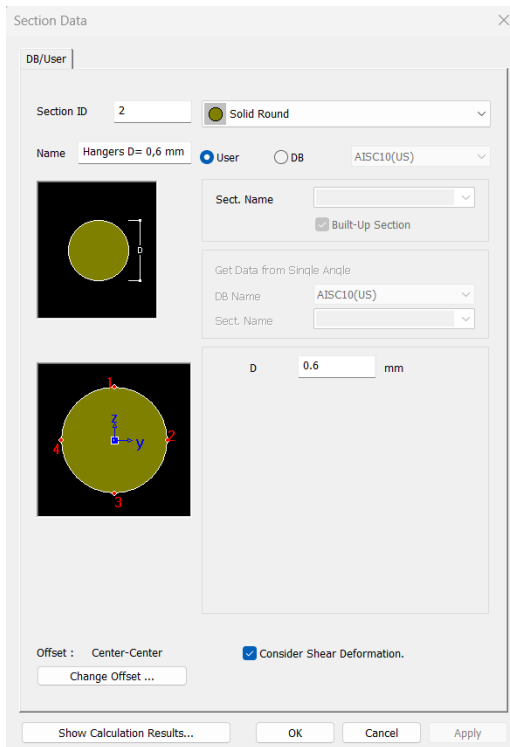


Figure 5.4: Hangers cross-sections in the FEM model (diameter 0.6 mm)



Figure 5.5: Main cables cross-sections in the FEM model

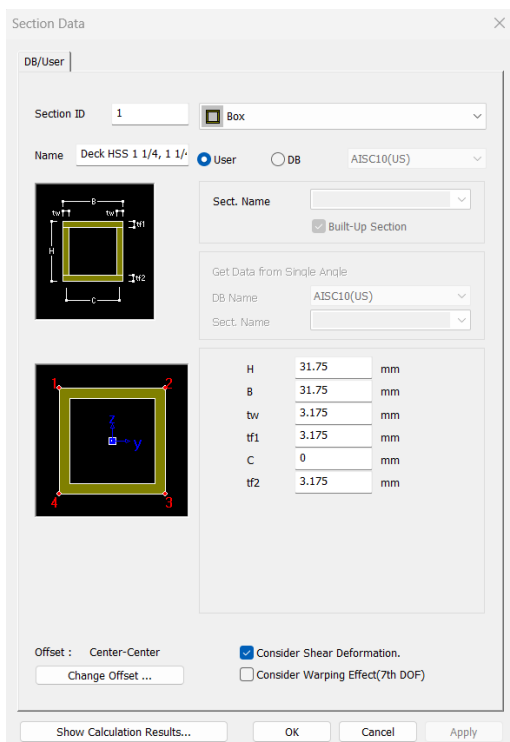


Figure 5.6: Deck cross-section in the FEM model

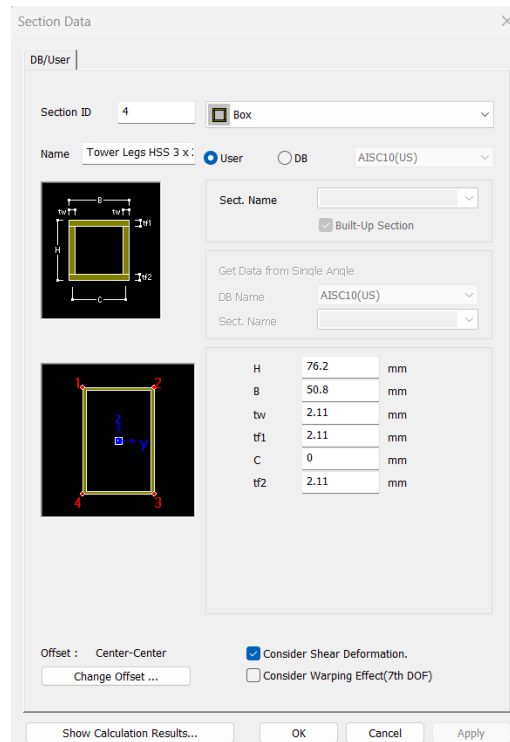


Figure 5.7: Towers cross-section in the FEM model

5.3 Final Model

In order to obtain the model desired, different changes have been made to the model, inclining the two towers with the designed width (30 cm at the base and 20 cm at the top). Moreover, both sidespans were adjusted removing an hanger and assigning the correct diameter for each one following the explained pattern. In between the two leg towers, the three cross beams have been implemented as well, for each tower. The final model is presented as the following:

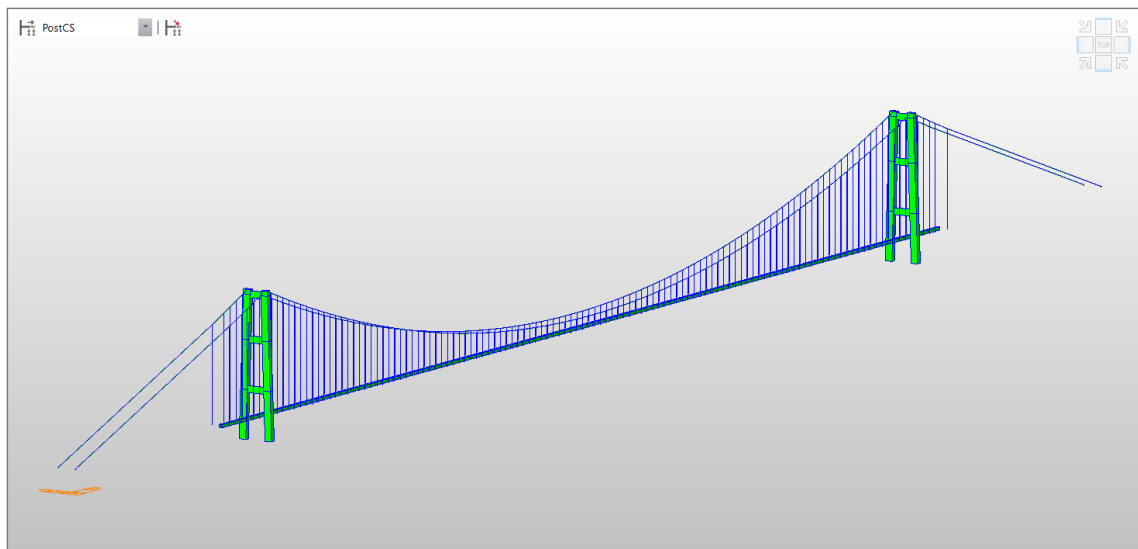


Figure 5.8: FEM model developed on Midas Civil

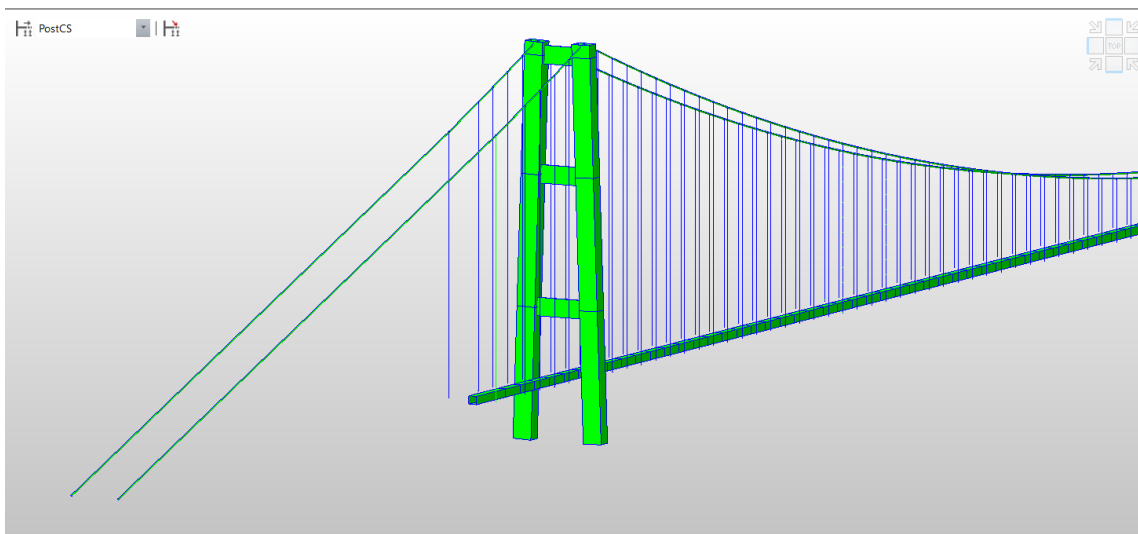


Figure 5.9: Tower- sidespan detail

5.3.1 Boundary Conditions

The boundary conditions assigned to this model, were the one that were assigned in the official document model, in order to have similarity also in each modeshape. For anchoring blocks, deck-tower interaction and end-supports of the deck rigid supports have been employed. Regarding the soil, linear springs in the transversal direction have been adopted, trying to simulate the spring-box system idealized in the experimental part (explained better in next chapter).

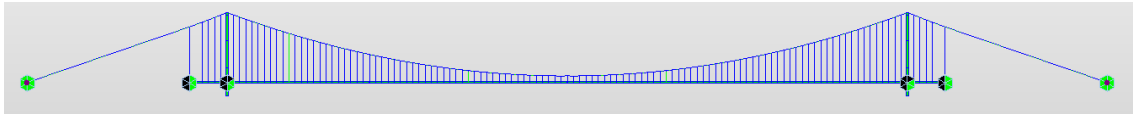


Figure 5.10: Rigid boundary conditions

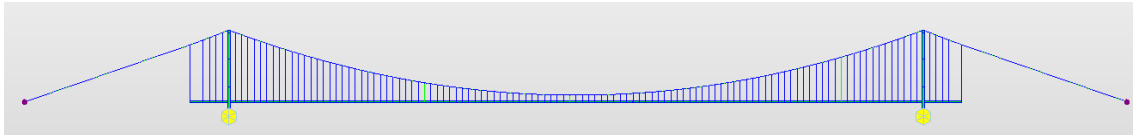


Figure 5.11: Elastic boundary conditions

To summarize, the following table is provided:

Table 5.3: Rigid and Elastic conditions for the model

Rigid	Support	Dx	Dy	Dz	Rx	Ry	Rz
	End Support	1	1	1	0	0	0
Tower Support	0	1	1	0	0	0	
End Cable Support	1	1	1	1	1	1	
Elastic	Support	KDx	KDy	KDz	KRx	KRy	KRz
	West Tower	1	KDy	1	1	1	1
	East Tower	1	KDy	1	1	1	1

where for rigid supports the Dx,Dy..ecc represents a fixed condition (1) or a degree of freedom (0). Instead, for the elastic ones, KDx,KDy represent the spring stiffness assigned to the model. Therefore, being interested in just the transversal behavior, KDy has been assigned for each tower leg, where all remaining direction have been fixed (1).

For the elastic spring supports, three different scenarios have been studied:

- **Fixed (high stiffness):** $KDy = 200 \text{ N/mm}$
- **Medium stiffness:** $KDy = 20 \text{ N/mm}$
- **Soft stiffness:** $KDy = 4 \text{ N/mm}$

To be specific, the latters are the total stiffness for each tower, so to clarify, in case of high stiffness where the total is 200 N/mm, for each leg 100 N/mm spring stiffness has been assigned, as shown in Figure 5.12

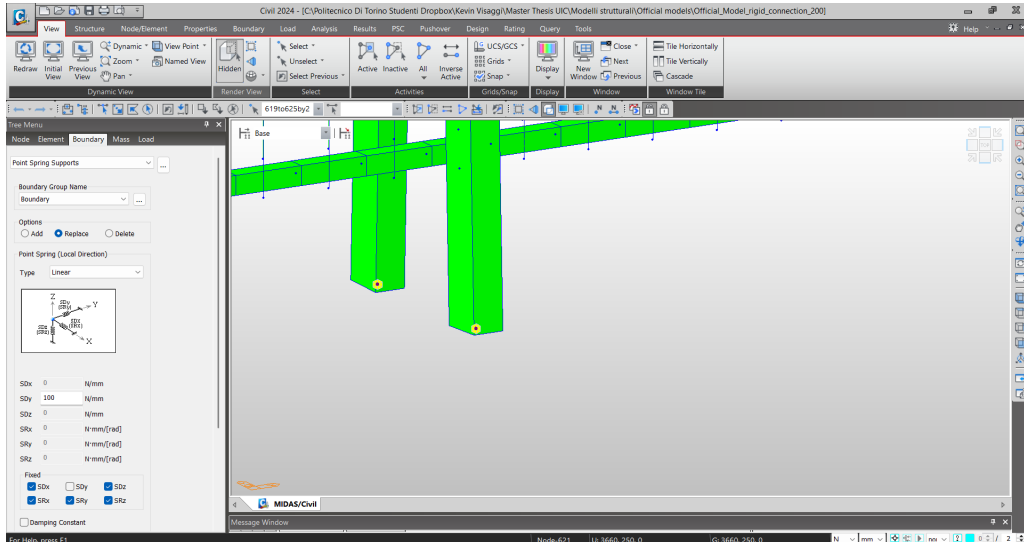


Figure 5.12: Spring-stiffness detail

5.3.2 Loads

By having defined the whole model, the last step before developing the different analysis, loads are needed. As already mentioned, in the experimental model a transversal plate of 1.5 kg plus 2 kg (1 kg + 1 kg) are attached to each hanger location. In the FEM model, it has been decided to model this load as two punctual loads in each hanger position. The total load for each hanger position (2 hangers) is the sum of 1.5 kg and 2 kg. It comes up that each hanger take half of this weight:

$$P_{hanger} = P_{tot}/2 = 3.5/2 = 1.75 \text{ kg} \rightarrow 17.5 \text{ N}$$

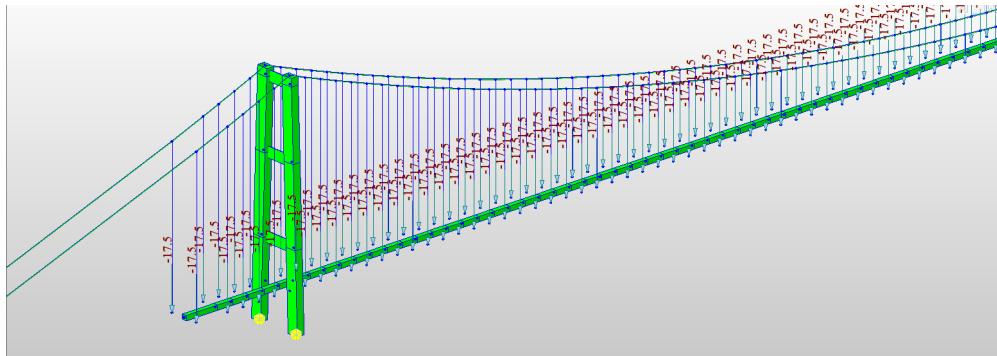


Figure 5.13: Nodal loads applied to the model to simulate additional masses

5.4 Suspension Bridge Analysis

The suspension bridge analysis is needed to understand the initial configuration of the bridge under a defined load pattern and specific conditions in a more accurate way. In detail, this function needs to be parametrized based on boundary conditions. Specifically, being an iterative method, boundary conditions able to be updated at every step are needed. Therefore, sag points and nodes of the suspension system are required to be defined and selected.

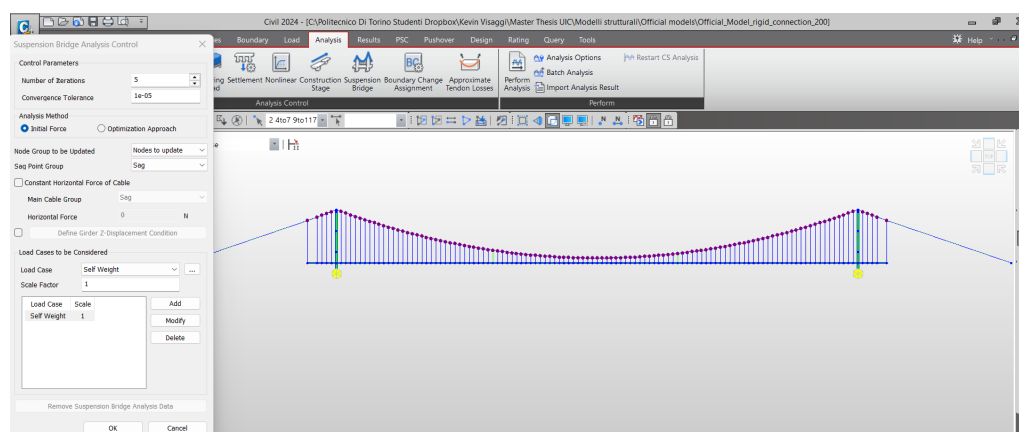


Figure 5.14: Nodes of the suspension system to be updated

5.5 Construction Stage Analysis

The influence of large displacements must be considered when determining forces during the erection of suspension bridges. A nonlinear construction stage analysis is performed, incorporating the equilibrium nodal forces obtained from the completed state analysis. The window of the construction stage analysis is shown in Figure 5.15.

Through the construction stage analysis, it is possible to check whether or not the suspension analysis has been carried correctly, checking the forces and deformation characteristics of members. In detail, looking to the deformation, the results presented in Figure 5.16 show that in the last construction-stage, where the final shape is the one wished, the vertical deformations (DXZ) are with practical null.

It is worth to mention that the displacement of around 1 mm in the mid-span is due to some computational issues, being in reality as all the other nodes, very close to zero.

The consequent forces inside the cables, to maintain the wished shape and null deformation are going to be plotted in Figure 5.17

5.5 Construction Stage Analysis

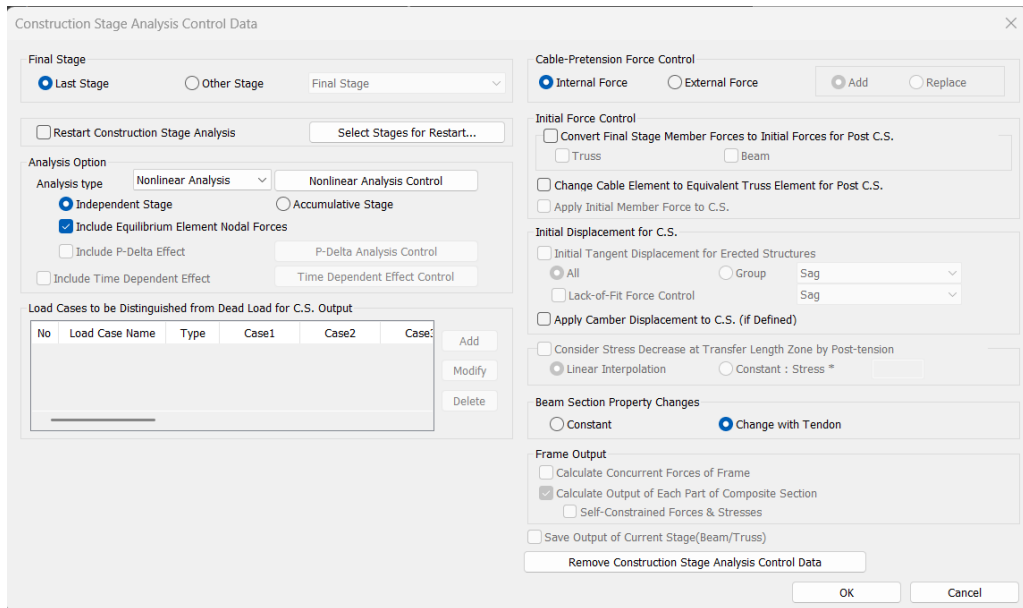


Figure 5.15: Construction stage analysis

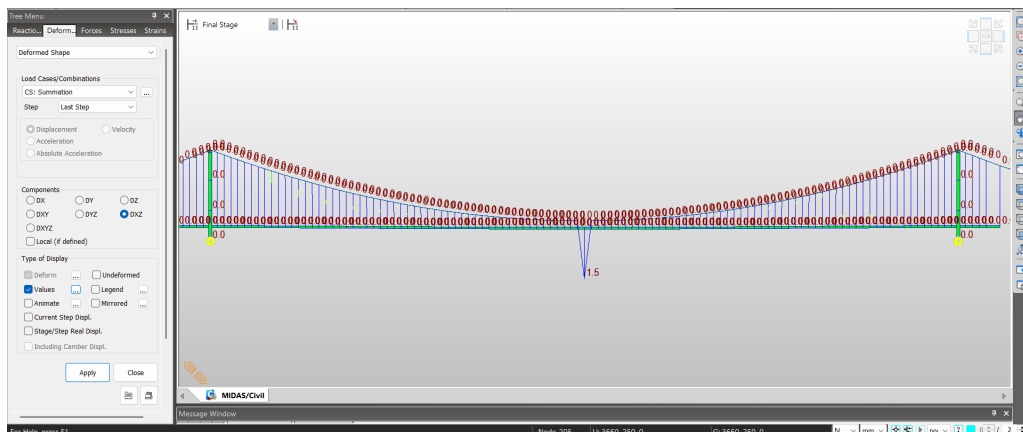


Figure 5.16: Null vertical deformation of the suspension system after applying the load pattern

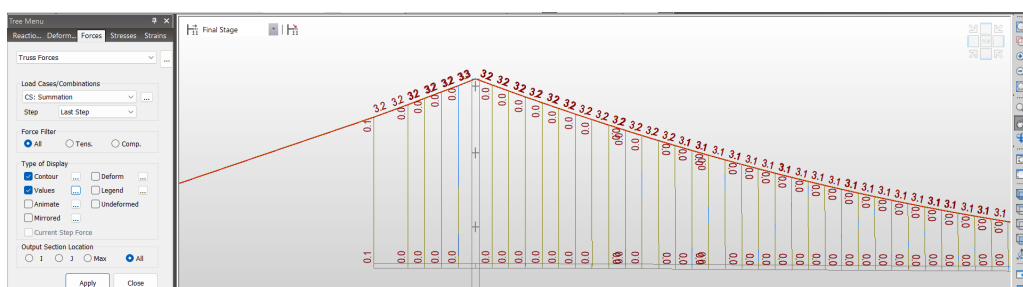


Figure 5.17: Tension forces in main cables after load applied

5.6 Eigenvalue Analysis

The first step towards the final results was the eigenvalue analysis used to compare the dynamic properties of the scaled model with the prototype structure.

In detail, 10 frequencies have been reached, focusing the study in the first 3-4 most important frequencies. Lanczos method have been adopted, according to the following window:

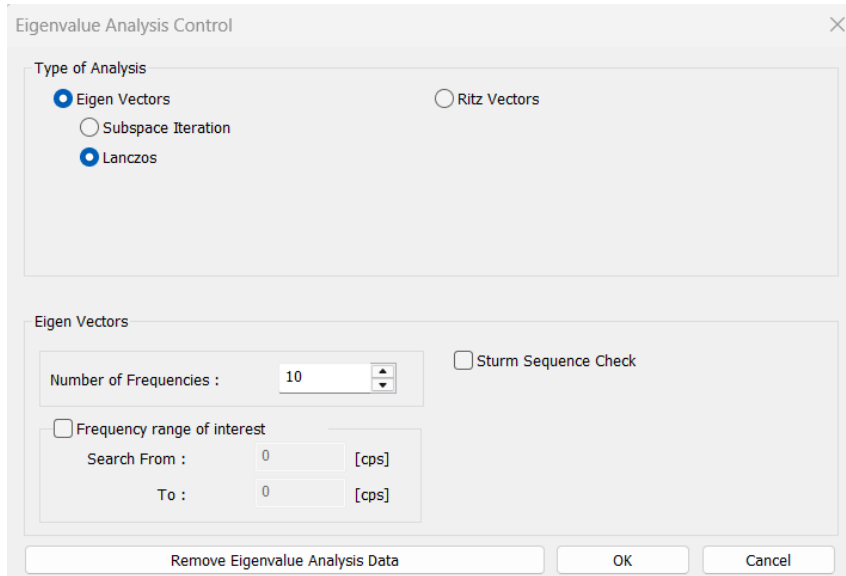


Figure 5.18: *Eigenvalue analysis control window*

The results from the eigenvalues analysis are the following:

Table 5.4: *Natural frequencies and periods for the first 10 modes in the numerical analysis*

Mode No.	Frequency [rad/sec]	Period [sec]	Mode Shape
1	3.892	1.614	Horiz.
2	7.799	0.806	Horiz.
3	9.733	0.646	Vert.
4	13.550	0.464	Horiz.
5	14.734	0.426	Vert.
6	21.525	0.292	Horiz.
7	24.823	0.253	Vert.
8	24.987	0.251	Vert.
9	31.648	0.199	Horiz.
10	34.288	0.183	Vert.

where the following first 5 vibration modeshapes are plotted:

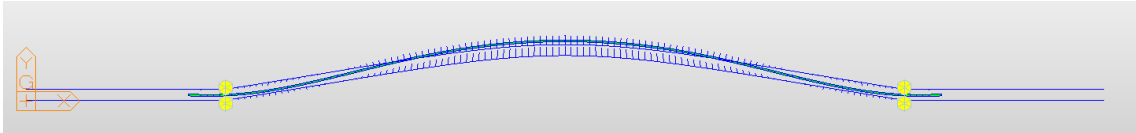


Figure 5.19: *First vibration mode: horizontal mode shape*

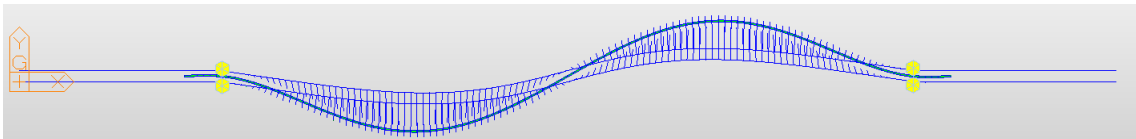


Figure 5.20: *Second vibration mode: horizontal mode shape*

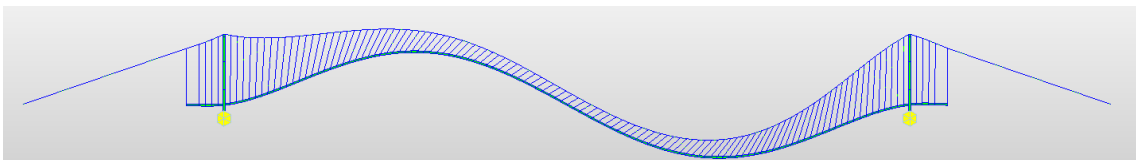


Figure 5.21: *Third vibration mode: vertical mode shape*

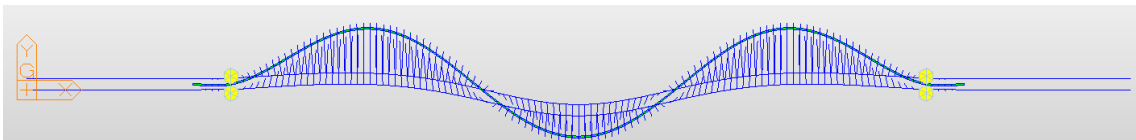


Figure 5.22: *Fourth vibration mode: horizontal mode shape*

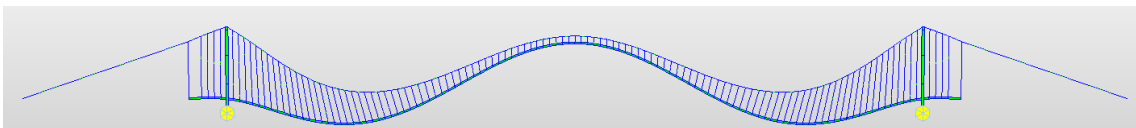


Figure 5.23: *Fifth vibration mode: vertical mode shape*

As shown, the third and fifth mode shapes are vertical and are therefore not relevant to the focus of this study. The analysis will instead concentrate on the first, second, and fourth mode shapes, which exhibit horizontal motion.

To summarize, the following table presents the differences between the theoretical periods (derived from the prototype) and the numerical results:

Table 5.5: Comparison of theoretical and numerical periods for selected modes.

Mode	Prototype [s]	Theoretical	Numerical	Error [%]
1	33.17	2.04	1.61	20.8
2	18.23	1.12	0.81	28.1
4	12.59	0.77	0.46	40.0

The error encountered clearly stems from the very low mass added to the system (1 kg per hanger) compared to the mass that should have been added (10 kg per hanger).

Therefore for having the order of magnitude, these are the differences in terms of stresses in the suspension system considering the static analysis:

Table 5.6: Stresses in the suspension system in Prototype and Scaled Model

Element	Prototype [MPa]	Actual scaled model [MPa]
Main cable	580	113
Hangers	345	87.5

5.7 Time History Analysis

By understanding the dynamic properties of the system, a Linear Time History Analysis has been performed. In this chapter, the analysis will be explained without delving into the earthquake selection process, which will be detailed in Chapter 7.

First, a load case was created, as shown in Figure 5.24. The analysis chosen for this case, as previously mentioned, was a linear analysis using the direct integration method.

The earthquake duration, after time scaling, is approximately 6-7 seconds, so a 15-second recording was selected to also capture the natural response of the bridge after the seismic load application. A time increment of 0.01 seconds was chosen for this study, which results in a reasonable computational cost (1500 iterations).

Another important aspect of this analysis is that it begins after the initial element forces, ensuring the correct final results in terms of forces and stresses. Finally, the damping factor, which is not the focus of this research, was set to 0.02.

After creating the dynamic load case, the software requires the application of the load case in one or more specific directions. For this study, the earthquake was applied only in the y-direction, which corresponds to the transversal direction of the towers.

Add/Modify Time History Load Cases

General

Name : Description :

Analysis Type: Linear Nonlinear

Analysis Method: Modal Direct Integration Static

Time History Type: Transient Periodic

End Time : sec Time Increment : sec

Step Number Increment for Output :

Order in Sequential Loading:

Subsequent to Load Case
 Initial Element Forces(Table)
 Initial Forces for Geometric Stiffness

Cumulate D/V/A Results Keep Final Step Loads Constant

Geometric Nonlinearity Type

None Large Displacements

Damping

Damping Method :

Direct Specification of Modal Damping

Damping Ratio for All Modes :

Modal Damping Overrides

	Mode	Damping Ratio
1		

Time Integration Parameters

Newmark Method : Gamma Beta

Constant Acceleration Linear Acceleration User Input

Nonlinear Analysis Control Parameters

Perform Iteration

OK Cancel Apply

Figure 5.24: Time history load case

6 Construction Stage

In this section all details of the construction stage will be illustrated, explaining every aspect faced during the assembling and preparation parts of the suspension bridge.

6.1 Laboratory Capacity

The construction stages, as already mentioned in the Chapter 4, was influenced by the laboratory's size. The length of the laboratory is around 16.45 m ($\approx 54ft$), and the bridge cables have been anchored wall-to-wall for the whole length.

6.2 Materials Preparation

6.2.1 Hanger Anchorages

One of the primary actions to take was setting up the anchorages between the plates masses of the deck and the hangers to ensure a solid connection, using steel bars and nuts. Specifically, the initial ordered material included 5 steel (around 1.8 m each) bars and 500 nuts.

First, it was necessary to assemble the nuts (in pairs), screwing them onto the bars and tightening them every 3.81 cm (1.5 inches), as shown in Figure 6.2.



Figure 6.1: Raw material for hangers anchorages



Figure 6.2: Couple of nuts inserted in the bar every 3.81 cm (1.5 inches)

Therefore, after assembling all the 5 bars, was necessary to cut each piece maintaining the cutting point around the mid-point between two nuts. It was used for cutting the bars a band saw, as illustrated in Figure 6.3



Figure 6.3: *Band saw used for cutting the bars in single pieces*

As a result, more than 240 pieces (240 was the amount that was needed for the bridge, one for each hanger) have been realized, according to the process above described, with the following final result:

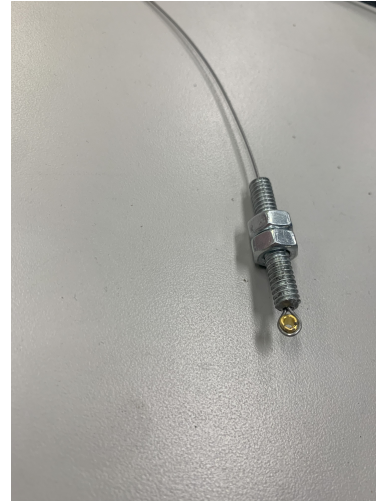


Figure 6.4: *Final anchorages for hangers*

In the final configuration, a small hole was drilled through the screw to allow the hanger to pass through it. This hole provided the necessary space to secure the hangers within the screw. To ensure a secure connection, the hanger cable was twisted multiple times around its end and then looped around a small ring. This gold ring prevents the cable from slipping out of the screw.



(a) Drilling the hole inside the screw.



(b) No-slippery system for the tip of the hanger.

Figure 6.5: Details of the drilling process and the no-slippery connection system for the hanger.

6.2.2 Bridge Deck

By considering all the aspects developed in Chapter 5, the cross-section of the deck has been selected as a hollow square tube $31.75 \times 31.75 \times 3.175$ mm (HSS $1\frac{1}{4} \times 1\frac{1}{4} \times \frac{1}{8}$). Also, the deck, as for the hangers, has been ordered in 2 bars, as shown in the following Figures 6.6 and 6.7:



Figure 6.6: Raw bars for the bridge's deck.



Figure 6.7: Cross-section of the bridge's deck bars HSS $1\frac{1}{4} \times 1\frac{1}{4} \times \frac{1}{8}$.

6.2.3 Plate Masses

The additional masses that have been attached to the deck for reaching the dynamic properties of the bridge, have been connected at the location of each hangers, with singular steel plates, to increase the overall mass of the bridge and reaching the frequency target (Chapter 4).

As with all the components of the bridge, rectangular bars have been ordered for the plates and then trimmed to size correctly reaching the amount of weight requested by the FEM model. In detail, the density of the steel is $8100 \frac{kg}{m^3}$ ($505.8 \frac{lb}{ft^3}$) and the sides of the rectangular cross-section are $50 \times 12 \text{ mm}$ ($1.97 \times 0.47 \text{ inches}$).

Based on this calculation, the length of the plate to reach the target values of mass of each plate analyzed in Chapter 4, 1.5 kg (3.31 lb), the length of the plate has been trimmed with a length L of:

$$\rho_{steel} = \frac{Mass_{plate}}{Volume_{plate}} \rightarrow L = \frac{Mass_{plate}}{\rho_{steel}} * \frac{1}{b * h}$$

Where b and h are respectively the base and the height of the rectangular plates. Therefore, it has been found:

$$L = \frac{1.5kg}{8100 \frac{kg}{m^3} * 10^{-9}} * \frac{1}{50mm * 12mm} \approx 310 \text{ mm (12.20 inches)}$$



Figure 6.8: Plates weight for matching dynamic properties of the bridge

6 CONSTRUCTION STAGE

After trimming the single plates, holes were created to connect the hangers to the plates. This process involved three repeated steps for the entire task: marking the location of the hole, drilling the hole, and refining the surface to ensure smoothness, as shown in Figure 6.9. It is worth to mention that the whole system has been implemented to guarantee 20 cm of distance between the two holes (correspondent to the main cables distance to ensure perfect verticality of hangers).

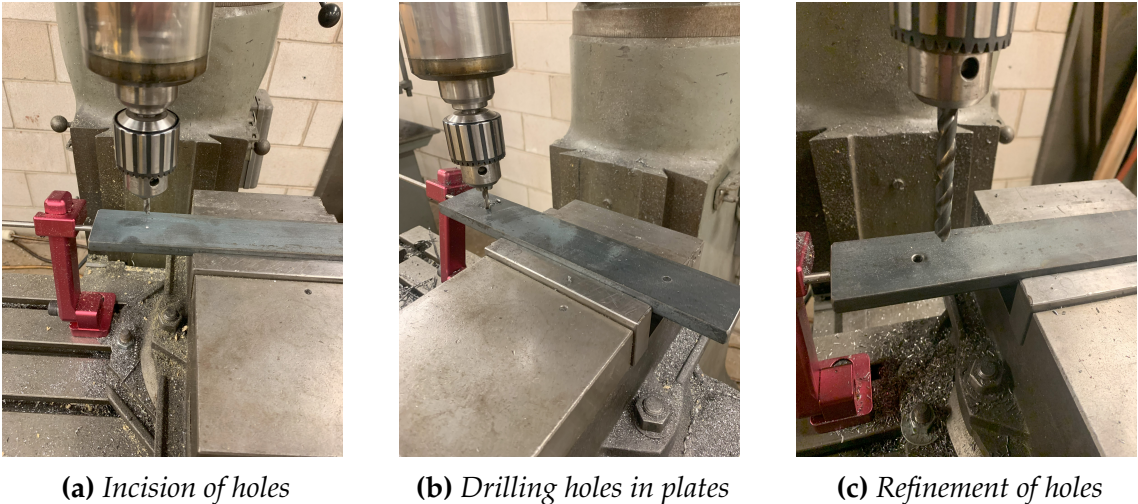


Figure 6.9: Steps in preparing plates for hanger connections: incision, drilling, and refinement of holes.

The final plates are presented as in the following picture:



Figure 6.10: Final plates after the whole process

6.2.4 Towers

The raw material for building the two towers of the suspension bridge are also in this case tubular sections, with a cross-section $76.5 \times 50.8 \times 2.11$ mm (HSS $3 \times 2 \times \frac{1}{12}$) rectangular shape. The following Figure 6.11, depicts the initial state of the material.



Figure 6.11: *Rectangular shape bars for the tower's legs*

First the length of the bars have been set up according to the design of the project. Then, the top of the towers has been bent and welded to fill the gap between the four edges, while simple thin plates have been used for the cross-beams between the two legs, as shown in the Figure 6.12.



(a) *Top of tower bended and welded*



(b) *Cross-beams of towers*

Figure 6.12: *Combined Caption for Both Images*

6 CONSTRUCTION STAGE

The plates have a cross-section of 0.4 x 75 mm (0.016 x 2.95 inches) and are welded directly to the legs of the towers. The length of the cross-beams is variable being that two towers are inclined.

The base of towers have been created with welded plate to anchor legs to the base foundation spring-box (explained in the next chapters).

The final configuration of the towers after the addition of the foundation system, is presented in the Figure 6.13



Figure 6.13: *Completed tower*

6.2.5 Wall Anchorage

For the anchorages to the wall connection a plug system have been deisgned. In detail, three plugs have been adopted for the anchoring plate and a screw system have been designed to set (increase/decrease) the tension in the cables.



(a) Anchoring plate to the wall

(b) Anchoring block with the cable

Figure 6.14: Details of the anchoring system.

6.3 Bridge Assembling

For the assembling the following logical scheme was adopted for building the entire bridge:

1. Erection of the towers.
2. Installation of the main cable.
3. Assembly of the clamping system and hangers.
4. Placement of the deck (supported at multiple points but not yet suspended).
5. Welding of mass plates onto the deck.
6. Temporary fastening of the hangers through the plates.
7. Welding of additional cube-shaped masses onto each plate.

6 CONSTRUCTION STAGE

8. Final tightening of the hangers.
9. Tensioning of the main cables to achieve the final shape.

Further details will be provided where necessary.

For the erection of the two towers, it is important to note that a saddle was welded at the top of each tower to create a frictionless system.

Next, the main cables were installed after being cut to the correct length. Once the clamping system was placed around the main cables—one clamp per hanger—the system appeared as follows:



Figure 6.15: *Tower-cable system.*

From the image above, it is evident that the deck was positioned according to the design drawings, supported at several predefined points. This was particularly useful in shaping the deck-cable system correctly. Additionally, all hangers were attached to the clamping system and initially tightened slightly to set their longitudinal positions, spaced approximately 11.3 cm apart.



Figure 6.16: *Hanger positioned at the correct distance.*

The next step involved welding each plate to the deck, aligning with the spacing of each hanger. The process is illustrated below:

6 CONSTRUCTION STAGE



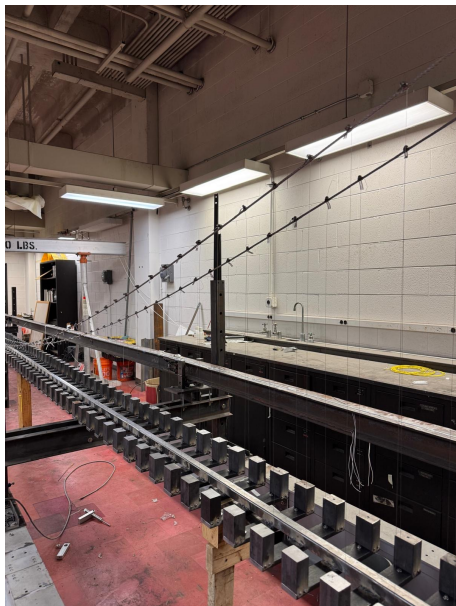
(a) *Partial welding of mass plates.*



(b) *Complete welding of mass plates.*

Figure 6.17: *Welding process of the mass plates onto the deck.*

Once the plates were positioned in the correct location along the entire deck, the steel cubes were welded to the top of each plate. After placing the expected load on the deck (plates + cubes), the length of each hanger was adjusted according to Table 4.2. Each nut was then tightened, putting the hanging system in tension.



(a) *Cube masses addition*



(b) *Tensioned hanging system*

Figure 6.18: *Completed bridge and tensioned hanging system.*

7 Experimental Set-up Test

7.1 Ground Motion

One of the key point for the experimental part, is the selection of the earthquake input load.

7.1.1 Near-Fault and Far-Fault

Before going in detail in the earthquake process of the project, it is necessary to describe the concept of Near-Fault (NF) and Far-Fault (FF). These latter two concept are really important because the seismic response of a structure can be really dependent on the seismic source; therefore a near-fault seismic action can have significant differences in term of structural response.

By having a near-fault earthquake, long-period pulses are shown in the seismic accelerogram, as it has been recorded on January 17th 1994, Northridge, California earthquake (Figure 7.1 on the left). However, far-fault earthquakes exhibit different characteristics in terms of the accelerogram. Specifically, no distinct pulse appears in the acceleration time history, as shown on the right in Figure 7.1, illustrating the Kern County, California, earthquake of July 21, 1952.

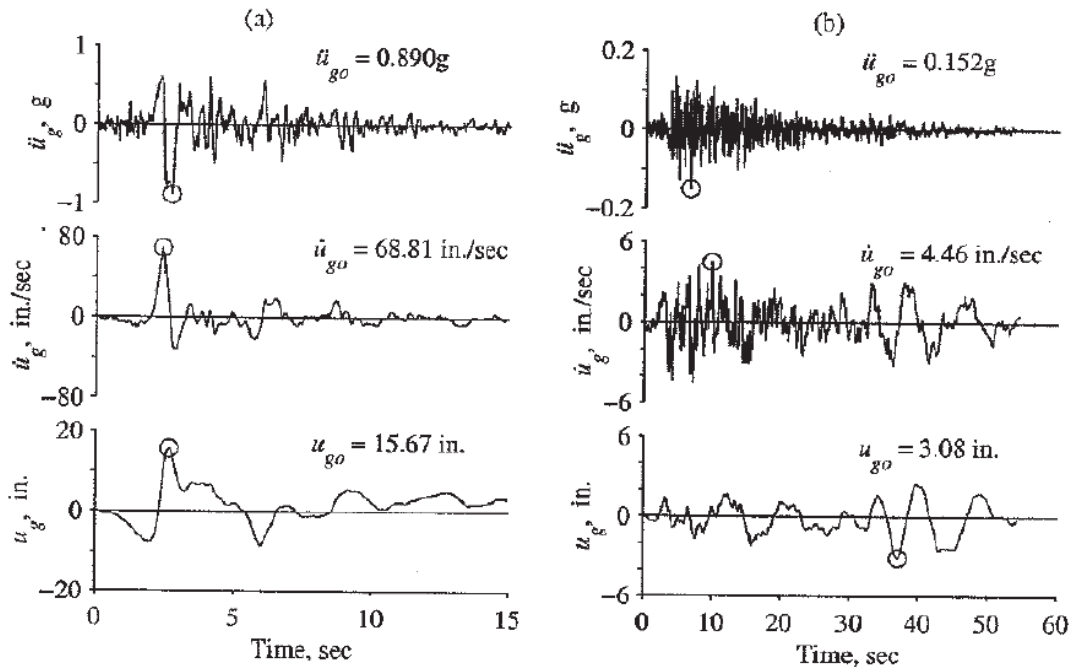


Figure 7.1: Ground motions recorded at (a) 1994 Northridge earthquake, and (b) 1952 Kern County earthquake.

By closely analyzing the case study reported in [20], it is evident that the long-period pulse observed in the NF case has a relatively longer duration compared to the FF case, where more rapid typical oscillations occur. The same trend is reflected in the displacement and velocity time history of both earthquake, where the pulse, more than longer, it is different also in the intensity/amplitude.

This concept is also crucial for structural engineers, as these long-period excitations can be particularly critical for flexible, long-period structures, such as suspension and cable-stayed bridges or high-rise buildings.

Also [21], show that the pulse signals is easier to detect from the velocity time history, as depicted in the following picutre:

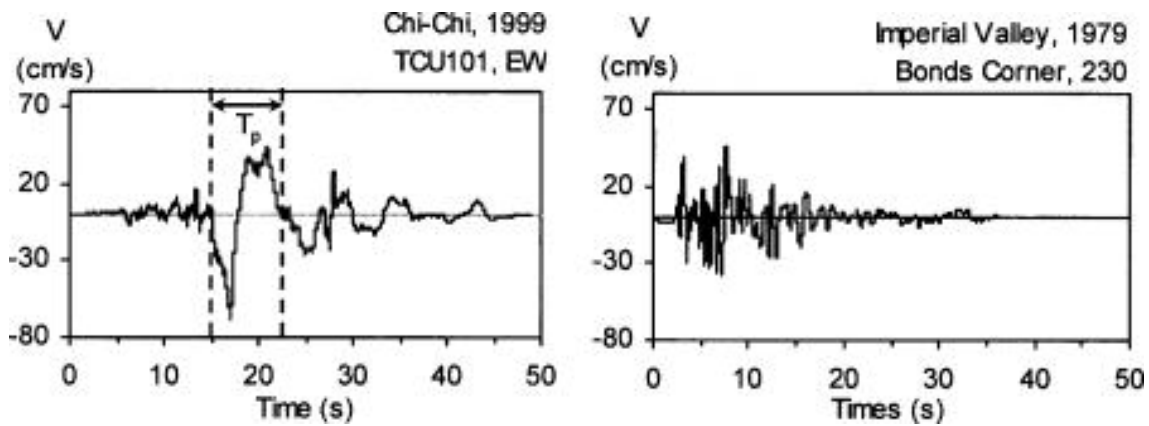


Figure 7.2: Velocity time history with pulse behaviour and without

7.1.2 Selection of Seismic Records for Testing

For the experimental part, it has been decided based on concepts above illustrated, to use two different input ground motions records, belonging to the same earthquake. The idea was to employed in the experiment, a significant earthquake in terms of characteristics and importance in the Italian history. Following this purpose, it should have been adopted the Messina earthquake of 1908, one of the most destructive earthquake in Italy, but also in Europe [22]. However, this earthquake occurred when seismology was just beginning to take its first steps, and nowadays limited information are available like the magnitude (7.1 Mw) and the source of the earthquake, but no real accelerograms exist of it.

By moving forward in the Italy's history and the advancements in seismology, one of the most significant earthquake in the Peninsula in last decades, is the 2009 Aquila earthquake (Figure 7.3).

The L'Aquila earthquake, with a magnitude of 6.2 (M_w), stands as one of the most significant and destructive events in the Italian history. The city of L'Aquila is situated in a high seismic zone and with the vulnerability of its structures (many of which were masonry buildings), contributed to the extensive destruction.



Figure 7.3: 6th April 2009 Aquila earthquake

<https://www.lacnews24.it/italia-mondo/quindici-anni-fa-il-terremoto-che-fece-309-morti-laquila-si-ferma-per-ricordare-ydh2kcv4>

This catastrophic event marked a turning point, launching significant efforts in both academic research and practical applications to enhance understanding and improve the seismic performance of structures. These efforts have led to advancements in areas such as the detailing of nodes, reinforcement techniques, and the overall state of the art in seismic design.

The site of the earthquake was presented like the following Figure 7.4 , where the triangles represent all measurements stations of acceleration.

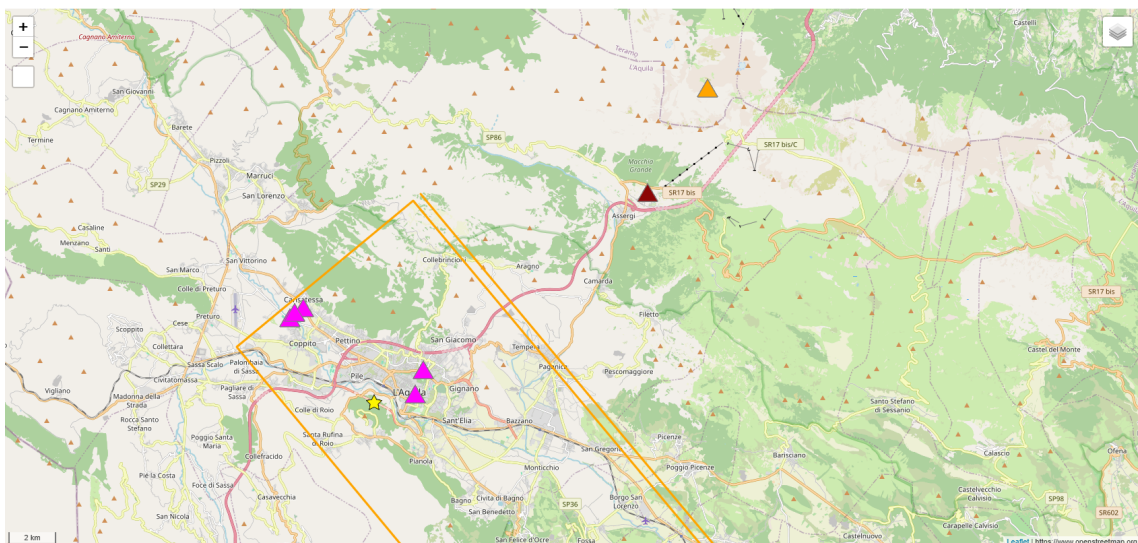


Figure 7.4: Site of the Aquila earthquake with accelerometers stations [23]

The legend that represent the intensity of PGA measurements is the following:



Figure 7.5: Legend based of the PGA intensity (cm/s^2) [23]

The data availability of this seismic event, have been gained by different agencies between INGV (Istituto Nazionale DI Geofisica e Vulcanologia), EMSC (European-Mediterranean Seismological Centre) and the USGS United States Geological Survey, as it reported in next Table 7.1.

Table 7.1: Seismic event data from different agencies.

Agency	Latitude	Longitude	Focal Depth (km)	Magnitude (Mw)
INGV	42.33	13.33	8.8	6.2
EMSC	42.38	13.32	2.0	6.3
USGS	42.423	13.395	10.0	6.3

Several stations have been recorded data from the Aquila earthquake, and in the following the main and significant stations have been reported [24]:

Table 7.2: Seismic station data of the L'Aquila earthquake, including location, soil type, PGA, and R_{jb} distance.[24]

Station Code	Province	Lat (N)	Long (E)	EC8 Soil Type	PGA (g)	R_{jb}	Distance (km)
AQV	L'Aquila	42.377	13.344	B	0.675	0	
AQG	L'Aquila	42.373	13.337	B	0.515	0	
AQA	L'Aquila	42.376	13.339	B	0.487	0	
AQK	L'Aquila	42.345	13.401	C	0.373	0	
GSA	L'Aquila	42.421	13.519	A	0.152	9	
CLN	L'Aquila	42.085	13.521	A	0.091	20	
AVZ	L'Aquila	42.027	13.426	C	0.069	25	
ORC	L'Aquila	41.954	13.642	A	0.066	37	
MTR	L'Aquila	42.524	13.245	A	0.063	16	
GSG	L'Aquila	42.460	13.550	A	0.030	14	
FMG	Rieti	42.268	13.117	A	0.027	17	
ANT	Rieti	42.418	13.079	A	0.026	19	
CSO1	L'Aquila	42.101	13.088	A	0.019	32	
LSS	Rieti	42.558	12.969	A	0.009	36	
MMP1	Rieti	42.249	12.748	A	0.009	46	

For the experiment, the same earthquake (L'Aquila) has been employed analyzing data coming from two different stations, one in proximity of the fault, while the other one could be considered far-fault. This choice was made based on the different response that a structure could have depending on the distance to the fault, as already mentioned.

The first selection was the AQK station (Figure 7.6) with an R_{jb} (Joyner-Boore distance) of 0 km, which means that the recording site was exactly in the surface projection of the rupture plane, as better explained in Figure 7.7 [25]:

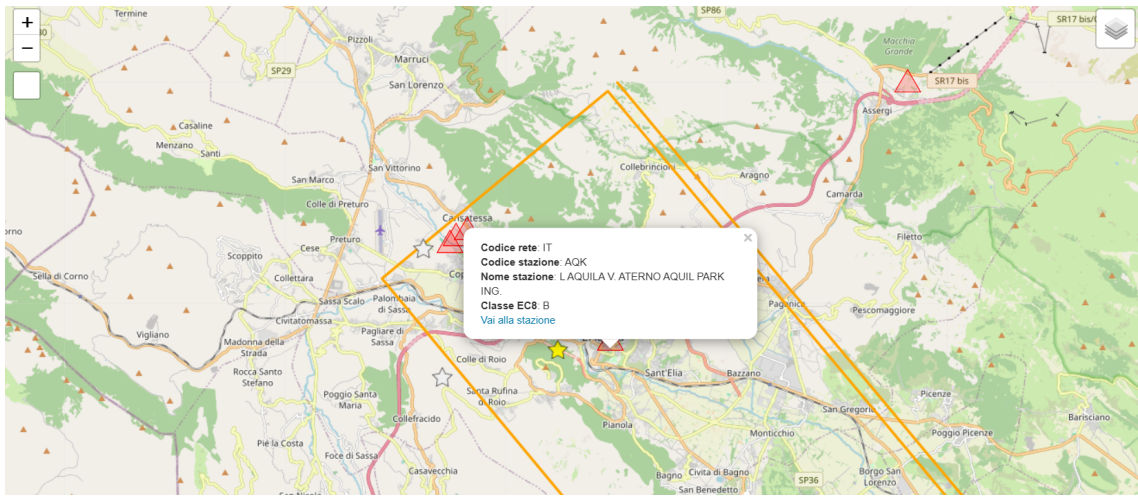


Figure 7.6: AQV station (Near-Fault)[23]

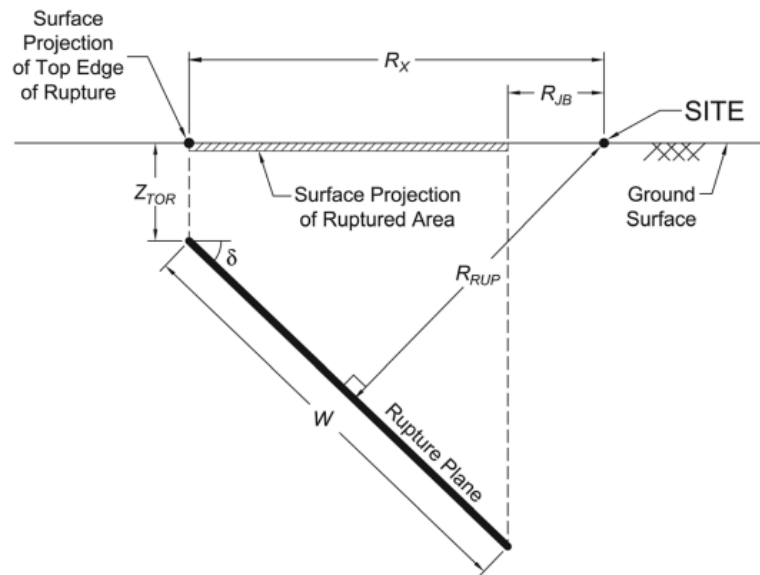


Figure 7.7: Illustration of a vertical cross section through a rupture plane and main important distances measurements

7 EXPERIMENTAL SET-UP TEST

In order to use the worst condition earthquake the East-West direction has been selected instead of the North-South being more significant, as shown in the below picture:

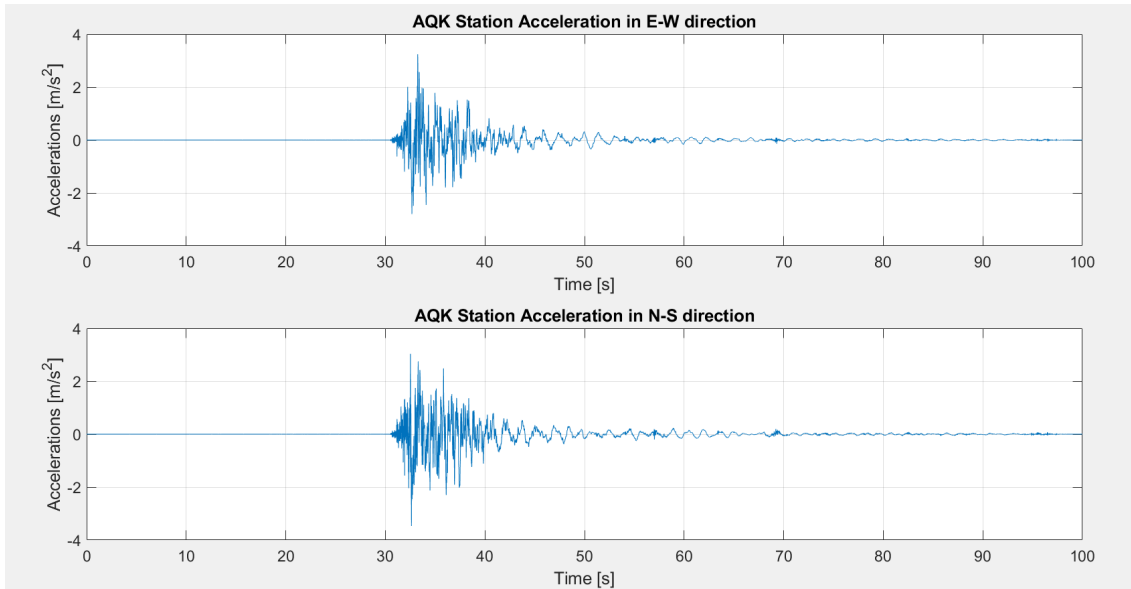


Figure 7.8: AQK station accelerograms records for East-West and North-South direction

For the Far-Fault condition, the station MTR has been selected with an R_{jb} of 16 km; the location of the station has been depicted in the following:

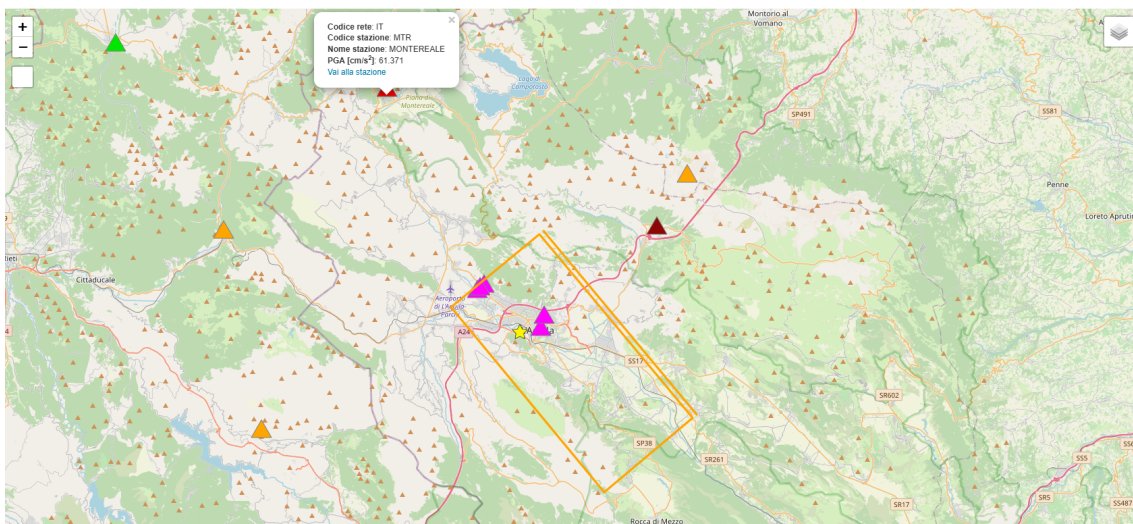


Figure 7.9: MTR station (Far-Fault) [23]

By selecting the far-fault station, the North-South has been employed for the current study; in the following Table 7.3, the two input ground motions of the research are shown, with the main characteristics

Table 7.3: Earthquake data, including station type, distances, and peak ground acceleration (PGA) and velocity (PGV).

Earthquake	Station	Type	Rjb [km]	Epicentral [km]	PGA [cm/s ²]	PGV [cm/s]	PGV/PGA [s]
L'Aquila	AQK EW	Near-fault	0.0	1.8	346.784	35.798	0.103
L'Aquila	MTR NS	Far-fault	16	23.1	61.371	2.886	0.047

The AQK records shows significant strong pulses, which contributed greatly to structures damages, as it is very clear from the velocity and displacement time-history, shown in Figure 7.10.

In fact, it is stated that in the near-fault case, strong velocity pulses at the beginning of the shaking occurred, giving a lot of energy to the structures [26].

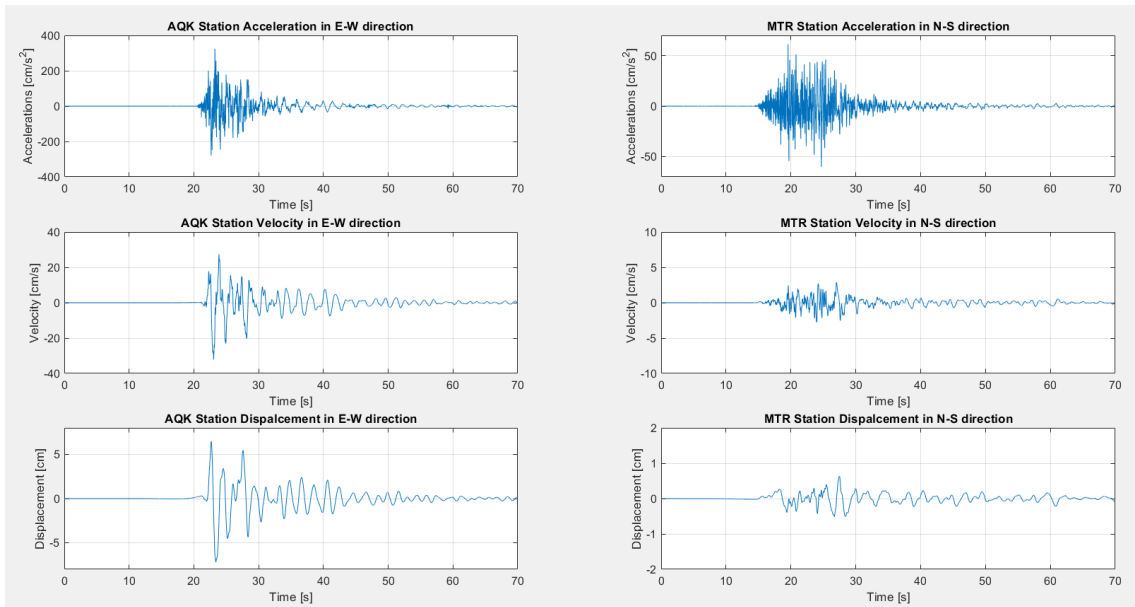


Figure 7.10: AQK EW and MTR NS time-history Acceleration, Velocity, Displacement

The two acceleration spectra are shown in the following figure. It can be observed that, regardless of the peak magnitude (PGA dependency), the AQK earthquake exhibits a distinct short range of frequencies where the motion is highly impulsive. In contrast, the MTR earthquake presents a more evenly distributed spectrum, without a specific frequency amplification.

7 EXPERIMENTAL SET-UP TEST

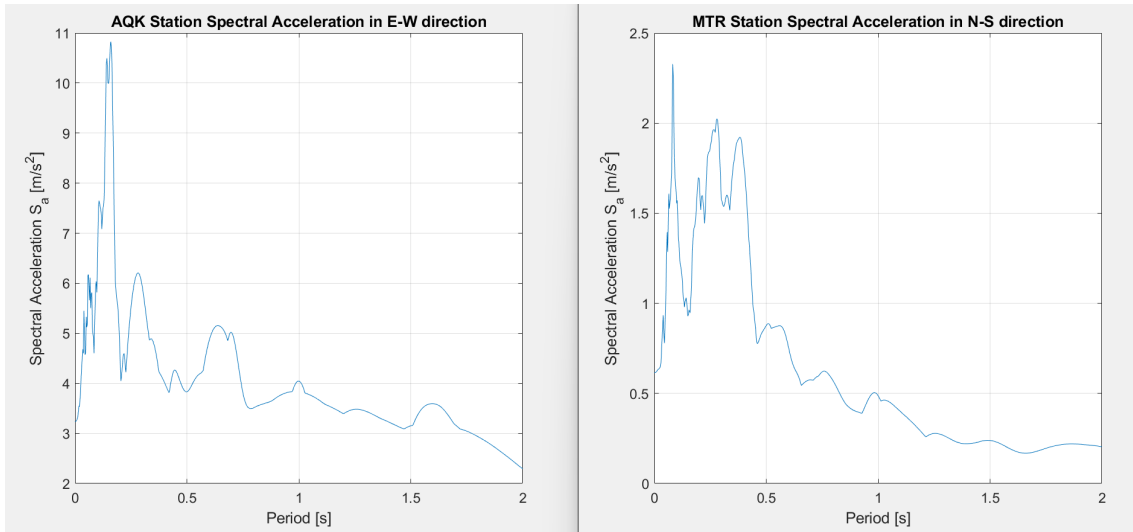


Figure 7.11: Spectral acceleration of AQK and MTR

Both ground motions were then scaled in time to meet the requirements of similarity laws expressed in Chapter 4. In detail, ground motions acceleration time history are presented as:

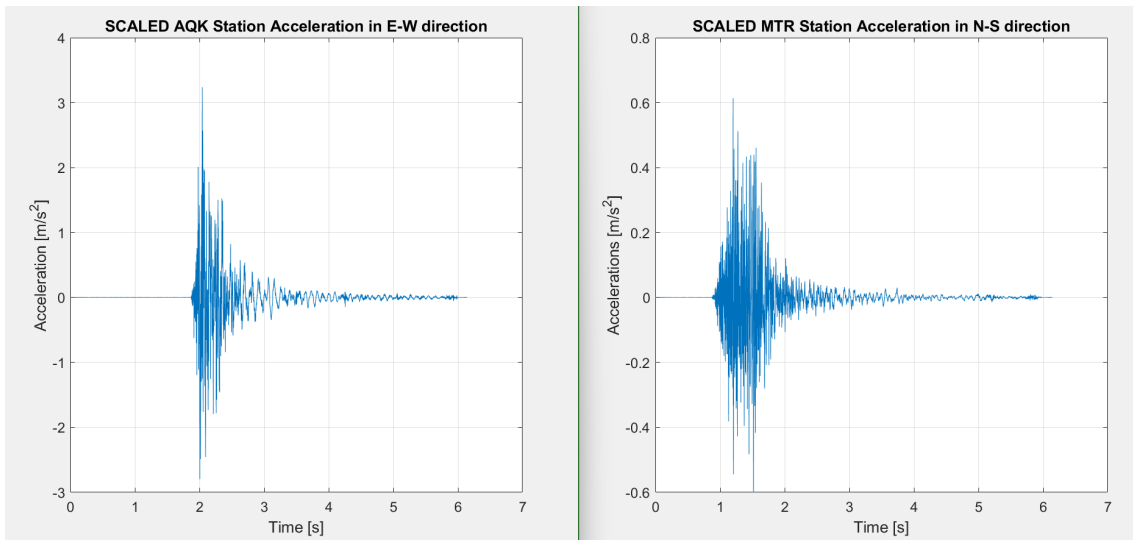


Figure 7.12: Time scaled acceleration time-history records

It is important to note that, as will be discussed in the results section, the large scaling factor applied to the mode is automatically reflected in the time scaling factor, leading to a significant compression of the records. This effect is clearly demonstrated when comparing Figure 7.10 and Figure 7.12, which illustrates how the Near and Far fault concept becomes much less prominent in the analysis, due to the substantial compression of the record.

Additionally, to maintain consistency, both ground motions are scaled to the same PGA of 0.4g. Scaling the ground motion is critical, as the focus of the research is on the structural response of the bridge, highlighting the characteristics of the seismic motion rather than the specific PGA of the earthquake. Consequently, the seismic ground motions applied to the FEM model are as follows:

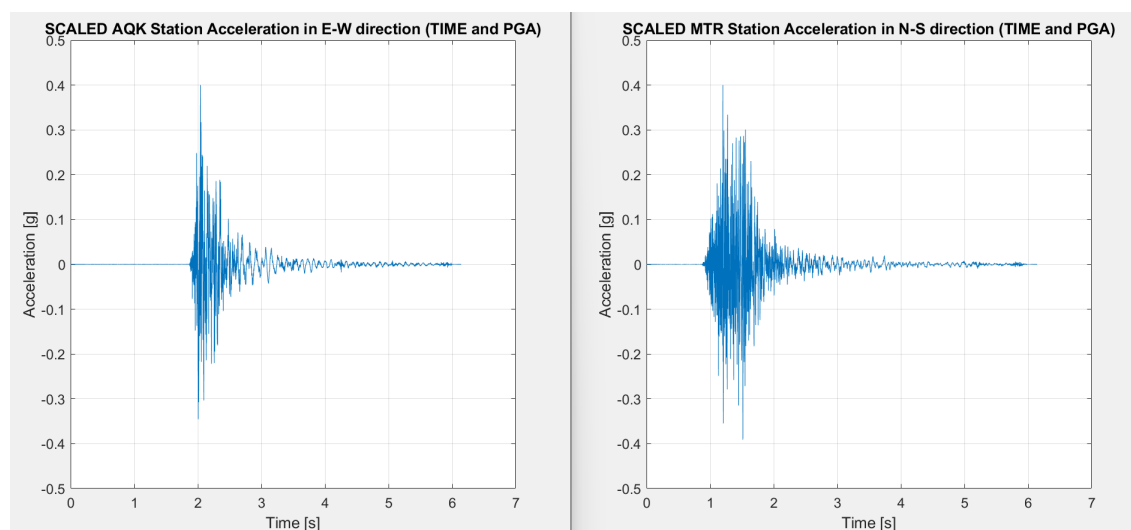


Figure 7.13: Time and PGA scaled acceleration time-history records

7.2 Soil-Foundation System

The focus of this study, as already mentioned is the understanding of the structural response of the bridge under different soil conditions. For this study 3 different cases are analysed, as already mentioned in the Chapter 5.

To achieve, and being able to reproduce a soil interaction, a box spring system has been realized. In detail, this spring box system, works through different springs, that are able to decrease or increase the stiffness of the base foundation. In the following more detail explanation of the system are provided

7.2.1 Box-Spring System

The interaction between the soil and the structure has been tested using a spring-box system, as shown in Figure 7.15.

The system consists of a thick base plate with four roll bearings positioned on top (Figure 7.16). Above the roll bearings, a massive translating plate is placed. This plate has holes on each side (square-shaped) to accommodate up to three springs per side, as illustrated in Figure 7.17.

Connected to different braces, the system features both movable and fixed parts. The tower base is attached to the movable part, allowing the transversal

shaking movements to be absorbed by the springs. This mechanism effectively simulates a non-fixed boundary condition.

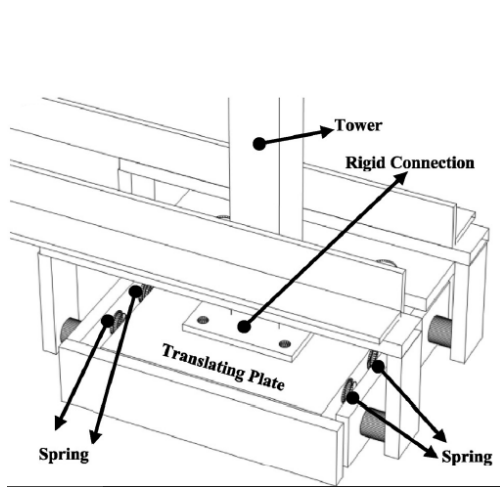
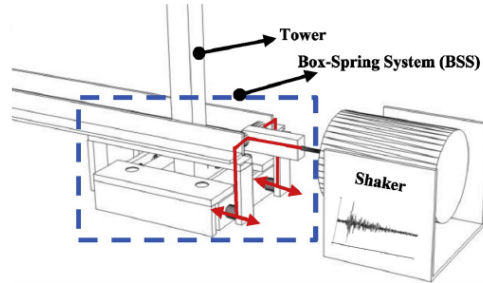
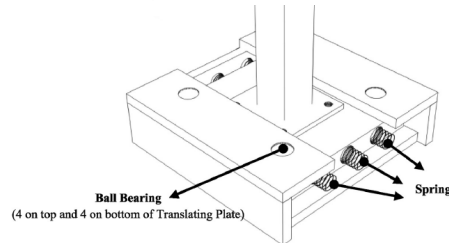


Figure 7.14: Spring-box system



(a) Spring-box system with shaker



(b) Springs location

Figure 7.15: Different components of the Spring-box system



Figure 7.16: Base plate with roll bearings



Figure 7.17: Whole system set-up

7.3 Sensors and Instrumentation

Several instrumentation and sensors have been set-up for monitoring the bridge and applying the earthquake input. Here in the following the most important are listed.

7.3.1 Shakers

Two shakers have been set-up at the base of each tower. The shaker works with a code written in LabVIEW for application of the ground motions through the shakers, based on the recorded ground motions selected before.

In detail, the displacement series data is provided as input, which represents the desired seismic motion over time. This displacement signal is taken from the time history displacement before shown or just from the time-history accelerogram using double integration. The shaker controller converts the displacement into electrical signals, which drive the actuator to generate the corresponding physical motion. The shaker then applies this motion to the base of the structure. Moreover, a load cell at the tip measures the resulting force, having in this way the control of the system.

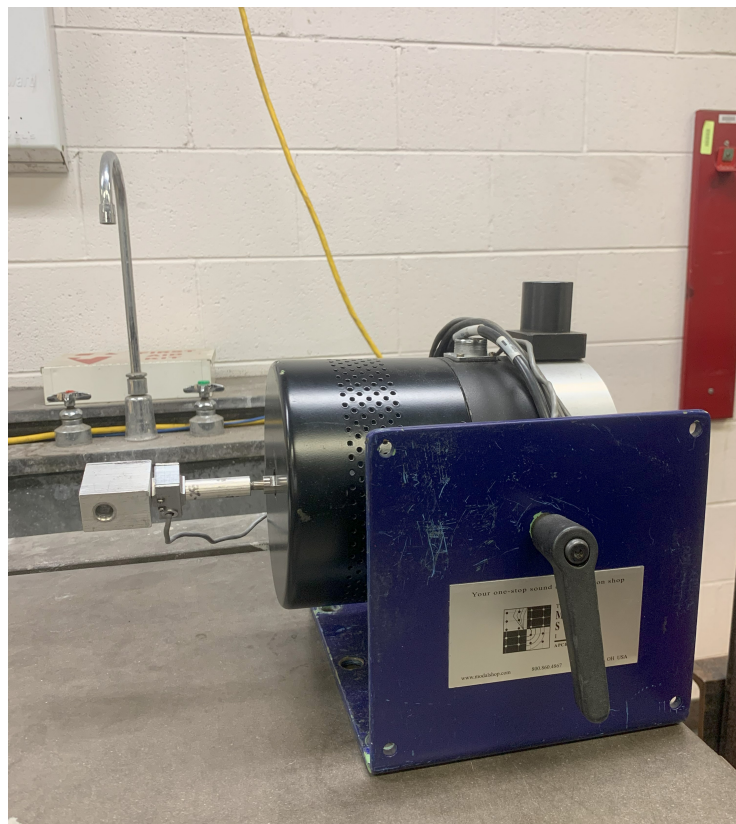


Figure 7.18: Shaker used for the experimental analysis

7.3.2 Accelerometers and LVDT

For the structural response of the bridge accelerometer and LVDT have been adopted.

Specifically accelerometers have been used to find experimentally the dynamic properties of the bridge, like the natural frequencies. In detail, an accelerometer was employed to measure the dynamic response of the structure and identify its natural frequencies. The sensor was securely mounted on the structure at a critical location (midspan) to capture the predominant vibration modes. An external excitation from the shakers, was applied to induce vibrations. The recorded acceleration data was processed through a Fast Fourier Transform (FFT) to obtain the frequency spectrum. Peaks in the spectrum correspond to the natural frequencies of the structure.

An LVDT (Linear Variable Differential Transformer), instead, was used to measure the displacement of the structure during dynamic testing. The sensor was positioned to track the relative motion of a specific point on the structure (midspan and towers), ensuring high accuracy in capturing small deformations. As the structure vibrated, the core of the LVDT moved within the coil assembly, inducing a voltage change proportional to the displacement.

The recorded signal was then processed and converted into displacement time histories.



Figure 7.19: Accelerometer used for calculating the dynamic properties of the bridge



Figure 7.20: LVDT used to calculate displacement in midspan

7.3.3 Fiber Bragg Gratings (FBG)

Fiber Bragg Grating (FBG) is an optical sensing technology commonly used for measuring strain, temperature, and pressure in various applications. It operates based on the principle of light reflection, where a periodic variation in the refractive index is inscribed along an optical fiber. These periodic refractive index changes, known as the Bragg grating, cause certain wavelengths of light to be reflected while others pass through. The key property of an FBG is its ability to reflect light at a specific wavelength, known as the Bragg wavelength, which is determined by the spacing of the refractive index modulations and the incident light's wavelength.

The Bragg wavelength (λ_B) is given by the equation:

$$\lambda_B = 2n\Lambda \quad (1)$$

where n is the effective refractive index of the fiber core, and Λ is the grating period (the distance between the refractive index modulations). When the fiber experiences external stimuli such as strain or temperature changes, the grating period or the refractive index of the fiber changes, leading to a shift in the Bragg wavelength. This shift can be precisely measured, allowing the FBG to act as a sensor.

In this study, FBGs are used to measure the tension in the cables of a bridge. As the cables undergo stress, the strain changes cause a shift in the Bragg wavelength, which can be correlated to the tension in the cables. This allows for continuous monitoring of the structural health of the bridge, providing valuable data on the forces acting on the system.

It is important to note that in order to accurately measure the tension using FBGs, a calibration process is required. This involves establishing a relationship between the shift in the Bragg wavelength and the specific amount of strain or force. The calibration ensures that the readings from the FBG sensor are accurate and reliable, enabling precise monitoring of the structural components under various loading conditions. A typical calibration of FBG is something like this:

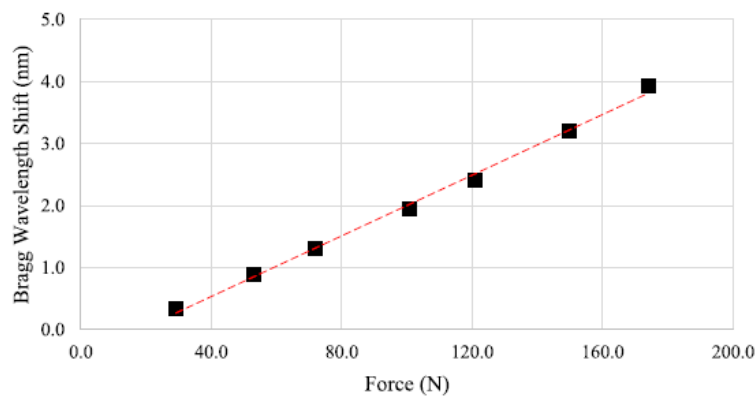


Figure 7.21: Example of calibration for FBG sensors

FBG sensors offer high sensitivity, accurate measurements, and long-term stability. They are widely used in structural health monitoring, where they provide real-time data on the condition of the structure. By monitoring the strain and temperature across various points, engineers can assess the performance and safety of critical infrastructure, detecting potential failures or anomalies before they escalate into serious issues.

8 Results

In the following numerical results are presented from the analyses for the six scenarios (2 earthquakes and 3 soil conditions).

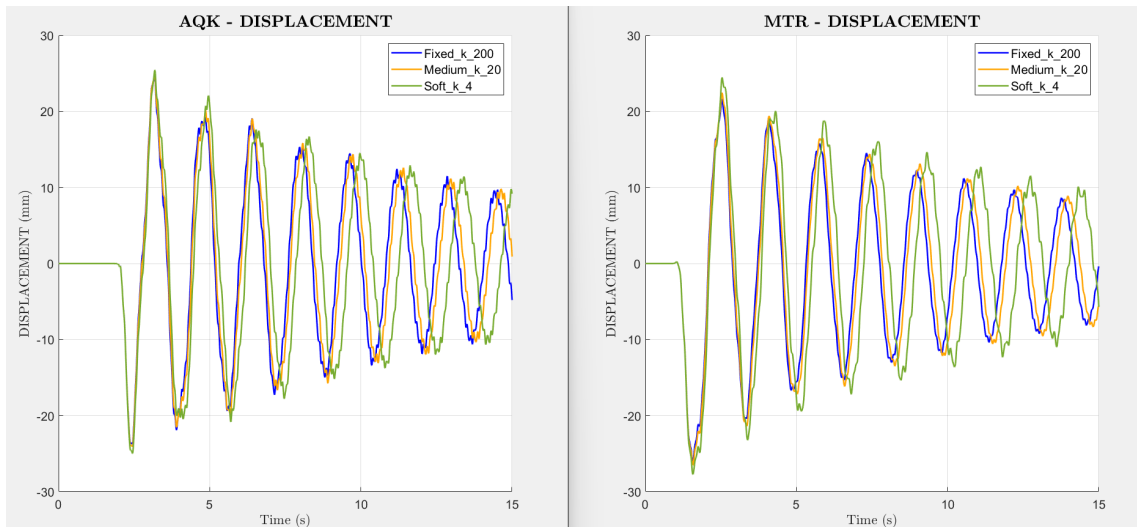


Figure 8.1: Displacement midspan results

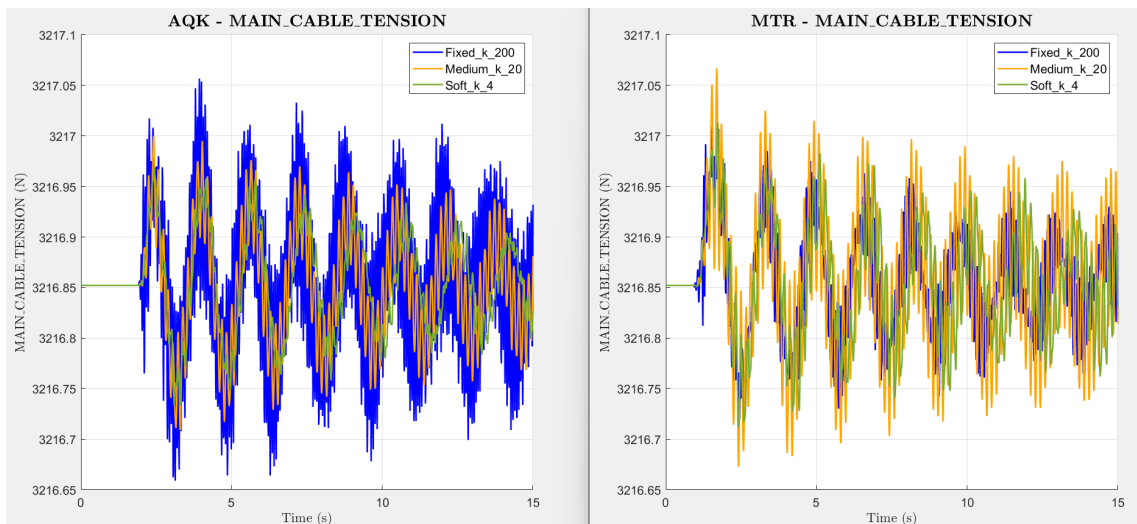


Figure 8.2: Most loaded main-cable results

By going through the displacement analysis in the midspan, it is possible to visualize how the structure starts shaking almost with similar period, while a shift of phase is present once the earthquake excitation ceases. In detail, as mentioned, the earthquakes last around 6-7 seconds, while the rest is free vibration.

As expected, a softer foundation results in greater midspan displacement, particularly during the seismic excitation. However, once the external excitation ceases, the displacement magnitude becomes similar across all cases, with only a phase shift in the oscillations.

Analyzing the seismic input motions, the AQK ground motion presents a more compact signal, whereas MTR has a longer duration and more uniform energy distribution. This is reflected in the bridge's structural response, where average displacements are higher for AQK compared to MTR.

As shown in Figure 8.2, for the AQK case, the softer the foundation, the lower the main cable tension. This behavior is expected, as a rigid foundation transmits seismic forces directly to the main cables, whereas a softer foundation allows more dissipation at the base.

For the MTR case, the same trend is observed, except for the high-stiffness case, where cable tensions are lower than in the soft foundation configurations. This deviation suggests an anomaly in the high-stiffness case, possibly due to differences in energy dissipation mechanisms or an unexpected interaction with the dynamic characteristics of the bridge.

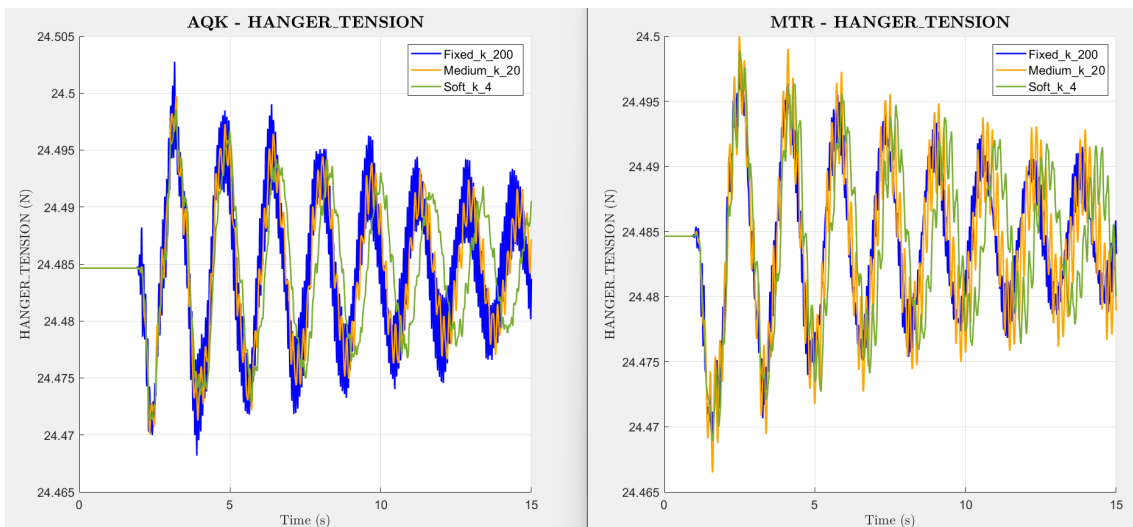


Figure 8.3: *Most loaded hangers tension results*

By analyzing Figure 8.3, it presents the hanger tension results. In the AQK case, the trend follows that of the main cables: softer foundations dissipate more seismic energy at the base, reducing the forces transmitted to the suspension system.

In the MTR case, however, the variation in hanger tension across different foundation conditions is less pronounced. Instead, a phase shift in the oscillation period is observed, which can be attributed to the damping effect of the structure.

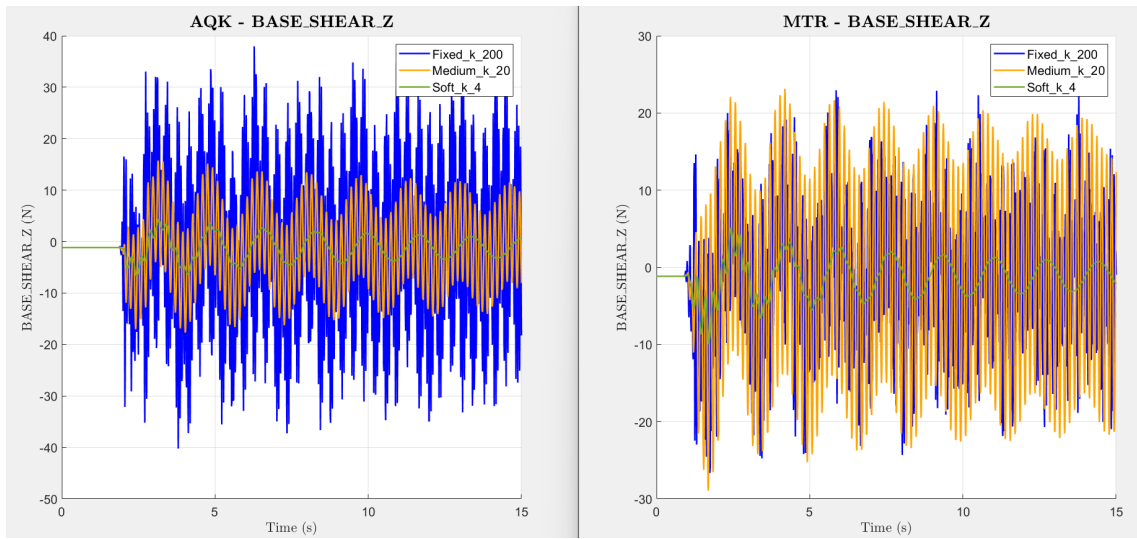


Figure 8.4: Base shear z direction East tower results

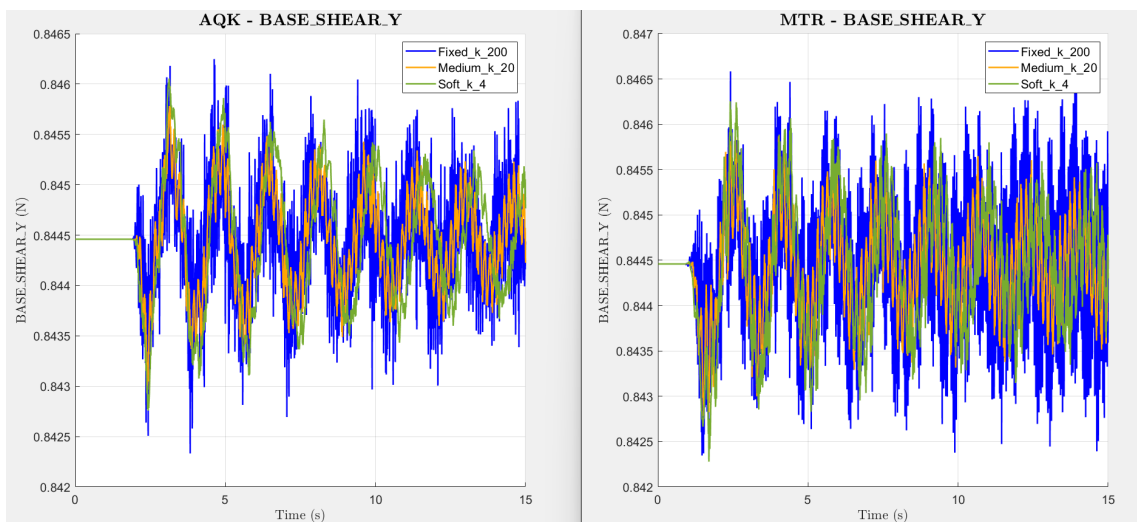


Figure 8.5: Base shear y direction East tower results

Figures 8.4 and 8.5 show the base shear forces in the two principal directions. The results confirm that increasing the foundation stiffness leads to higher seismic force absorption by the towers, as forces are primarily attracted to the stiffer elements.

The effect of foundation stiffness is more significant in the primary shear direction (z-axis), where the seismic forces are larger. In contrast, in the secondary shear direction (y-axis), the differences between stiffness cases are present but less pronounced.

For the MTR seismic action, an interesting observation is that the fixed configuration exhibits a base shear similar to the medium stiffness case ($k = 40 \text{ N/mm}$), suggesting a possible redistribution of forces within the system.

9 Conclusions

This study aims to understand the structural dynamic response of the Messina Bridge under seismic excitation, exploring different soil conditions. The reproduction of the scaled model follows a distorted similitude approach, where not all similarity requirements could be fully satisfied. However, the time compression in the seismic records was a necessary consequence of the large length scale factor adopted for the bridge. This adjustment was required to achieve perfect similarity in the time domain. Nevertheless, the distinction between near-fault and far-fault earthquakes was somewhat reduced, leading to similar magnitudes in the structural response across the two seismic scenarios.

Regarding displacement analysis, it is evident that the softer the foundation, the higher the midspan displacement amplitude. While there is a slight difference, the near-fault case results in a higher magnitude compared to the far-fault case. However, an anomaly is observed in the fixed configuration of the MTR case, which does not follow the general trend of the results. This could be attributed to localized dynamic effects and the interaction between cables, towers, and foundations, potentially leading to a local reduction in forces and stresses. As a result, this case behaves similarly to the medium-stiffness scenario.

These findings highlight the significant role of foundation stiffness in the global seismic response of the bridge and suggest that soil-structure interaction must be carefully considered in the seismic design of long-span suspension bridges. The results align with existing studies on similar structures, confirming that foundation stiffness plays a crucial role in determining dynamic behavior under seismic loads.

Ultimately, this study aims to compare the numerical results obtained with experimental data, which will be collected in a subsequent phase. As discussed throughout this thesis, all the necessary instrumentation and sensor components have been set up. The next steps of this research, which will be valuable for a future publication, involve first identifying the natural frequencies of the bridge. This will be achieved by applying a white noise excitation to the structure through shakers and using accelerometers along with the Fast Fourier Transform to extract the natural frequencies. Secondly, seismic input signals will be applied to the structure, again using shakers, to analyze its response under controlled conditions.

Beyond these experimental analyses, future research could investigate the effects of different foundation configurations or seismic isolation systems to assess potential mitigation strategies. Furthermore, incorporating fiber optic techniques for bridge health monitoring or introducing damping strategies in the analysis could offer valuable insights for enhancing the seismic design of suspension bridges.

In conclusion, this study provides a preliminary contribution to understanding the dynamic response of the Messina Bridge under seismic loading, emphasizing the importance of foundation conditions on the overall structural behavior.

The numerical results obtained lay a solid foundation for future experimental investigations.

References

- [1] Emad Norouzzadeh Tochaei, Todd Taylor, and Farhad Ansari. “Effects of near-field ground motions and soil-structure interaction on dynamic response of a cable-stayed bridge”. In: *Soil Dynamics and Earthquake Engineering* 133 (June 2020), p. 106115. DOI: [10.1016/j.soildyn.2020.106115](https://doi.org/10.1016/j.soildyn.2020.106115).
- [2] J. D. Bray and A. Rodriguez-Marek. “Characterization of forward-directivity ground motions in the near-fault region”. In: *Soil Dynamics and Earthquake Engineering* 24.11 (2004), pp. 815–828.
- [3] JP Stewart and S Tileylioglu. *Input ground motions for tall buildings with subterranean levels*. TBI Task 8 Final Report. Berkeley, CA: Pacific Earthquake Engineering Research Center, 2010.
- [4] National Institute of Standards and Technology. *Soil-Structure Interaction for Building Structures*. Tech. rep. National Institute of Standards and Technology, 2012. URL: <https://www.nist.gov/publications/soil-structure-interaction-buildingstructures>.
- [5] Wenming Zhang, Genmin Tian, and Yupeng Chen. “Evolution of suspension bridge structural systems, design theories, and shape-finding methods: A literature survey”. In: *Journal of Traffic and Transportation Engineering (English Edition)* 11.2 (2024), pp. 225–244. ISSN: 2095-7564. DOI: <https://doi.org/10.1016/j.jtte.2024.03.002>. URL: <https://www.sciencedirect.com/science/article/pii/S2095756424000291>.
- [6] Niels J. Gimsing and Christos G. Georgakis. *Cable Supported Bridges: Concept and Design*. Third. Chichester, West Sussex, UK: John Wiley & Sons, 2012.
- [7] Tadaki Kawada Stephens. *History of the Modern Suspension Bridge: Solving the Dilemma Between Economy and Stiffness*. Reston, VA: ASCE Press, 2010. ISBN: 978-0-7844-1105-0.
- [8] Tadaki Kawada. *History of Modern Suspension Bridge: Solving the Dilemma Between Economy and Stiffness*. ASCE Press, 2002. ISBN: 9780784409480. DOI: [10.1061/9780784410189](https://doi.org/10.1061/9780784410189).
- [9] A. Angelini. *Il mitico ponte sullo Stretto di Messina: da Lucio Cecilio Metello ai giorni nostri : la storia, la cultura, l'ambiente*. Sociologia urbana e rurale. FrancoAngeli, 2011. ISBN: 9788856833195. URL: <https://books.google.com/books?id=dDCmcQAACAAJ>.
- [10] E. Vismara. *Proposta di studi per una galleria sotto lo Stretto di Messina*. Comunicazione fatta al Congresso Geografico tenutosi in Firenze nel marzo-aprile 1921. Milano: Turati Lombardi, 1921.
- [11] Italiana. *Bridge over the Strait of Messina: A Work Never Built*. Accessed: 2024-10-14. 2024. URL: <https://en.italiani.it/bridge-over-the-strait-of-messina-a-work-never-built/>.

- [12] E. Verzera. "Sotto lieti auspici si è iniziato il convegno per il Ponte sullo Stretto". In: *Notiziario di Messina* 199 (Aug. 23, 1953). Cited in Franco Angelini, *Il mitico ponte sullo stretto di Messina.*, p. 6.
- [13] N. Calarco. "Iniziati a Messina i sondaggi per il ponte". In: *Giornale del Mezzogiorno* 3-39 (Sept. 22, 1955). Cited in Franco Angelini, *Il mitico ponte sullo stretto di Messina.*
- [14] Autori sconosciuti. "I vincitori del concorso per il Ponte sullo Stretto di Messina". In: *L'Industria Italiana del Cemento* 11 (1970). Cited in Franco Angelini, *Il mitico ponte sullo stretto di Messina.*, p. 875.
- [15] Consorzio Stretto di Messina. *Stretto di Messina S.p.A.* Sito ufficiale della Stretto di Messina S.p.A. 2024. URL: <https://strettodimessina.it/> (visited on 11/03/2024).
- [16] Jack R. Janney et al. "The Use of Models in Structural Engineering". In: *ACI Symposium Publication* 24 (1970). DOI: 10.14359/17582.
- [17] G. M. Sabnis et al. *Structural Modeling and Experimental Techniques*. Illustrated edition, 585 pages. Englewood Cliffs, NJ: Prentice-Hall Civil Engineering, 1983.
- [18] Junjun Guo et al. "Shake table test and numerical model update for a viscous damper isolated cable-stayed bridge". In: *Soil Dynamics and Earthquake Engineering* 176 (2024), p. 108308. ISSN: 0267-7261. DOI: <https://doi.org/10.1016/j.soildyn.2023.108308>. URL: <https://www.sciencedirect.com/science/article/pii/S0267726123005535>.
- [19] Ltd. MIDAS Information Technology Co. *MIDAS Civil Software*. 2024. URL: <https://www.midasuser.com>.
- [20] Anil K. Chopra. *Dynamics of Structures: Theory and Applications to Earthquake Engineering*. 4th. Upper Saddle River, NJ: Prentice Hall, 2012. ISBN: 9780132858038.
- [21] Sinan Akkar, Ufuk Yazgan, and Polat Gülkan. "Drift Estimates in Frame Buildings Subjected to Near-Fault Ground Motions". In: *Journal of Structural Engineering* 131.7 (2005), pp. 1014–1024. DOI: 10.1061/(ASCE)0733-9445(2005)131:7(1014).
- [22] Redazione Focus. *L'origine del terremoto di Messina del 1908*. Accessed: 2024-11-13. 2020. URL: <https://www.focus.it/scienza/scienze/origine-terremoto-messina-1908>.
- [23] C. Felicetta et al. *Italian Accelerometric Archive v4.0*. Istituto Nazionale di Geofisica e Vulcanologia, Dipartimento della Protezione Civile Nazionale. 2023. DOI: 10.13127/itaca.4.0.

REFERENCES

- [24] T. Rossetto et al. "Field observations from the Aquila, Italy earthquake of April 6, 2009". In: *Bulletin of Earthquake Engineering* 9.1 (2011), pp. 11–37. ISSN: 1573-1456. DOI: 10.1007/s10518-010-9221-7. URL: <https://doi.org/10.1007/s10518-010-9221-7>.
- [25] James Kaklamanos, Laurie G. Baise, and David M. Boore. "Estimating Unknown Input Parameters when Implementing the NGA Ground-Motion Prediction Equations in Engineering Practice". In: *Earthquake Spectra* 27.4 (2011), pp. 1219–1235. DOI: 10.1193/1.3650372.
- [26] Aybige Akinci, Luca Malagnini, and Fabio Sabetta. "Characteristics of the strong ground motions from the 6 April 2009 L'Aquila earthquake, Italy". In: *Soil Dynamics and Earthquake Engineering* 30.5 (2010), pp. 320–335. ISSN: 0267-7261. DOI: 10.1016/j.soildyn.2009.12.006. URL: <https://doi.org/10.1016/j.soildyn.2009.12.006>.